Journal of Cleaner Production 538 (2026) 147402

Contents lists available at ScienceDirect

Journal of Cleaner Production

journal homepage: www.elsevier.com/locate/jclepro

Changing global vegetation-climate interactions constrain photosynthesis in the 21st century

Rahul Kashyap, Jayanarayanan Kuttippurath *

CORAL, Indian Institute of Technology Kharagpur, Kharagpur, 721302, India

HIGHLIGHTS

- Investigation of changing global vegetation-climate interactions and photosynthesis.
- Temperature is the key climatic control on photosynthesis, followed by soil moisture.
- A shift in control from temperature and energy to water availability on photosynthesis.
- Greening continues, but slowdown for grasses, and tropical/arid biomes due to drying.
- Intense greening is projected for the cold and arid biomes in the future climate.

GRAPHICAL ABSTRACT

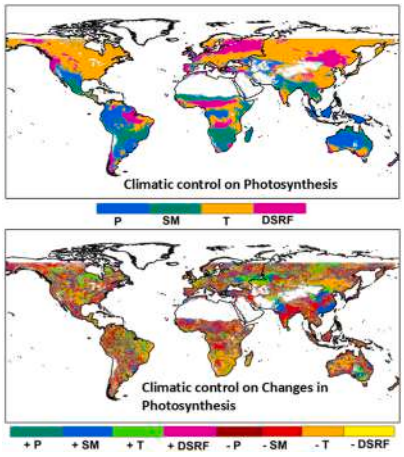

ARTICLE INFO

Keywords:
Greening
Browning
Vegetation-climate feedbacks
Land-atmosphere interactions
Carbon cycle
Machine learning

ABSTRACT

Photosynthesis drives life on the Earth and it is essential to examine the response of terrestrial ecosystems to climate change. This study investigates the changing vegetation-climate interactions and the response of global photosynthesis to it in the current (2000–2021) and future climate scenarios (until 2100). The study finds temperature (T, 31 %) as the dominant driver of global photosynthesis, followed by soil moisture (SM, 26 %), precipitation (P, 23.4 %) and downward shortwave radiation flux (DSRF, 19.5 %) as suggested by Random Forest (RF). Across biomes and land covers, T controls photosynthesis in forests (36.4 %), croplands (35 %), and temperate (36.1 %) and cold (29.7 %) biomes, but P in grasses (35.5 %), and tropical (26.8 %) and arid (27 %) biomes. Photosynthesis has causal feedbacks with SM (croplands), P (forests, tropical and temperate), and T (temperate and cold); reveals Granger Causality that goes beyond correlations as it indicates directional effects. Water availability (SM, 5 %; P, 2.4 %) has strengthened its control on the global photosynthesis, and weakened the influence of T (−4.4 %) in recent decade (2010–2019) from its previous (2000–2009). The enhanced Solar-Induced Fluorescence (SIF, 4.2 %), Enhanced Vegetation Index (EVI, 2.8 %) and Fraction of Photosynthetically Active Radiation (FPAR, 0.8 %) confirm the “Greening Earth”, as also attested by the positive cumulative growth rate (FPAR, 1.2 % CGR). Greening is intensified in croplands (1.7 % CGR), arid (1.6 % CGR) and temperate (1.4

* Corresponding author.
E-mail address: jayan@coral.iitkgp.ac.in (J. Kuttippurath).

https://doi.org/10.1016/j.jclepro.2025.147402
Received 24 November 2024; Received in revised form 18 November 2025; Accepted 23 December 2025

% CGR) biomes, and forests (0.4 % CGR); conversely, slowdown/reversed in grasses (−4.1 % CGR), and tropical (−1.8 % CGR) and cold (−0.2 % CGR) biomes. Greening is projected to continue until the end of the century (2090–2100), predominantly in the cold (45.9 %) and arid (31.6 %) biomes. Future greening can expedite the hydrological cycle and strengthen land-atmosphere coupling. This calls for effective utilisation of land resources, judicial management of green cover and climate adaptation policies to attain sustainability in a warmer and drier world with an unprecedented human population rise.

1. Introduction

Land-atmosphere interactions are vital to the climate and the functioning of various components of the Earth system. Vegetation plays a crucial role in regulating the fluxes of carbon, water, energy and momentum between land and atmosphere (Piao et al., 2020; Humphrey et al., 2021). To improve our understanding of fluctuations in these fluxes within the climate system, and to monitor natural ecosystems and agricultural lands, it is essential to study global photosynthesis (Ryu et al., 2019; Keenan et al., 2023). The terrestrial ecosystems act as major carbon sinks as they absorb about 30 % of human-caused CO_2 emissions and store them as vegetation biomass, and control the stability of carbon cycle (Ruehr et al., 2023; Bar-On et al., 2025). Thus, measuring global photosynthesis is essential for comprehending the global carbon cycle and climate system as both are closely connected through various feedbacks (Nemani et al., 2003; Sellers et al., 2018). Furthermore, the increase in population and economic growth necessitates an increase in crop yield and wood production, that depend on photosynthesis (Piao et al., 2020).

Quantification of global photosynthesis is very challenging as it requires a vivid understanding of various linear and non-linear biophysical processes that vary in space and time. In recent decades, collaborative efforts among plant physiology, biogeochemistry, ecology and earth observations have greatly enhanced our understanding of photosynthesis on multiple scales (Ryu et al., 2019). However, there remains uncertainties regarding the spatio-temporal patterns of global photosynthesis due to differences among the selected models, algorithms, parameters, and measurements (Rogers et al., 2017). The establishment of eddy covariance flux towers has greatly enhanced our comprehension of canopy photosynthesis processes (Baldocchi, 2020). However, flux towers do not represent global processes, particularly in the tropics with limited measurements (Schimel et al., 2015; Kashyap et al., 2023a). Contextually, the emergence of satellite remote sensing has made significant strides in the study of global photosynthesis (Nemani et al., 2003; Piao et al., 2020).

Monitoring the changes in global photosynthesis is essential for comprehending the alterations in the functioning of terrestrial biosphere and to assess climate feedback mechanisms (Nemani et al., 2003; Piao et al., 2020). It is also of great significance because of the unprecedented rise in human population, exorbitant resource consumption and accelerated environmental degradation (Zhu et al., 2016; Chen et al., 2019). Satellite-derived vegetation indices reveal varied regional changes, with an overall increase in vegetation greenness (i.e. greening) (Zhu et al., 2016; Chen et al., 2019; Cortés et al., 2021; Chen et al., 2024a) over the years and a recent decrease in vegetation greenness (i.e. browning) (Brandt et al., 2018; Pan et al., 2018; Liu et al., 2023). The global vegetation dynamics is influenced by both climate (Nemani et al., 2003; Zhu et al., 2016; Piao et al., 2020) and non-climate (land management and environmental factors) (Zhu et al., 2016; Chen et al., 2019; Piao et al., 2020) drivers. Land management such as agricultural intensification and afforestation contributes to greening (Chen et al., 2019; Kuttippurath and Kashyap, 2023). Environmental factors such as the CO_2 fertilization effect (CFE) and nitrogen deposition (ND) also contribute to greening (Zhu et al., 2016). However, the land use land cover change (LULCC) (Tagesson et al., 2020), dryness stress (Liu et al., 2023), extreme events such as droughts and heatwaves (Bastos et al., 2020), and strong El Niño (Wigneron et al., 2020) trigger browning.

The role of non-climate drivers on global vegetation dynamics is rather straightforward. The vegetation response to climate trends is intricate and exhibits significant spatial and temporal variability (Nemani et al., 2003; Higgins et al., 2023). In the warming world (Trenberth, 2015), with erratic rainfall and enhanced evapotranspiration (ET), soil moisture (SM) has been drying in 40 % of the global vegetated lands in recent decades (Lal et al., 2023). This dryness stress impacts global ecosystems as it limits photosynthesis (Liu et al., 2020) and reduces terrestrial carbon uptake (Feng et al., 2021). Changes in climate have altered the functioning of terrestrial ecosystems in recent decades on global (Higgins et al., 2023) and regional (Kashyap and Kuttippurath, 2024a; b) scales. One of the major challenges in Earth System Science is the identification of these alterations and their attribution. First, the detection of changes in global vegetation is difficult due to the inherent stochasticity of the system, the limited data availability, uncertainty in the observations, and the significant impact of LULCC (Higgins et al., 2023). Next, the attribution is also challenging due to the heterogeneity of vegetation response and nonlinearity of ecosystem dynamics, further limited by the highly correlated climate drivers (Winkler et al., 2021; Kashyap et al., 2023a).

A study based on multiple machine learning (ML) models finds global greening to be stronger in the future, particularly in the northern hemisphere (Zhang et al., 2025). Advancements in trend estimation techniques find a decrease in the greening areas in recent decades (Gutiérrez-Hernández and García, 2025). The global vegetation dynamics also impacts global climate through complex vegetation-climate feedbacks (Miralles et al., 2025; Liu et al., 2025). A clear understanding of the dominant climate drivers of global photosynthesis, its changes, and the climatic control that drives these changes is of paramount significance in assessing vegetation dynamics, and land-atmosphere and carbon-climate interactions in a warmer and drier world. Furthermore, in the context of unprecedented human population growth in the background of a changing climate, attaining global sustainability is a big challenge. There is a need for robust assessments aimed at effective terrestrial carbon sink management and climate adaptation policies to ensure the global food security and to timely meet sustainable development goals (SDGs). Thus, this study hypothesises that with the changing climate, the global vegetation-climate interactions will be altered, and in response, global photosynthesis will change in the current and future climate scenarios. Therefore, the study presents a comprehensive assessment of the following: (i) What is the spatio-temporal variability in global photosynthesis? (ii) What are the dominant climate drivers of global photosynthesis? (iii) How does the vegetation-climate relationship evolve with time? (iv) What is the role of key climatic factors in driving changes in global photosynthesis? and (v) What is the future of global photosynthesis for various land covers and biomes? The study employs a set of statistical and ML techniques on remote sensing measurements, reanalyses data and climate model projection results for this assessment. The findings would shed light on the complex vegetation-climate interactions and their feedback, which are crucial for drafting policies to mitigate the threats of climate change, to attain food security and global sustainability.

2. Data and methods

The study employs a range of remote sensing observations, reanalyses and climate projection data of land cover types, biomes,

photosynthetic activity, and climate. A suite of statistical and machine learning techniques such as correlation, Partial Correlation (PC), Limiting Factor analysis, Multiple Linear Regression (MLR), ML based Random Forest (RF) model, Growth Rate (GR) analysis, sensitivity analysis and Granger Causality (GC) are also employed to unravel the evolution of global vegetation-climate interactions and the response of photosynthetic activity to them. These would provide information on their spatio-temporal variability, decadal changes, relationship, causal connection, relative control, sensitivity and growth rate, and their climate drivers. The data, parameters, computational techniques, and the outputs are presented in the overall conceptual and methodological framework in Fig. 1. Details of data and methods are given in this section.

2.1. Data

2.1.1. Proxies of photosynthesis

The abbreviations and their meaning are mentioned in Table 1. The data used in this study with their resolution, purpose and sources are mentioned in Table 2. Earth observations enable a synoptic scale view of the global terrestrial biosphere and are key to its timely monitoring (Nemani et al., 2003; Crowther et al., 2015). The moderate resolution imaging spectroradiometer (MODIS) is a highly effective instrument in monitoring the terrestrial biosphere (Chen et al., 2019; Kashyap et al., 2023a). To accurately measure plant photosynthetic activity, it is essential to determine the fraction of photosynthetically active radiation (FPAR) absorbed by the green components of vegetation canopy and is one of the essential climate variables (Sellers et al., 1996; Kashyap et al., 2022). The study utilises MODIS Normalised Difference Vegetation Index (NDVI) to compute FPAR through the Linear Scaling technique (Sellers et al., 1996) (detailed in methods). The study also utilises the MODIS Enhanced Vegetation Index (EVI) as it is more sensitive to changes in canopy structure and does not saturate in high biomass regions like Amazon, unlike NDVI (Huete et al., 2002; Kashyap et al., 2023b; Patel et al., 2024a). The study also considers solar-induced fluorescence (SIF), as it is an efficient indicator of photosynthesis and productivity being closely related to plant physiological processes (Rascher et al., 2015; Shekhar et al., 2022). The global Orbiting Carbon Observatory (OCO-2) SIF (GOSIF v2) dataset is employed for quantifying plant photosynthetic activity and terrestrial productivity (Li and Xiao, 2019; Kashyap et al., 2023b).

2.1.2. Land covers and biomes

The study delineates various land cover types based on MODIS land cover data as per the International Geosphere and Biosphere Programme (IGBP) classification as it has an overall classification accuracy of around 75 % (MODIS Land Team, 2014). The study reclassifies the land covers for our analysis, wherein the overall vegetated land comprises croplands, forests, and all other natural vegetation such as grasslands, shrublands and savannah. The other natural land cover types will be called grasses hereafter (Fig. S1a). The study also performs analysis for the four major biomes in the world, the tropical, temperate, cold and arid, based on the Köppen-Geiger climate classification (Beck et al., 2023) (Fig. S1b). The study additionally focusses 10 countries with the largest vegetated area and population (Chen et al., 2019) (Fig. S1c).

2.1.3. Climate data

Global photosynthesis is greatly controlled by climatic drivers (Nemani et al., 2003; Higgins et al., 2023). Here, the study considers moisture availability as precipitation (P) and soil moisture (SM), Warmth as temperature (T) and energy as downward shortwave radiation flux (DSRF) as the key climatic drivers. The P data are obtained from the Global Precipitation Measurement (GPM) system, a comprehensive dataset that combines precipitation measurements from multiple satellites (Skofronick-Jackson et al., 2018). The Global Land Data Assimilation System (GLDAS) utilises satellite and ground-based observations through sophisticated data assimilation techniques to produce accurate representations of land surface conditions. This study incorporates the

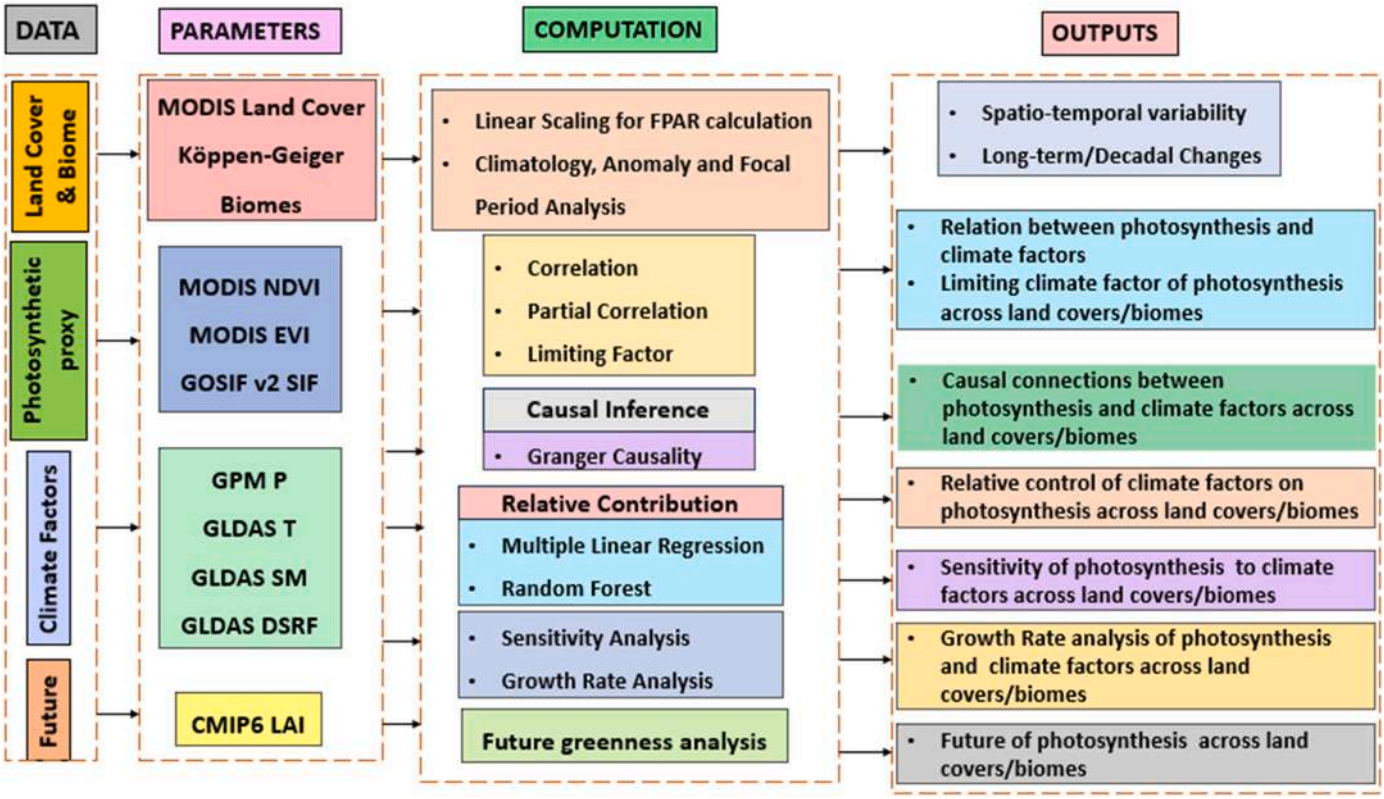

Fig. 1. A schematic diagram of the working methodology of the study.

Table 1
The list of abbreviations used in the manuscript.

Abbreviation	Meaning
CFE	CO_2 Fertilisation Effect
CGR	Cumulative Growth Rate
CMIP6	Coupled Model Intercomparison Project Phase 6
CSA	Climate-Smart Agriculture
DGVM	Dynamic Global Vegetataion Model
DJF	December, January and February
DSRF	Downward Shortwave Radiation Flux
EbA	Ecosystem-based Adaptation
ENSO	El Niño Southern Oscillation (ENSO)
ET	Evapotranspiration
EVI	Enhanced Vegetation Index
FPAR	Fraction of Photosynthetically Active Radiation
GC	Granger Causality
GLDAS	Global Land Data Assimilation System
GNSS	Global Navigation Satellite Systems
GPM	Global Precipitation Measurement
GPP	Gross Primary Productivity
GR	Growth Rate
IGBP	International Geosphere and Biosphere Programme
ISIMIP	Inter-Sectoral Impact Model Intercomparison Project
JJA	June, July and August
LAI	Leaf Area Index
LULCC	Land Use Land Cover Change
MAM	March, April and May
ML	Machine learning
MLR	Multiple Linear Regression
MODIS	Moderate Resolution Imaging Spectroradiometer
NbS	Nature-based Solutions
ND	Nitrogen Deposition
NDVI	Normalised Difference Vegetation Index
NPP	Net Primary Productivity
OCO	Orbiting Carbon Observatory
P	Precipitation
P1	historical period (2015–2019)
P2	mid-century (2040–2050)
P3	end-century (2090–2100)
PC	Partial Correlation
REDD+	Reducing Emissions from Deforestation and Forest Degradation
RF	Random Forest
SDGs	Sustainable Development Goals
SIF	Solar-Induced Fluorescence
SM	Soil Moisture
SON	September, October and November
SSP	Shared Socioeconomic Pathways
T	Temperature
VAR	Vector Autoregressive
UN	United Nations

Table 2
The datasets, their resolution, purpose and the sources are listed.

Data	Resolution	Purpose/Use	Source
MODIS LULC (MCD12Q1)	500 m	LULC data to extract vegetated land covers	(https://lpdaacsvc.cr.usgs.gov/)
MODIS NDVI (MOD13A1)	500 m	calculation of FPAR	(https://lpdaacsvc.cr.usgs.gov/)
MODIS EVI (MOD13A1)	500 m	EVI & calculation of change in photosynthesis	(https://lpdaacsvc.cr.usgs.gov/)
GOSIF SIF (v2)	0.05° × 0.05°	SIF & calculation of change in photosynthetic activity and productivity	(http://data.globalecology.unh.edu/)
GPM Level–3 precipitation	0.1° × 0.1°	Precipitation, relationship with photosynthesis and changes	(https://daac.gsfc.nasa.gov/)
GLDAS Soil Moisture	0.25° × 0.25°	Soil Moisture, relationship with photosynthesis and changes	(https://daac.gsfc.nasa.gov/)
GLDAS Skin Temperature	0.25° × 0.25°	Temperature, relationship with photosynthesis and changes	(https://daac.gsfc.nasa.gov/)
GLDAS DSRF	0.25° × 0.25°	DSRF, relationship with photosynthesis and changes	(https://daac.gsfc.nasa.gov/)
Köppen-Geiger classification	1 km	Biome delineation	(https://www.gloh2o.org/koppen/)
CESM2 LAI	1° × 1°	Future LAI and changes	(https://esgf-node.llnl.gov/projects/cmip6/
CSM-2 MR LAI	1.25° × 1.25°	Future LAI and changes	(https://esgf-node.llnl.gov/projects/cmip6/
CNRM LAI	1.40° × 1.40°	Future LAI and changes	(https://esgf-node.llnl.gov/projects/cmip6/
ACCESS LAI	1.875° × 1.25°	Future LAI and changes	(https://esgf-node.llnl.gov/projects/cmip6/
MPI-ESM LAI	1.88° × 1.86°	Future LAI and changes	(https://esgf-node.llnl.gov/projects/cmip6/
Can-ESM LAI	2.81° × 2.77°	Future LAI and changes	(https://esgf-node.llnl.gov/projects/cmip6/

GLDAS-based SM, land temperature (T) and DSRF data (Wang et al., 2016; Liu et al., 2019).

2.1.4. Future projections

To explore the future of photosynthesis, the study employs the Coupled Model Intercomparison Project Phase 6 (CMIP6) based future projection of a proxy of photosynthesis in terms of Leaf Area Index (LAI). The data from six CMIP6 models CESM2 (1° × 1°), CSM-2 MR (1.25° × 1.25°), CNRM (1.40° × 1.40°), ACCESS (1.875° × 1.25°), MPI-ESM (1.88° × 1.86°) and Can-ESM (2.81° × 2.77°) are employed, as these are high resolution models with good reliability (Zhao et al., 2020). Since the study investigates changes in the most extreme cases, an examination of future projections is conducted under high emissions scenarios (Shared Socioeconomic Pathways, SSP585). Three time periods are selected for comparison: (a) historical (P1, 2015–2019), (b) mid-century (P2, 2040–2050) and (c) end-century (P3, 2090–2100).

2.2. Methods

This study identifies and attributes the role of climate change on terrestrial ecosystems. Our approach effectively deals with the complications arising from limited time series data, constraints of correlative techniques, and uncertainties in interpreting biophysical proxies (e.g. LAI, Gross Primary Productivity: GPP and Net Primary Productivity: NPP) from satellite data (Higgins et al., 2023). The study employs high-resolution, recent remote sensing data (e.g. FPAR, SIF and EVI) that are highly responsive indicators of plant photosynthesis and depend solely on the radiometrically and geometrically corrected satellite measurements. Additionally, terrestrial vegetation dynamics is influenced by various environmental factors through complex, non-linear processes (Winkler et al., 2021; Kashyap et al., 2023a). Therefore, this study employs a suite of statistical techniques such as partial correlation, MLR, ML based RF, and Granger Causality for robust analysis. The climatology and varbility estimates in the study extends from 2000 to 2021 ensuring data quality remains intact and consistent across metrics. For the analysis of long-term decadal changes, we have selected the study period from 2000 to 2019, to avoid the anomalous vegetation response during the COVID-19 lockdown in 2020 and 2021, as those data may compromise the integrity of long-term data analysis (Kashyap et al., 2023b; Patel et al., 2024a). The working methodology is presented as a schematic (Fig. 1) and are described below.

2.2.1. Quantification of FPAR: linear scaling

Remotely-sensed FPAR is determined by the distribution of carbon to foliage and the regulation of photon flux for photosynthesis. This study employs Sellers' linear scaling technique to estimate FPAR from the MODIS-based NDVI data as per Equation (1):

$$\mathrm{FPAR} = \frac{[(\mathrm{NDVI} - \mathrm{NDVImin}) \times (\mathrm{FPARmax} - \mathrm{FPARmin})]}{(\mathrm{NDVImax} - \mathrm{NDVImin})} + \mathrm{FPARmin} \quad (1)$$

where, NDVI max and NDVI min are defined as 98th and 2nd percentiles, respectively, of maximum and minimum NDVI during its growth cycle. FPAR min and FPAR max are set equal to 0.01 and 0.95, which represents the extremes of potential canopy absorption of PAR (Sellers et al., 1996).

2.2.2. Spatio-temporal variability

This study computes the spatio-temporal patterns of FPAR, the seasonal, interannual and decadal variability and its key climatic drivers P, SM, T and DSRF. The four seasons considered are, winter (DJF: December, January and February), spring (MAM: March, April and May), summer (JJA: June, July and August) and autumn (SON: September, October and November). These are opposite in the southern hemisphere, where DJF is summer, MAM is autumn, JJA is winter and SON is spring. The change in different parameters during the period (2000–2019) is quantified in terms of percentage as per Equation (2):

$$\%\, X_{R-P} = \frac{X_R - X_P}{X_P} \times 100 \quad (2)$$

Here, X is any variable, R is the mean of X in recent decade (2010–2019) and P is the mean of X in the previous decade (2000–2009). To complement our analysis based on FPAR, the study also employs other proxies of global photosynthesis SIF and EVI.

2.2.3. Relation with drivers

To understand the relation of photosynthesis (FPAR) with key climate drivers (P, SM, T and DSRF) the study employs Pearson's correlation analysis. However, to examine the link between two variables, it is necessary to limit the impact of a third variable (covariate), and the partial correlation (PC) does it. Therefore, we employ PC analysis to examine the relationship between FPAR and its key climate drivers using Equation (3):

$$r_{xy.z} = \left(\frac{r_{xy} - r_{xz} . r_{yz}}{\sqrt{1 - r_{xz}^2} \cdot \sqrt{1 - r_{yz}^2}} \right) \quad (3)$$

Here, r_{xy} = correlation coefficient between variables x and y.

$r_{xy.z}$ = first order partial correlation between x and y by elimination of covariate (z) from the other variables (x and y).

2.2.4. Limiting factor and change in climatic control analysis

The limiting factor of photosynthesis is estimated by computing the mean of the partial correlation per pixel and then the climatic driver with the largest value is the limiting factor or the dominant climatic control of photosynthesis. To account for the change in the relation of the climatic driver with global photosynthesis, the study detects change in the coupling (correlation) between them over the two decades converted to percentage values using equation (4):

$$\%\, C_{R-P} = \frac{C_R - C_P}{C_P} \times 100 \quad (4)$$

Here, C is the coupling (correlation) between FPAR and a climate driver in recent decade (2010–2019) and P is C in the previous decade (2000–2009).

2.2.5. Causal relationship of climatic drivers

Correlation analysis simply states the relation between two parameters, which does not imply causation. Therefore, to determine the presence of causal relationships among FPAR and its key drivers, Granger causality test is performed. This examines a causal relationship between two variables based on the concepts of "cause" and "effect" with an option of time lag. Instead of relying on basic correlation between the effect(response) and the cause(driver), the Granger causality is grounded in the concept of predictability. A causal relationship is Granger if the ability to predict future responses of variable Y improves by incorporating all pertinent information, excluding the present value of variable X (Granger, 1969). To conduct a Granger causality test, a bivariate model is established between the time series (X and Y) that are stationary per equations (5) and (6):

$$Y_t = \sum_{i=1}^{n} a_i Y_{t-i} + \sum_{i=1}^{n} b_i X_{t-i} + \varepsilon_t \quad (5)$$

$$X_t = \sum_{i=1}^{n} c_i X_{t-i} + \sum_{i=1}^{n} d_i Y_{t-i} + \delta_t \quad (6)$$

Where, X and Y are two stationary time series; a, b, c and d are coefficients; and ε and δ are white noise. For X to Granger cause Y, $b_i \neq 0$; for Feedback between X and Y, $d_i \neq 0$.

The determination of stationarity for each time series is conducted through a non-parametric test known as the Augmented Dickey-Fuller (ADF) test. In the case of non-stationary time series, the difference function is employed in conjunction with vector autoregressive (VAR) models to create the adjusted time series. Subsequently, VAR models are constructed to find the relationship between the "response variable (Y)," specifically FPAR, and the "explanatory variable (X)," which represents the driver. The evaluation of the null hypothesis (Ho: X does not Granger cause Y) is conducted using the Granger causality test. The maximum allowable temporal lag between photosynthesis (FPAR) and climate drivers (P/SM/T/DSRF) is assigned as 3 months and its statistical significance is computed at the 95% confidence interval based on multiple iterations and previous studies for similar bioclimatic regions (Krich et al., 2020; Winkler et al., 2021; Kashyap et al., 2023a; Kashyap and Kuttippurath, 2024b). This particular lag is also selected to keep the causal effects of drivers on FPAR intact within the same season to avoid seasonal influence (Winkler et al., 2021; Kashyap and Kuttippurath, 2025a).

2.2.6. Contribution of drivers

ML has demonstrated significant efficacy in effectively managing multidimensional data, rendering it highly valuable for modelling systems characterised by intricate nonlinear structures. An ensemble model, RF, combines the boosting and regression trees to generate multiple individual tree models. These models are then combined to form a final optimised model. A variety of decision trees, each serving as a distinct method for data classification, guarantee that RF assesses each tree separately, choosing the one that accumulates the greatest number of votes as the prediction. The RF algorithm exhibits the capability to assign priority to input variables and address the constraints of conventional approaches by virtue of its ability to handle extensive datasets and its robustness against noise and overfitting (Breiman, 2001). The study employs the RF model in R Studio version 4.2.1 based on packages "randomForest" and "caret" to quantify the relative role of climate drivers (P, SM, T and DSRF) on the photosynthesis (FPAR) (Kashyap and Kuttippurath, 2024a; b). In the RF model, a total of 500 decision trees are generated with two variable splitting allowed in each tree. Here, 70 % of the data are split for training and 30 % for testing. The utilisation of hyperparameters in ML algorithms serves to augment the predictive capability and efficiency of the model. The RF model's default hyperparameters have been chosen for their exceptional efficacy and efficiency in executing the algorithm. The first step involves evaluating the specimen obtained directly from the bag in terms of its predictive accuracy. Afterwards, the stability of all other variables is maintained, while the values of the variables in the outlier sample are generated randomly. This study assesses the accuracy of forecast by calculating the average decrease in precision across all trees. The value indicator is further divided into various categories of outcomes. It can be deduced

that the stochastic rearrangement of a variable leads to the total elimination of its predictive capability. The importance of a variable is a measure of the degree to which its omission results in a decrease in precision as per Equation (7):

$$I_x = \sum_{k=1}^{K} \left[\frac{1}{K} \left(MSE_k{}^{xprem} - MSE_k \right) \right] \quad (7)$$

Here, I_x is the variable importance or contribution, K is the number of trees in the forest, $MSE_k{}^{xprem}$ is the estimation error with predictor x being eliminated for the *k*th decision tree, and MSE_k is the forecasting error with all predictors included in the *k*th decision tree. The RF model is run for the global vegetated land and three broad land cover types and four broad biomes.

The study also employs MLR to complement the contribution analysis with standard errors. MLR is a conventional statistical approach to model the relationship between the dependent variable i.e. response with independent variables i.e. predictors. This statistical approach enables multiple predictors to explain the variability in the response. Here, the study utilises climate drivers (P, SM, T and DSRF) to explain the variability in photosynthesis (FPAR) as per Equations (8) and (9):

$$Y = \beta_0 + \beta_1 X_1 + \beta_2 X_2 + \ldots + \beta_n X_n + \epsilon \quad (8)$$

$$FPAR = \beta_0 + \beta_P.P + \beta_{SM}.SM + \beta_T.T + \beta_{DSRF}.DSRF + \epsilon \quad (9)$$

Here, Y i.e. FPAR is the dependent variable or the response, X_1, X_2 to X_n i.e., P, SM, T and DSRF are independent variables or predictors, β_0 is the intercept (value of Y when all X = 0), β_1, β_2 to β_n are coefficients (effect of each predictor on Y) and ϵ is the uncertainty or error term (unexplained variation).

2.2.7. Sensitivity analysis

The study estimates the sensitivity of global photosynthesis to climatic drivers (P, SM, T and DSRF) as per Equation (10):

$$Sx = \frac{\Delta S}{\Delta X} \quad (10)$$

Here, Sx is the sensitivity of S to X, S is FPAR and X is its driver (P, SM, T and DSRF). The change in S (ΔS) and X (ΔX) are the percentage change in recent decade (2010–2019) from the previous decade (2000–2009). Furthermore, Sx is also normalised for better understanding and easier comparison.

2.2.8. Growth rate analysis

This concept is widely utilised in the domains of economics and finances to detect the intermediate change and the overall cumulative changes within a span of time. This method is also widely utilised in determining the variability in the atmospheric CO_2 concentration (Keenan et al., 2016). It is the difference in the value (X) in the current time period (t) from the previous time period (t-1) based on Equation (11):

$$X_{GR} = X_t - X_{t-1} \quad (11)$$

Here, X_{GR} is the growth rate (GR) in X (FPAR and its climate drivers) among time periods t and t-1. The study also estimates the cumulative growth rate (CGR, Equation (12)) and mean growth rate (MGR, Equation (13)) in FPAR and its climate drives for three time periods: (i) Study period (2000–2019); (ii) previous decade (P, 2000–2009) and (iii) recent decade (R, 2010–2019) (Kashyap and Kuttippurath, 2025b).

$$CGR = \sum_{i=1}^{n} X_{GR} \quad (12)$$

$$MGR = \left(\sum_{i=1}^{n} X_{GR} \right) \Big/ n \quad (13)$$

Here, n is the number of years of the study.

To understand the change in the MGR and CGR, the study also estimates the change in them among the decades as per equation (14):

$$\%\, CGR/MGR_{R-P} = \frac{CGR/MGR_R - CGR/MGR_P}{CGR/MGR_P} \times 100 \quad (14)$$

3. Results

3.1. Spatio-temporal variability in global photosynthesis

The regions with higher global photosynthetic activity (FPAR > 0.7) are tropical forests in Amazonia, Central Africa, Indonesia and the Western Ghats in India (Fig. 2a). Forests and grasses in temperate regions such as South America, western and eastern coasts of North America, Europe, China, and some regions in Russia also exhibit high photosynthesis (FPAR = 0.5–0.7). Grasses and croplands in temperate and cold regions in North America, India, eastern Europe, Russia, and north and western Australia show moderate photosynthesis (FPAR = 0.3–0.5). The arid regions such as western North America, southern South America, sub-Sahara, central Asia, northwest India, and western Australia depict low photosynthesis (FPAR = < 0.3) (Fig. 2a). We also utilise SIF and EVI, and find the spatial patterns of global photosynthesis are consistent across these metrics (Figs. S2 and S3). Seasonally (Fig. 2b), global photosynthesis peaks in JJA (FPAR = 0.63), followed by SON (FPAR = 0.55), and lower in MAM (FPAR = 0.49) and DJF (FPAR = 0.43). During DJF, the cold biomes such as western Europe and Russia show lower photosynthesis (FPAR < 0.3). However, temperate biomes in regions like India, sub-Sahara, southernmost Africa, western coast of South America and Australia exhibit moderate photosynthesis (FPAR = 0.3–0.5). Contrarily in MAM, these cold biomes exhibit higher photosynthesis (FPAR = 0.8–0.9) and temperate and arid biomes in North America, Africa and Australia show lower photosynthesis (FPAR <0.3). In JJA, most vegetated lands exhibit higher photosynthesis than other seasons. The cold biomes exhibit very high photosynthesis, and temperate and arid biomes also exhibit relatively higher photosynthesis. In SON, the spatial pattern is similar to that of JJA in most regions with relatively lower photosynthesis in the cold and temperate biomes. The hotspots of global photosynthesis in the pan-tropical forests exhibit high photosynthesis across the seasons (Fig. 2b). SIF and EVI also exhibit similar seasonality to FPAR for most regions in the study period (Figs. S2 and S3).

The annual global photosynthesis except for 2011–2013 (steep decline in P, SM and spike in DSRF, Fig. S4) has shown a positive anomaly. Seasonally, the negative anomaly peaked in JJA during 2002 and 2009, and the positive anomaly in SON during 2006, 2010 and 2012. Post-2012, high positive anomaly is exhibited in MAM and SON, that peaked during 2020 and 2021 (Fig. 2c). Cold biome contributes a very high positive anomaly in 2006 (large spike in T, Fig. S4c), which makes the overall positive anomaly. The negative anomalies during 2006–2009 and 2012 (rise in T, decline in P and SM, Fig. S4) are contributed by all biomes, peaked in the arid and cold biomes during 2009. Post-2012, the positive anomaly exhibited by all biomes peaked with the arid and cold biomes. Temperate biomes also exhibit a very sharp increase that peaked in 2020 (Fig. 2d). Grasses and forests contribute to negative anomalies in 2002, 2009 and 2012, and positive anomalies in 2006, 2010, 2016 and 2018. The croplands also exhibit a persistent positive anomaly in recent decade that peaked in 2020 (Fig. 2e). This is predominant with the noticeable positive anomalies in India (2020 and 2021) (Fig. 2f). The temperate croplands such as in India, western Europe, and eastern China exhibit an increase in photosynthesis due to extended growing periods during COVID-induced improvement in air quality during 2020 and 2021 (Kashyap et al., 2023b; Patel et al., 2024a).

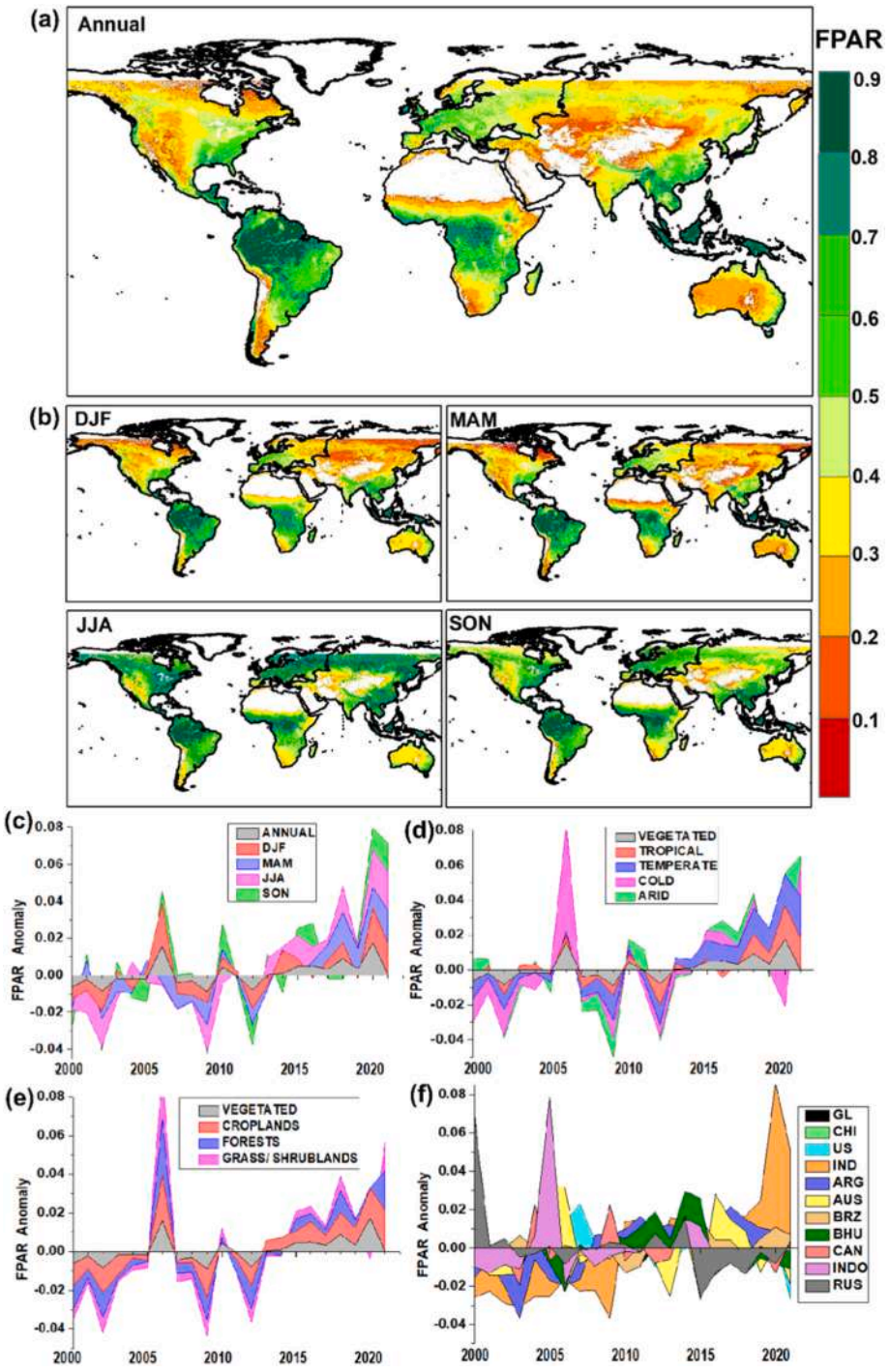

Fig. 2. Spatio-temporal variability in Global Photosynthesis (measured as Fraction of Photosynthetically Active Radiation, FPAR) during 2000–2021 for **(a)** Annual; **(b)** Seasonal: [(DJF: December, January and February), (MAM: March, April and May), (JJA: June, July and August), (SON: September, October and November)]; interannual anomaly for **(c)** a, b; **(d)** biomes; **(e)** land cover types; **(f)** global vegetation (GL) and countries as China (CHI), United States (US), India (IND), Argentina (ARG), Australia (AUS), Brazil (BRZ), Bhutan (BHU), Canada (CAN), Indonesia (INDO) and Russia (RUS).

3.2. Climate controls of global photosynthesis

To understand the role of drivers, the study examines the key climatic controls (P, SM, T and DSRF) of global photosynthesis (FPAR). Here, P exhibits a high positive control (> 0.6) in northern North America, sub-Sahara, Central Africa, and northern and eastern Asia. Contrarily, negative (< −0.2) relation is prevalent in western North America, Amazonia, western Europe and Indonesia (Fig. 3a). FPAR–SM relation exhibits a distinct pattern, where a strong positive influence (> 0.6) is observed in temperate and some tropical regions of southern North America, northwestern South America, Africa, India, China and eastern Australia. Contrarily, cold biomes and tropical forests in Amazonia and Indonesia have a negative control (< −0.2) (Fig. 3b). FPAR–T relationship is homogeneous across biomes, wherein strong positive (>0.8) control is observed in cold biomes in northern North America, Eurasia, China and some areas in central Asia. However, a strong negative (−0.4 to −0.8) control is found in southern North America, northeastern and southern South America, northern and central Africa,

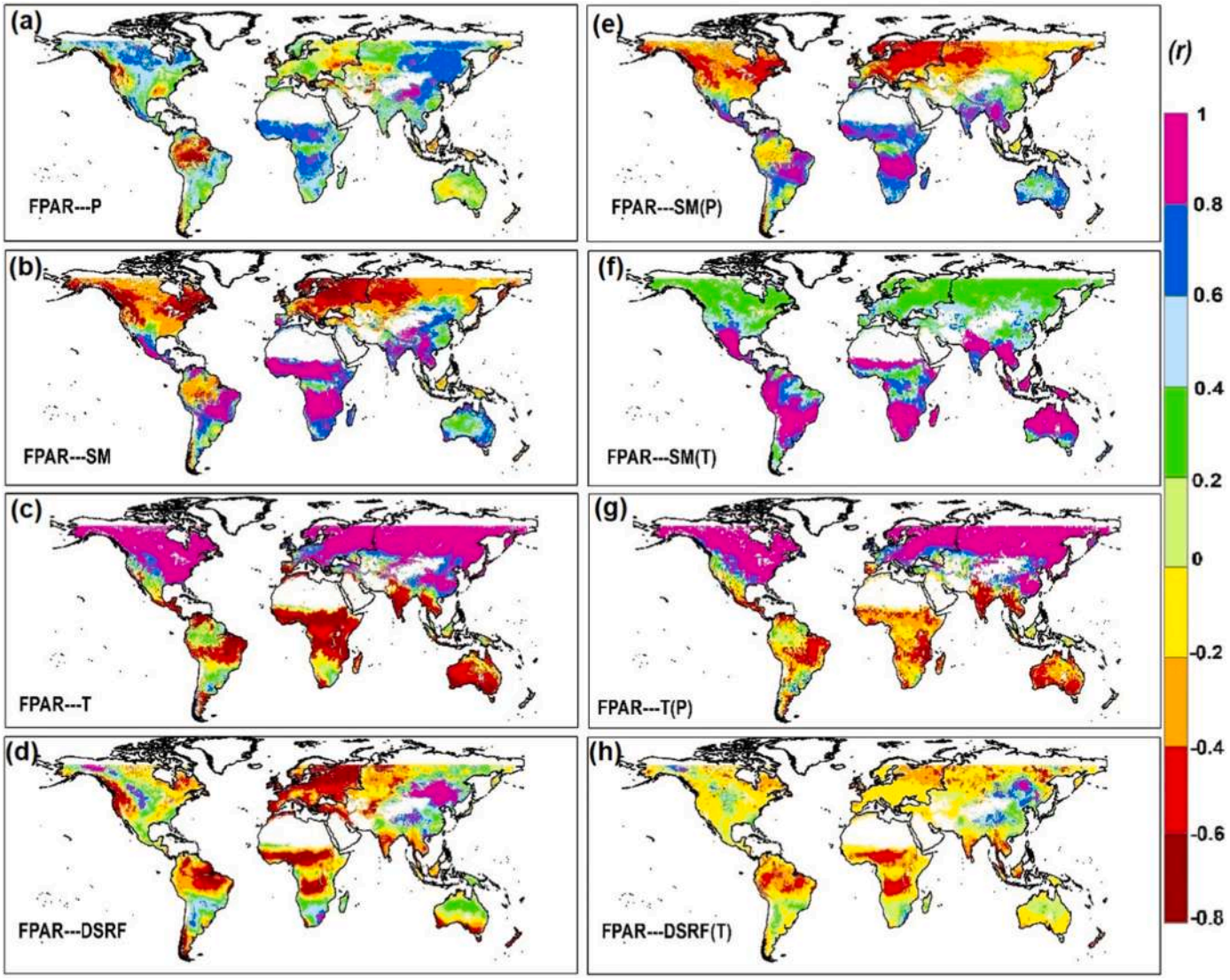

Fig. 3. Climatic controls such as **(a)** Precipitation (P, mm/day), **(b)** Soil Moisture (SM, kg/m^2), **(c)** Temperature (T,°C) and **(d)** Downward Shortwave Radiation Flux (DSRF, W/m^2) on global photosynthesis (measured as Fraction of Photosynthetically Active Radiation, FPAR) based on correlation (left) and partial correlation (right) FPAR with **(e)** SM limiting the influence of P, **(f)** T limiting the influence of P, **(g)** SM limiting the influence of T, **(h)** DSRF limiting the influence of T during 2000–2021.

India, some areas in southeast Asia, and Australia (Fig. 3c). DSRF has a peculiar relationship with photosynthesis, wherein it has a strong positive influence (0.4–0.8) in cold biomes in the northern latitudes and a positive control (<0.4) in temperate and arid regions such as southern North America, central South America, sub–Sahara, southern Africa, northwest India, eastern China and northern Australia. In contrast, some tropical and temperate regions like western North America, northern and southern South America, northern and central Africa, southeast Asia, and southern Australia show a negative influence of DSRF on FPAR (Fig. 3d).

Furthermore, for a vivid understanding of these relationships, limiting the influence of a climate driver (covariate), this study employs partial correlation (PC) analysis. First, PC of FPAR and SM with P as covariate is examined, and there is a strong positive relation (> 0.6) in temperate and arid biomes in southern North America, eastern South America, northern and central Africa, India, eastern southeast Asia and peripheries of Australia. Contrarily, cold biomes largely show a strong negative relation (<−0.2) as SM is largely the snow water equivalent there (Fig. 3e). The FPAR–SM relationship is very vivid when T is taken as covariate. The relation is stronger in tropical (0.72), arid (0.68) and temperate (0.65), but weaker in cold (0.32) biomes. The relation is stronger in croplands (0.56) than for grasses (0.54) and forests (0.52) (Fig. 3f and Fig. S5). Next, FPAR–T relationship with P as covariate is investigated, and there is a very strong positive (> 0.8) relation for cold biomes in eastern China, central North America, eastern Europe, and Eurasia. However, the southern hemisphere shows a negative relation, very strong (−0.4 to −0.8) in eastern South America, sub-Sahara, eastern Africa, India, eastern southeast Asia, and western and eastern Australia (Fig. 3g). The relation is a very strong positive for cold (0.94), weak positive (0.23) in temperate, negligible in arid and negative (−0.36) in tropical biomes. The relation is stronger in forests (0.44) than in grasses (0.34) and croplands (0.31) (Fig. S5). FPAR–DSRF PC with T as covariate relation is largely weak negative (−0.2) in cold and temperate biomes, and strong negative (<-0.2) in some regions such as tropical Amazonia, northern and Central Africa, southern India and Indonesia (Fig. 3h). The results from partial correlation analysis across the land cover types and biomes are presented in Supplementary material (Table S1).

3.3. Global photosynthesis: limiting factor, contribution and causal relations with drivers

The analysis finds, P as the limiting factor for photosynthesis in regions like central North America, Amazonia, western and southern South America, central Africa, some areas in central Asia, northwest and northeast India, Indonesia, and western and central Australia. However, SM limits photosynthesis in southern North America, eastern and central South America, sub–Sahara, eastern and southern Africa, northern India, eastern southeast Asia, and northern and eastern Australia. Moisture availability limits photosynthesis in tropics and temperate regions. However, T limits photosynthesis in cold biomes of North America, southern Europe, most of Eurasia, eastern Asia, southern India, eastern and central Africa, northeastern South America, and southeastern and southwestern Australia. Energy (DSRF) limits photosynthesis in northwestern and western North America, northern and central Africa, northern Europe, southeastern Eurasia, central China, Western Ghats in India, and southeastern and southwestern Australia (Fig. 4a).

The dominant drivers of photosynthesis across various biomes and land covers and their relative contribution are largely unknown. Therefore, this study employs the RF algorithm for the same and for global vegetated lands, and finds T (30.9 %) to be the dominant driver of photosynthesis followed by SM (26.1 %), P (23.4 %) and DSRF (19.5 %). T is the dominant driver for photosynthesis in forests (36.4 %) and croplands (35 %), but P (35.5 %) is the major control for grasses. Interestingly, T has limited influence on photosynthesis for grasses (19.7 %). SM has the highest influence on FPAR for grasses (26.5 %) followed by forests (24.8 %) and croplands (22.2 %). P has a higher influence on FPAR for croplands (23 %) than forests (18.2 %). P is the major control on FPAR in tropical (26.8 %), arid (27 %), T in temperate

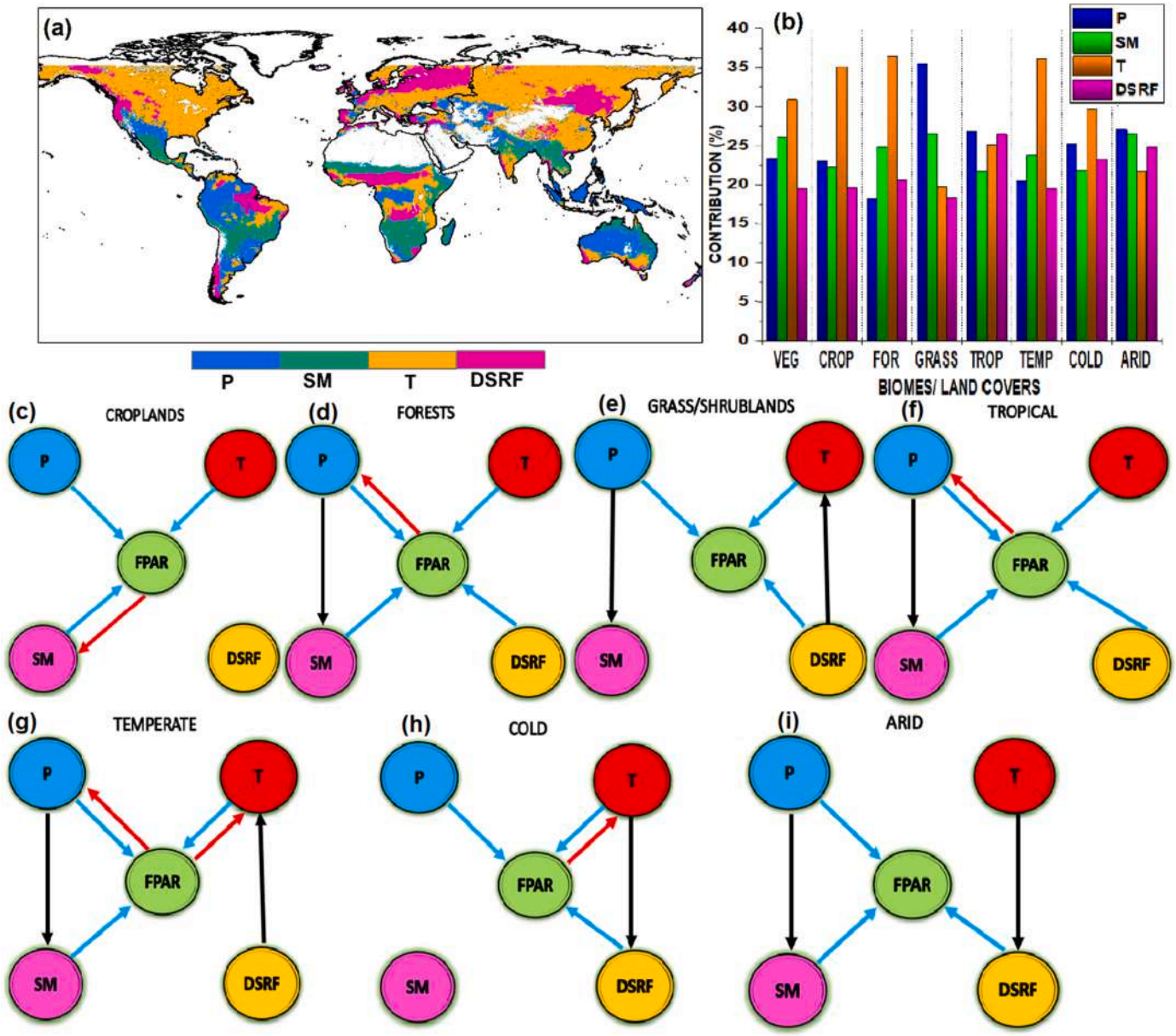

Fig. 4. Global Photosynthesis (measured as Fraction of Photosynthetically Active Radiation, FPAR): **(a)** Limiting climate factor [Precipitation (P), Soil Moisture (SM), Temperature (T) and Downward Shortwave Radiation Flux (DSRF)]; **(b)** Contribution of climate factors (P, SM, T and DSRF) percentage (%) to FPAR variability; **(c–i)** Causal links between FPAR and climate factors across land cover types: [net vegetated land (VEG), Croplands (CROP), Forests (FOR), other natural vegetation (GRASS)] and biomes: [Tropical (TROP), Temperate (T), Cold (COLD), Arid (ARD)] in 2000–2021 at lag of 0–3 months (blue line: positive impact, red line: negative impact) and no lag (black line).

(36.1 %), and cold (29.7 %) biomes. DSRF in tropical (26.4 %), SM in temperate (23.8 %) and arid (26.4 %), and P in cold (25.2 %) biomes also have key roles in photosynthesis (Fig. 4b). The climate drivers (P, SM, T, and DSRF) are ranked based on their relative control on photosynthesis (FPAR) across land cover types and biomes, and are provided in Supplementary material (Table S2). The RF model performs better for tropical ($R^2 = 0.79$) and temperate ($R^2 = 0.74$) than arid ($R^2 = 0.69$) and cold ($R^2 = 0.71$) biomes. Amongst the land cover types, RF has a higher accuracy for forests ($R^2 = 0.78$) and croplands ($R^2 = 0.75$) than grasses ($R^2 = 0.73$) (Table S3). The study also employs MLR to estimate the influence of climate factors on global photosynthesis across land cover types and biomes, and have found similar results as detailed in Supplementary material (Table S4–S11).

The relation and contribution of drivers is now deciphered, but their causal connection with photosynthesis is unknown. Henceforth, the study employs Granger Causality test with a maximum allowable temporal lag as 3 months for various land covers and biomes; significant at the 95% confidence interval. In croplands, SM, P, and T have direct causal links with FPAR, where SM has a feedback causal link (Fig. 4c). In forests, all drivers have causal link with FPAR, but P has a causal feedback relationship (Fig. 4d). Grasses have causal links between FPAR and P, T and DSRF (Fig. 4f). FPAR has causal connection with all drivers in tropical biome, where P has a feedback relationship (Fig. 4g). In temperate biome, there is a causal association of drivers with FPAR except DSRF. DSRF has a causal link with T that has a direct causal connection with FPAR. Here, both P and T have feedback relationships with FPAR (Fig. 4h). In cold biome, all drivers except SM have causal links with FPAR, and T has a feedback relationship with FPAR (Fig. 4i). In arid biome, except T, all drivers have direct casual links with FPAR, and T influences FPAR through DSRF (Fig. 4j).

3.4. Changes in relation of climatic drivers with photosynthesis

The study investigates the change in the relation (correlation) of climatic drivers with photosynthesis (FPAR) in recent decade from the previous decade (Fig. 5a). The FPAR–P coupling has strengthened in northern latitudes of North America and Eurasia, sub-Sahara, central and southern most Africa, southwest and northeast Europe, India and Australia. However, the FPAR–P coupling has weakened in coastal North America, western, central and southern South America, eastern Europe, western and northern Eurasia, eastern China, and peripheries of Australia. FPAR–P coupling has strengthened for all land cover types with a higher increase in forests (8 %) than in grasses (1.7 %) and croplands (1.6 %). The relationship has strengthened for temperate (3 %), tropical (1.2 %) and arid (0.6 %), but declined for cold (−3.6 %) biomes (Fig. 5b). The FPAR–SM coupling has increased in northern and central North America, northwest and southern South America, sub-Sahara, central and southern Africa, eastern and western Europe, eastern Asia, India and Australia. Contrarily, FPAR–SM coupling has declined in eastern and southern North America, central South America, southern Africa, central and northeastern Europe, eastern and western Eurasia and western Australia (Fig. 5a). The FPAR–SM relationship has substantially tightened for croplands (20.9 %), but declined for forests (−6.7 %) and grasses (−3 %). For biomes, it has increased for all, higher in temperate (3.3 %) and arid (2.2 %) than tropical (1 %) and cold (0.2 %) regions (Fig. 5b).

The FPAR–T coupling has strengthened marginally in northern North America, eastern Europe, eastern Asia, India, northwestern Australia, northern and peripheries in Africa, and northeastern and central South America. However, FPAR–T coupling is greatly weakened in western North America, northwestern, west central and southern South America, central and southern Africa, eastern Europe, northwest India, eastern southeast Asia, and central and eastern Australia (Fig. 5a). FPAR–T relation has weakened for all land cover types, and is larger for forests (−8 %) and croplands (−7.6 %) than grasses (−2 %). Temperate (−15.7 %) and arid (−5.6 %) biomes exhibit substantial weakening in FPAR–T relation, where cold (−1.2 %) and tropical (7.5 %) biomes exhibit marginal decline and marked strengthening, respectively (Fig. 5b). The FPAR–DSRF relationship has strengthened in most regions like central and eastern North America, northern, eastern and southern South America, central Africa, central and southern Europe, central Asia, eastern Asia, India, and northern and central Australia. Conversely, this relation has weakened in northern North America, central and eastern Eurasia, and Southeast Asia such as Indonesia, southern Australia,

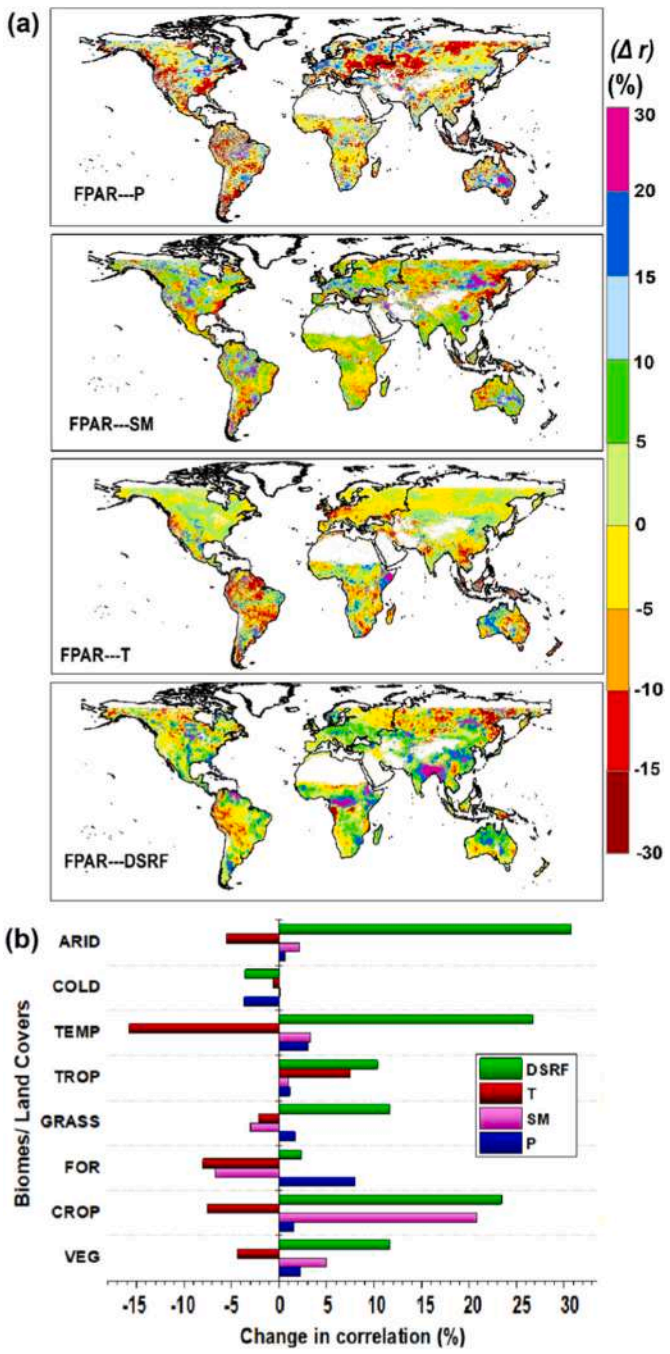

Fig. 5. (a) Change in the relation of climate drivers: [Precipitation (P, mm/day), Soil Moisture (SM, kg/m^2), Temperature (T, °C) and Downward Shortwave Radiation Flux (DSRF, W/m^2)] with photosynthesis (Fraction of Photosynthetically Active Radiation, FPAR) in percentage (%) during recent decade (2010–2019) from previous decade (2000–2009); **(b)** (a) for land cover types: net vegetated land (VEG), Croplands (CROP), Forests (FOR), other natural vegetation (GRASS) and biomes: Tropical (TROP), Temperate (T), Cold (COLD), Arid (ARID)].

southern Africa, and northwestern and central South America (Fig. 5a). FPAR–DSRF coupling has strengthened for all land cover types, higher for croplands (23.4 %) than grasses (11.7 %) and forests (2.3 %). The relationship has strengthened substantially for arid (30.7 %), temperate (26.8 %), and tropical (10.3 %) biomes, but weakened for the cold (−3.5 %) (Fig. 5b).

3.5. Change in global photosynthesis

There are changes in the relation of global photosynthesis with its drivers, and therefore, the study next explores the response of terrestrial ecosystems to it. There are substantial changes, wherein increased photosynthesis (greening) is intense (+FPAR, 10–20 %) in northwest India and northeastern China, moderate (2.5–7.5 %) in northern and southern North America, sub-Sahara, northern and western Europe, eastern Asia, India, China and southeastern Australia (Fig. 6a). Marginal greening (< 2.5 %) is found in Amazonia, central Africa, and Indonesia. The decrease in photosynthesis (i.e. browning) is severe (FPAR, −5 to −20 %) in northwestern North America, northeastern South America, southeastern Europe and western Eurasia. Moderate and marginal browning (i.e. FPAR, 0 to −5 %) is observed in central North America, central and southern South America, eastern and southern Africa, and western and northern Australia (Fig. 6a).

Seasonally (Fig. 6b), in DJF, greening is predominant in eastern and southern South America, southern Africa, central Asia, India, China, Southeast Asia and southeastern Australia. Contrarily, browning is prevalent in the northern latitudes of North America, Europe and Eurasia and some small areas in central North America, northeastern South America, eastern Africa, and northern and western Australia. In MAM, greening is found in northwestern North America, eastern and southern Europe, northern Eurasia, eastern Asia, China, India and eastern Australia. Browning is prevalent in central North America, eastern

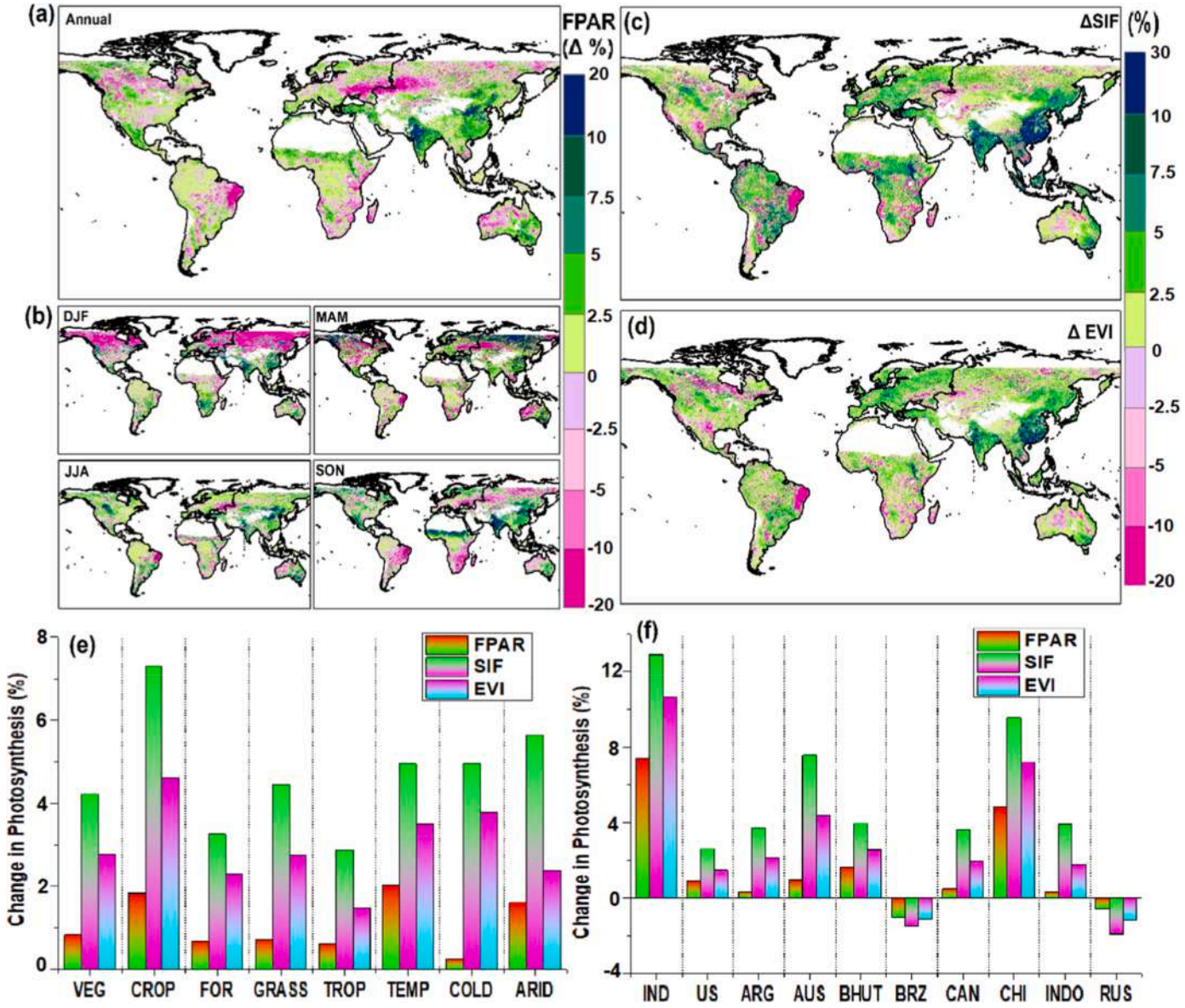

Fig. 6. Change (%) in Global Photosynthesis for: **(a)** Fraction of Photosynthetically Active Radiation, (FPAR), Annual; **(b)** FPAR, Seasonal: [(DJF: December, January and February), (MAM: March, April and May), (JJA: June, July and August), (SON: September, October and November)]; **(c)** Solar-Induced chlorophyll Fluorescence (SIF), Annual; **(d)** Enhanced Vegetation Index (EVI), Annual; **(e)** FPAR, SIF and EVI for land cover types: [net vegetated land (VEG), Croplands (CROP), Forests (FOR), other natural vegetation (GRASS)] and biomes: [Tropical (TROP), Temperate (T), Cold (COLD), Arid (ARID)]; **(f)** FPAR, SIF, EVI for countries: [India (IND), United States (US), Argentina (ARG), Australia (AUS), Bhutan (BHU), Brazil (BRZ), Canada (CAN), China (CHI), Indonesia (INDO) and Russia (RUS)] during recent decade (2010–2019) from the previous decade (2000–2009).

Europe, western Eurasia, western Australia, southern Africa and north-eastern South America. In JJA, greening is evident in the majority of lands, and it is intense in central east North America, northwest India, northeast China and eastern Australia. However, marginal browning is found in northeastern South America, peripheries of Africa, and western Australia. In SON, greening is intense in northern and southern North America, northern Europe, eastern Asia, China, India sub-Sahara and eastern Australia. Browning is evident in southern Europe, Eurasia, eastern and central South America, eastern and southern Africa, and western and northern Australia (Fig. 6b). Overall, except DJF (−3.2 %),

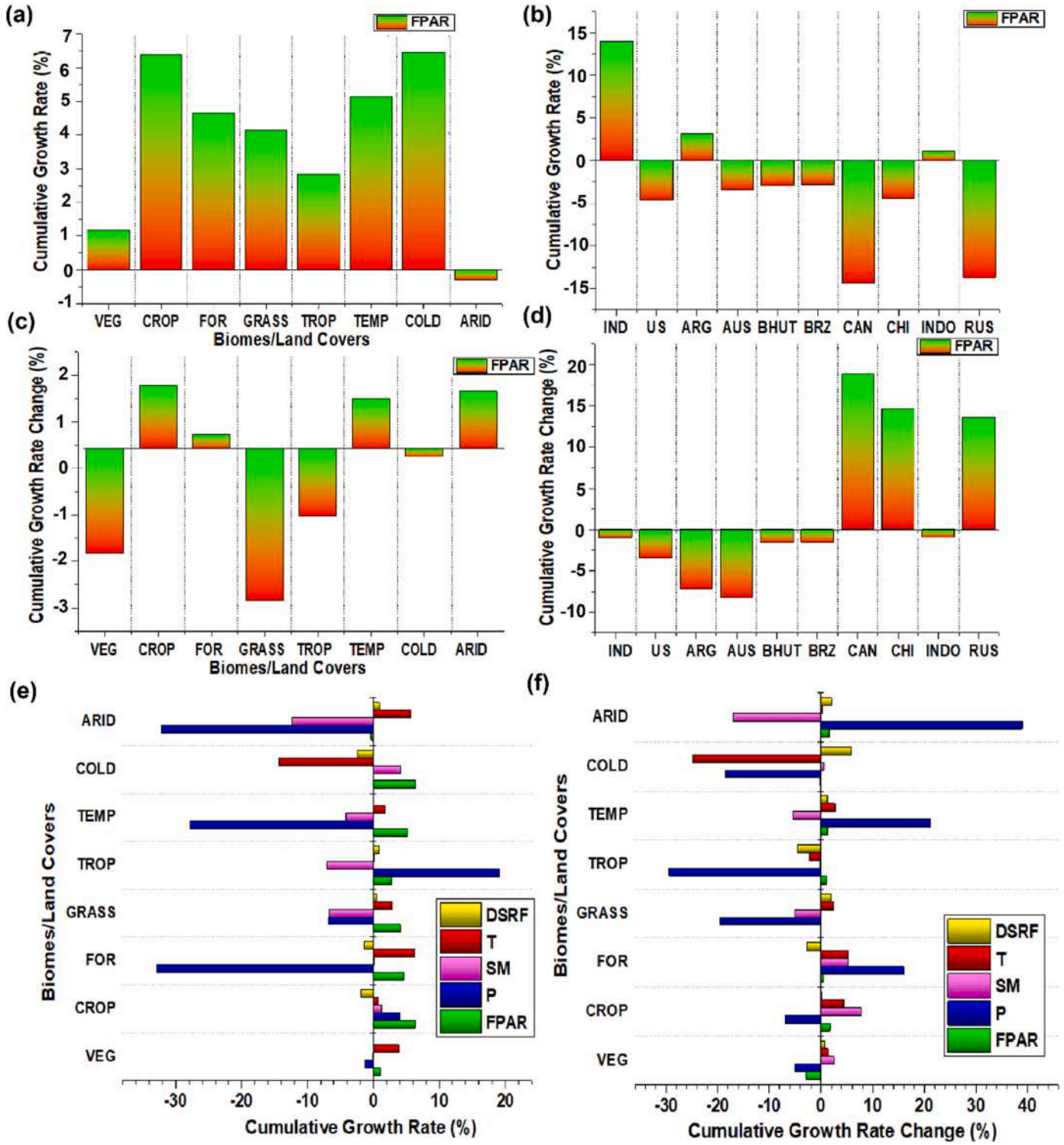

Fig. 7. Cumulative Growth Rate (CGR) of Fraction of Photosynthetically Active Radiation (FPAR) in percentage (%) for: **(a)** land cover types: net vegetated land (VEG), Croplands (CROP), Forests (FOR), other natural vegetation (GRASS)] and biomes: Tropical (TROP), Temperate (T), Cold (COLD), Arid (ARID); **(b)** countries: India (IND), United States (US), Argentina (ARG), Australia (AUS), Bhutan (BHU), Brazil (BRZ), Canada (CAN), China (CHI), Indonesia (INDO) and Russia (RUS) during 2000–2019; **(c)** change (%) in CGR of FPAR for (a); **(d)** change in CGR of FPAR for (b); **(e)** CGR for climate drivers: [(Precipitation (P), Soil Moisture (SM), Temperature (T) and Downward Shortwave Radiation Flux (DSRF)]; **(f)** change (%) in CGR for (e) during recent decade (2010–2019) from the previous decade (2000–2009).

MAM (2.18 %), JJA (1.63) and SON (0.67 %) exhibit greening.

The study also utilises the SIF (Fig. 6c) and EVI (Fig. 6d) data to find the changes in global photosynthesis. The spatial patterns of changes are largely consistent across the photosynthetic metrics, with variations in their magnitudes, but the trends (greening/browning) remain consistent. For instance, SIF exhibits more intense greening than FPAR and EVI. The change in EVI exhibits its magnitude between those of SIF (larger) and FPAR (smaller). All three photosynthetic proxies; SIF (4.2 %), EVI (2.8 %) and FPAR (0.8 %) show "Greening Earth" in recent decade (2010–2019) from the previous decade (2000–2009). Croplands exhibit more intense greening (1.8 % FPAR, 7.3 % SIF and 4.6 % EVI) than forests (0.68 % FPAR, 3.2 % SIF and 2.3 % EVI) and grasses (0.73 % FPAR, 4.5 % SIF and 2.8 % EVI). Temperate (2 % FPAR, 5 % SIF and 3.5 % EVI) and arid (1.6 % FPAR, 5.7 % SIF and 2.4 % EVI) biomes show more greening than cold (0.25 % FPAR, 5 % SIF and 3.8 % EVI) and tropical (0.6 % FPAR, 2.9 % SIF and 1.5 % EVI) biomes (Fig. 6e). Amongst the selected ten countries, except for Brazil (−1 % FPAR, −1.5 % SIF and −1.1 EVI) and Russia (−0.6 % FPAR, −1.9 % SIF and −1.2 EVI), others are greening. India exhibits most intense greening (7.4 % FPAR, 13 % SIF and 10.7 EVI) followed by China (4.8 % FPAR, 9.6 % SIF and 7.2 % EVI), Australia (1 % FPAR, 7.6 % SIF and 4.4 % EVI), Bhutan (1.6 % FPAR, 3.9 % FPAR and 2.6 % EVI) and the US (0.9 % FPAR, 2.6 % SIF and 1.5 % EVI) (Fig. 6f).

3.6. Growth rate of global photosynthesis and its climate drivers

To better comprehend the changes in global photosynthesis with climate change, this study computes the growth rates (GR) of FPAR and climate factors. The positive cumulative GR (CGR, 1.16 %) in FPAR during recent two decades affirms "Greening Earth". Croplands exhibit faster greening (CGR, 6.4 %; MGR, 0.3 %/yr) than forests (CGR, 4.64 %; MGR, 0.22 %/yr) and grasses (CGR, 4.14 %; MGR, 0.19 %/yr). Enhanced moisture availability (P, 4 % and SM, 1.3 % CGR) and relatively lower warming (T, 0.76 % CGR) facilitate rapid cropland greening. Contrarily, forests exhibit a large decline in P (−32.9 % CGR) accompanied by intense warming (T, 6.3 % CGR) and reduction in energy/radiation (DSRF, −1.4 % CGR). Cold (6.5 % CGR), and temperate (5.1 % CGR) biomes exhibit larger greening than tropical (2.8 % CGR) and arid (−0.3 % CGR) biomes. Most countries exhibit a negative photosynthetic GR, higher in Canada (−14.4 % CGR), Russia (−13.8 % CGR), the US (−4.7 % CGR) and China (−4.4 % CGR). India exhibits a massive positive photosynthetic GR (14 % CGR) followed by Argentina (3.2 % CGR) (Fig. 7 a, b, e).

For further insights, the study also estimates the changes in GR between the decades and find a slowdown of the global greening (−0.27 %/yr MGR, −2.8 % CGR). Both croplands (1.7 % CGR) and forests (0.4 % CGR) exhibit greening intensification; but grasses show a decline (−4.1 % CGR). Reduced moisture availability (P, −19.6 % and SM, −5.1 % CGR) accompanied by increased radiation (DSRF, 1.9 % CGR) in these natural vegetations led to a decline in greening. Interestingly, croplands exhibit a reduction in P (−6.9 % CGR), but enhanced SM (7.8 % CGR) highlights the influence of irrigation on greening. Arid (1.6 % CGR) and temperate (1.4 % CGR) biomes exhibit enhanced greening, whereas tropical (−1.8 % CGR) and cold (−0.2 % CGR) biomes exhibit slowdown/reversal of greening. The tropical biome experiences declined water availability (P, −29.5 % CGR) and radiation (DSRF, −4.6 % CGR); whereas cold biome exhibits cooling (T, −24.9 % CGR) and reduced water availability (P, −18.5 % CGR) that slowdown greening. P exhibits a substantial increase (39 % CGR) in the arid biome that boosts photosynthesis. Most countries exhibit a decline in photosynthetic GR such as Australia (−8.3 % CGR), Argentina (−7.2 % CGR), the US (−3.4 % CGR) and India (−1 % CGR). However, Canada (18.8 % CGR), China (14.6 % CGR), Russia (13.7 % CGR) and some other countries show a substantial increase in the photosynthesis GR (Fig. 7 c, d, f).

3.7. Mechanisms of changes in global photosynthesis: sensitivity to climatic drivers

Sensitivity analysis illustrates the change in global photosynthesis corresponding to the change in climate drivers, where the change in both (FPAR and climate driver) is in the same direction (positive) and opposite direction (negative) for various land covers, biomes (Fig. S6) and uncertainties (Table S12). Here, P exhibits an increase in various land covers, higher in grasslands (1.14 %) and croplands (0.94 %) than forests (0.23 %). Arid (2.8 %) and temperate (0.44 %) biomes show showering, but tropical (−1.1 %) and cold (−0.24 %) biomes exhibit P-drying (Fig. 8a and b). FPAR has a positive sensitivity to P in sub-Sahara,

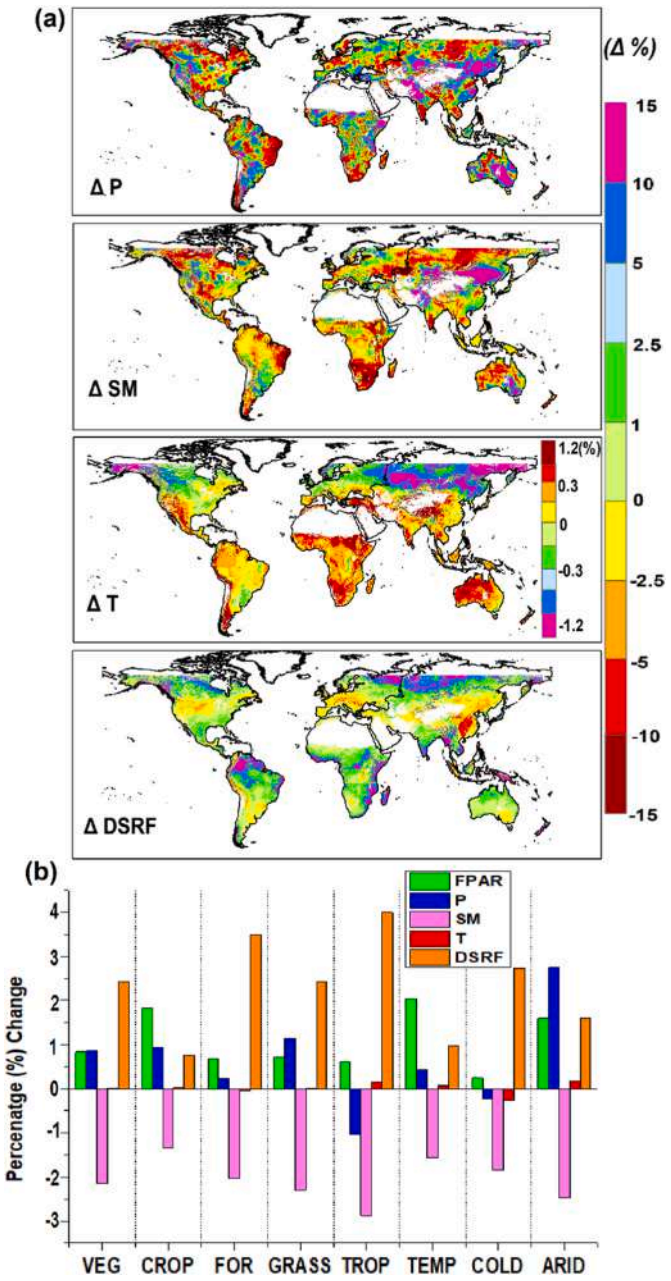

Fig. 8. **(a)** Change in climate factors: [Precipitation (P, mm/day), Soil Moisture (SM, kg/m^2), Temperature (T, °C) and Downward Shortwave Radiation Flux (DSRF, W/m^2)] in percentage (%) during recent decade (2010–2019) from the previous decade (2000–2009); **(b)** (a) for land cover types: [net vegetated land (VEG), Croplands (CROP), Forests (FOR), other natural vegetation (GRASS)] and biomes: [Tropical (TROP), Temperate (T), Cold (COLD), Arid (ARID)].

northwest India, southeastern Eurasia, eastern China, Indonesia and eastern Australia, where showering-induced greening is prevalent. Central North America, northeastern South America, southern Africa and westernmost Europe also exhibit positive sensitivity, wherein P-drying driven browning is prevalent. However, FPAR has a high negative sensitivity to P in northwest North America, western Eurasia, eastern and southern India, and northeastern China, wherein greening is observed, although P-drying is observed there (Fig. 8a, b, 9a). SM-drying is prevalent in all land cover types and biomes, most pronounced in grasses (−2.3 %) and tropical (−2.9 %) biomes (Fig. 8d). Similarly, for SM, FPAR has a positive sensitivity in central South America, sub-Sahara, northwest India and eastern China, wherein moisture-induced greening is observed. Central North America, northeastern South America, southernmost Africa, western Eurasia and western Australia also exhibit a positive sensitivity, but dryness stress driven browning is dominant there. Eastern and southern India, eastern Asia, and Indonesia show a negative sensitivity as they exhibit marginal greening despite dryness stress (Fig. 8a and 9a).

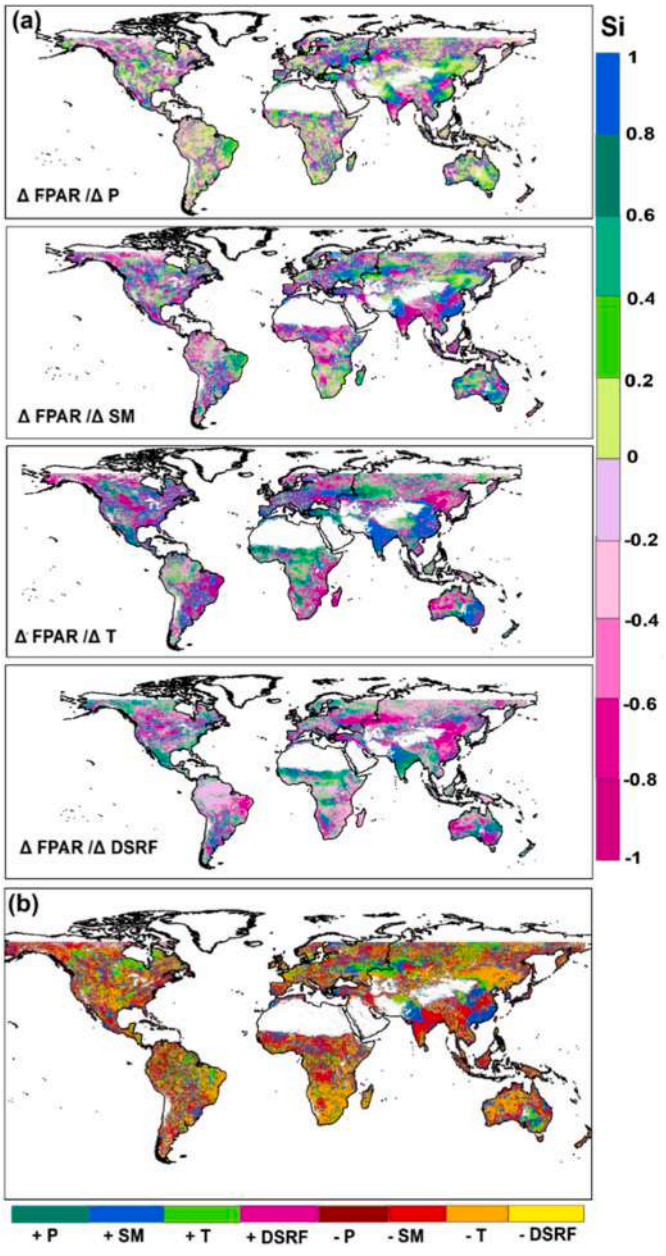

Fig. 9. **(a)** Sensitivity index (Si) of Global Photosynthesis to climate factors i.e. change in Fraction of Photosynthetically Active Radiation (ΔFPAR) to change in climate factor ((Precipitation (ΔP), Soil Moisture (ΔSM), Temperature (ΔT) and Downward Shortwave Radiation Flux (ΔDSRF)) during recent decade (2010–2019) from previous decade (2000–2009) scaled to (−1 to +1); **(b)** climate driven changes of Global Photosynthesis during the period 2000–2019. Here "+/−" represents increase/decrease in recent decade from previous decade.

In the climate change context, warming is intense in arid (0.17 %) and tropical (0.16 %) biomes, and cooling (−0.26 %) in cold biomes (Fig. 8d). FPAR has a positive sensitivity to T in India, eastern and southern China, Indonesia, central Africa and eastern Australia where greening is observed, despite the warming. Northeastern Eurasia exhibits a positive sensitivity as cooling-induced browning is prevalent in these cold regions. Contrarily, FPAR exhibits negative sensitivity to T in northeast South America, eastern and southern Africa and western Australia as warming-induced browning is observed there. Some areas in northern latitudes in North America, Europe, and eastern Eurasia show a negative sensitivity as greening with cooling is observed there (Fig. 9a). Energy/radiation (DSRF) has increased across land covers and biomes with its high enhancement in tropical (4 %) and cold (2.7 %) biomes; forests (3.5 %) and grasses (2.4 %) (Fig. 8d). FPAR has a positive sensitivity to DSRF in northern and southern North America, western Europe, India, eastern Australia and sub-Sahara, greening is observed with an increase in DSRF there. Contrarily, FPAR has a negative sensitivity to DSRF in northeastern South America, eastern Europe, western Eurasia and western Australia wherein with an increase in DSRF browning is exhibited. Also, central North America, eastern Europe and northeastern China exhibit greening with a decrease in DSRF (Fig. 9a).

4. Discussion

4.1. Shifting climatic controls of global photosynthesis

In recent decades, the global climate has experienced substantial changes like warming hiatus and enhanced warming (Trenberth, 2015), drying (Feng et al., 2021), brightening and dimming (Wild, 2016) and strengthening of land-atmosphere feedbacks (Humphrey et al., 2021). There is a need for a comprehensive study on the spatio-temporal evolution of global photosynthesis and its attribution to changing climate across various seasons, biomes and land covers. Here, the study finds that moisture availability (P, SM) is the key climatic control in tropical and arid, but warmth (T) in temperate and cold biomes. For croplands and forests, T is the predominant driver, but P is the key driver for grasses; consistent with Zhang et al. (2021) and Higgins et al. (2023). The study finds T to be the major control of photosynthetic activity for all vegetated lands, followed by SM. T remains the key climatic control of global photosynthesis, but the strength of the relation has declined recently, as also found by Zhang et al. (2021) and Higgins et al. (2023). This is due to the saturation of boreal greening to warming (Piao et al., 2017), warming hiatus in the tropical and temperate biomes (Trenberth, 2015), and enhanced drying (Feng et al., 2021). Croplands (SM), forests (P) and gasses (DSRF) show increasing influence of other drivers on global photosynthesis. For arid regions, water availability (P and SM) has enhanced and strengthened the control on photosynthesis (Patel et al., 2024b, Kashyap et al., 2025a). A recent ground-based study (Higgins et al., 2023) found SM to be the dominant driver of vegetation growth in the warm and dry regions, but cool and wet regions exhibited a combination of drivers dominated by T. The control of water availability (P and SM) and radiation (DSRF) has increased over global photosynthesis. Also, there is a shift in control from radiation to water limitation in ecosystems where an increase in DSRF and a decrease in SM are observed (Denissen et al., 2022). Thus, the climate control on global photosynthesis has shifted from warmth and energy to water availability in recent decades. This is due to the saturation of vegetation to positive influence of warming and enhanced dryness stress that override the dominance of other limiting factors.

4.2. Greening Earth

The study employs three proxies of photosynthesis FPAR, EVI and SIF, and their long-term change is largely consistent across all three metrics with variable magnitudes. The study finds greening in all land covers and biomes, which is highest in temperate and arid biomes and croplands. India and China exhibit the largest greening, followed by Australia, but Brazil and Russia exhibit browning, as also found by Chen et al. (2019). Greening is strongest in MAM and JJA. The moisture-induced greening regions are the central North America, sub-Sahara, northwestern India, northeastern Asia and eastern Australia (Fig. 9b). Although these are largely moisture-limited regions, where enhanced atmospheric moisture drives vegetation growth through improved P and SM (Patel et al., 2024b). Warming-induced greening is exhibited by northern high latitudes in North America and eastern Europe. The warming in these cold regions enhances the plant metabolism, extends the growing season and promotes the expansion of shrubs (Piao et al., 2017). However, drying-induced browning is observed in northeastern, northern and southern South America, central and southern Africa and western Australia (Feng et al., 2021). These regions are also predominantly warming, and thus warming-induced drying drives browning in these regions (Gampe et al., 2021). The reduced canopy photosynthesis during drying is further intensified by warming-induced heat stress (Huang et al., 2019). The persistent warming and drying will have a detrimental effect on tropical ecosystems for carbon sequestration (Tao et al., 2022; Liu et al., 2023). Changes in DSRF alone do not induce substantial changes in photosynthesis, but it modifies T, and thus, enhanced DSRF drives greening in northern Eurasia (Fig. 9b). SIF, particularly GOSIF is more closely related to photosynthesis and carbon sinks than MODIS based NDVI and EVI (Shekhar et al., 2022). The study finds that SIF exhibits a more intense greening than NDVI and EVI in the pan-tropical forests, provided the saturation of NDVI and EVI in dense canopy such as tropical forests. In recent years, there has been enhancement in greening heterogeneity (Myers-Smith et al., 2020; Qiu et al., 2022) and amplified browning (Pan et al., 2018; Liu et al., 2023).

4.3. Slowdown of global greening

The positive growth rate (GR) of global photosynthesis in recent two decades (FPAR, 1.2 % CGR) affirms global greening. However, there is a slowdown/reversal of greening in recent decade (FPAR, −2.8 %, CGR), predominantly for grasses and tropical biome due to dryness stress. There is a decline in the global greening rate, with the emergence and expansion of browning regions (Pan et al., 2018; Winkler et al., 2021). Greening is evident in areas of sparse canopies such as arid biomes, croplands and temperate forests. Contrarily, the areas of dense canopies such as the pan-tropical forests, and Eurasian tundra exhibit browning, owing to warming and drying (Feng et al., 2021; Qiu et al., 2022). There is also regime shift in the cold, arid and tropical regions in recent decades (Cooper et al., 2020; Southworth et al., 2023). Two of the largest contributors to global greening (Chen et al., 2019) show contrasting patterns. India has a very high positive GR and China has a negative GR in recent two decades, consistent with Chen et al. (2024). However, greening is largely intensified in China, but it has slowed down in India during recent decade. Greening in China is predominantly due to large scale afforestation (Chen et al., 2019; Tong et al., 2020), but largely irrigation-induced agricultural intensification in India (Chen et al., 2019; Kuttippurath and Kashyap, 2023). In previous decades, greening in China may have reached saturation, but recent afforestation and modernisation of agriculture have intensified the greening there (Tong et al., 2020). On the contrary, increasing moisture stress constrains the greening in India during recent decade (Kashyap and Kuttippurath, 2024a; b). Additionally, growing ecological implications of moisture stress during the moisture-rich summer monsoons drives regional browning in India (Kashyap et al., 2025b). In the warming world, the atmospheric evaporative demand is enhanced and leads to closer of stomata to preserve water, which would limit photosynthesis and CO_2 capture. Henceforth the global photosynthesis is largely becoming water constrained in the warming world. This leads to SM drying along with enhanced evaporative demands of land and atmosphere (Liu et al., 2023; Song et al., 2024). Thus, there is a slowdown/reversal of global greening due to the shift in climatic control to water availability and enhanced dryness stress.

4.4. Non-climatic drivers of vegetation dynamics

Apart from climatic drivers, regional changes in vegetation can be influenced by non-climatic drivers of CFE, land management, afforestation, or deforestation (Chen et al., 2019; Tagesson et al., 2020). The impacts (beneficial or detrimental) of these factors, largely remain stable over a long period in a specific region (Zhu et al., 2016; Piao et al., 2020). For instance, browning due to: (i) deforestation and forest degradation in tropical forests of Amazon (Qin et al., 2021) and central Africa (Zhao et al., 2024), and (ii) land clearance in Australia (Heagney et al., 2021), and greening due to: (i) afforestation in China (Tong et al., 2020), (ii) reforestation and woody encroachment in North America and Europe (Buitenwerf et al., 2018; Bueso et al., 2023), (iii) plantations growth in southeast Asia (Guillaume et al., 2018; Chen et al., 2019), and (iii) improved land management in India (Chen et al., 2019; Kuttippurath and Kashyap, 2023) have already been reported. These factors can intensify the magnitude of the change in global photosynthesis (greening/browning), but can rarely alter the direction of change (greening to browning or vice versa). For instance, warmer and drier climate generally provoke and intensify disturbances such as wildfires (Abatzoglou and Williams, 2016) and insect outbreaks (Deutsch et al., 2018). These effects can be found as indirect consequences of climate change that cause browning. CFE can facilitate greening by amplifying the influence of climate factors. CFE can partially counteract browning caused by climate change, but the overall vegetation dynamics is determined by the climate as CFE can never cause browning on its own (Zhang et al., 2021; Keenan et al., 2023). However, only temperate forests and cool grasslands exhibit CFE with no persistent impact on other biomes (Winkler et al., 2021). Additionally, CFE has weakened due to the growing limitations of foliar nutrient concentrations and water availability (Wang et al., 2020). Also, in the warming scenario, the radiative effects of CO_2 may counter the fertilisation effects and saturation of plants to CFE (Shi et al., 2021) due to enhanced land sinks (Keenan et al., 2016, 2023). Therefore, the impact of CFE is restricted, and possibly overshadowed by climatic factors (Zhang et al., 2021; Higgins et al., 2023).

4.5. Future of global photosynthesis

The majority of CMIP6 models predict a consistent greening pattern throughout the 21st century (Zhao et al., 2020). Additionally. Multiple ML model ensemble also suggests intensified greening in the 21st century, predominant in the northern hemisphere (Zhang et al., 2025). The study finds that greening continues in the future for most global regions until the end of the century (P3, 2090–2100), from the historical period (P1, 2015–2019), which is stronger in the cold (45.9 %) and arid (31.6 %) biomes, forests (28.5 %) and grasses (25.9 %). However, browning is projected in the Amazonia and much of northern South America (Fig. 10a–e). The ensemble uncertainty range in LAI for the global vegetation derived from CMIP6 models is in the Supplementary material (Table S13). For a better understanding, this study splits the periods and examine the changes in global photosynthesis during the mid-century (P2, 2040–2050) from the historical period (P1). Generally, there is widespread greening (6.4 %), more intense in the cold (16.4 %) and arid (9.2 %) biomes, forests (8.8 %) and grasses (7 %), as found before. Browning is largely observed in the southern hemisphere, and is intense in central and southern India (Fig. 10b–e). This study also investigates

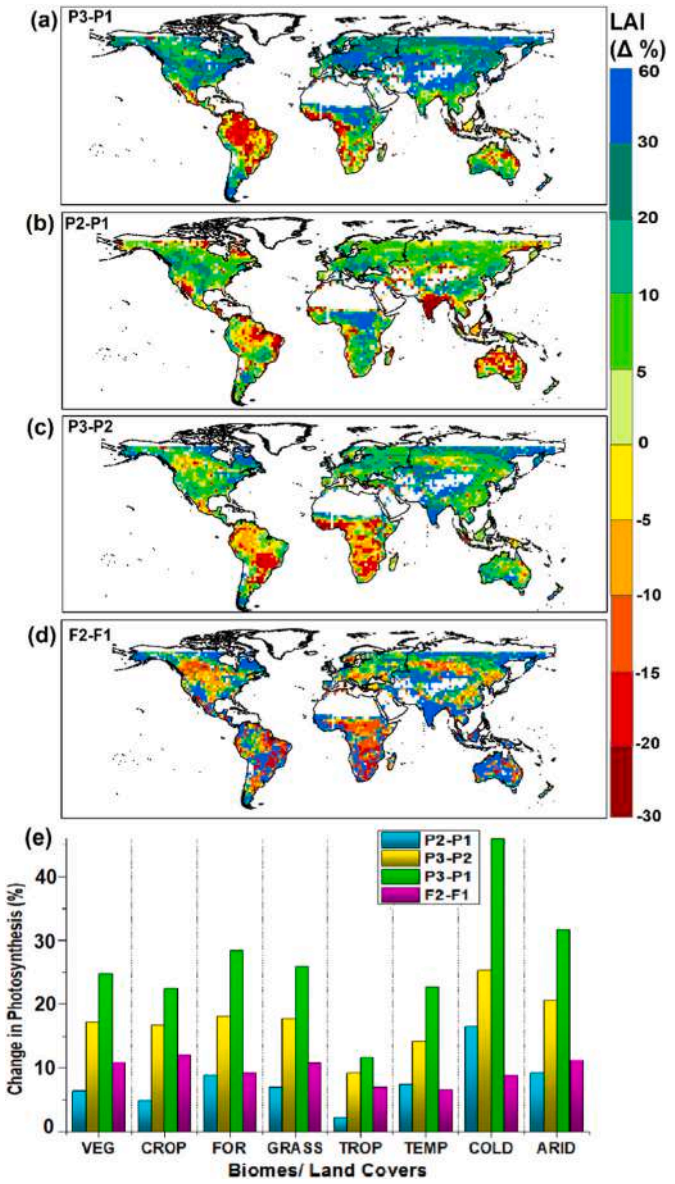

Fig. 10. Future change in Global Photosynthesis (Leaf Area Index, LAI) in percentage (%)during **(a)** historical (P1, 2015–2019) to end-century (P3, 2090–2100), **(b)** mid-century (P2, 2040–2050) to P1, **(c)** P3-P2, **(d)** mid-century to end-century (F2) from mid-century to historical period (F1); **(e)** (a–d) for land cover types: [net vegetated land (VEG), Croplands (CROP), Forests (FOR), other natural vegetation (GRASS)] and biomes: [Tropical (TROP), Temperate (T), Cold (COLD), Arid (ARID)].

the changes in global photosynthesis in the end-century (P3) from mid-century (P2). The greening is stronger (17.2 %) in the northern hemisphere, whereas browning is dominant in southern hemisphere regions such as Amazonia, northern and southern Africa and eastern Australia. Again, greening is larger in the cold (25.2 %) and arid (20.5 %) biomes, forests (18 %) and grasses (17.7 %) (Fig. 10c–e). Interestingly, in terms of changes between mid–end century and historical–mid-century, greening is intensified (10.9 %) and predominant in northern latitudes of North America and Eurasia, India, Southeast Asia, and Australia with larger magnitude in arid (11.4 %) and cold (8.8 %) biomes and croplands (11.9 %) (Fig. 10d and e).

Slowdown/reversal of greening is expected in central North America, central Eurasia, Africa and northeastern South America. Future warming will favour greening in northern high latitudes, but will have a detrimental impact on photosynthesis in the tropics and sub-tropics. Moistening will drive greening in tropical regions of Central Africa and mid-latitudes in central North America, north-central Asia and northeast China in the future. Drying-induced browning will be observed in western Europe, southern North America, northern South America, southern Africa and Australia. Water availability will play a strong positive role in enhanced cropland greening in the future (Wu et al., 2022). The future greening will be dominant in the northern latitudes in evergreen needleleaf forests and grasslands (Teng et al., 2023). CFE is expected to be the predominant driver of future greening in the cold and arid biomes (Zhao et al., 2020; Chai et al., 2025). However, there are uncertainties with the CMIP6 models in quantifying CFE, as some models are oversensitive to CFE, but others are less sensitive. This can lead to discrepancies in estimating the future greening based on multiple or ensemble model results (Wei et al., 2022; Chai et al., 2025). Conversely, Inter-Sectoral Impact Model Intercomparison Project (ISIMIP) based Dynamic Global Vegetation Models (DGVMs) are constrained with their dynamic vegetation modules with water (plant hydraulics) and nutrient (nitrogen and phosphorus) limitations, and have better land use patterns, weak CFE and greening; particularly in the semi-arid regions compared to the CMIP6 models (Warszawski et al., 2014; Molina Bacca et al., 2025). Also, ISIMIP models have relatively smaller inter-model variability and diverse dynamic vegetation mechanisms that better accounts for the plant biological successions than CMIP6 models (Warszawski et al., 2014; Rosenzweig et al., 2017). The ISIMIP models assume simplified plant functional types (PFTs) and use bias-corrected GCMs that smoothens out the extremes and thereby largely underrepresent the uncertain future climate variability and extremes (Warszawski et al., 2014; Frieler et al., 2017). Additionally, ISIMIP models suffer from uncertainties due to weak validation and very limited applications in these studies due to large inconsistencies in LAI definition (effective vs. true LAI) (Warszawski et al., 2014; Rosenzweig et al., 2017). Both CMIP6 and ISIMIP models simulate future greening, but have relatively weak patterns in ISIMIP due to restricted CFE in the semi-arid regions. Both CMIP6 and ISIMIP models also overestimate greening in water and nutrient limited regions due to the overestimation of CFE (Zhao et al., 2020; Chai et al., 2025). Also, with saturation of CFE, negative impacts of climate (e.g. enhanced warming and drying and extreme events), nutrient limitations, and human interventions (land use change and land management), the future photosynthesis will probably exhibit restrained influence of CFE (Peñuelas et al., 2017; Chen et al., 2024b). This can also be a major reason for the slowdown/reversal of future greening in the regions that previously exhibited strong CFE.

4.6. *Biophysical implications of changes in global photosynthesis*

The vegetation-climate feedbacks are key to terrestrial biogeochemical cycling and the exchanges of carbon, water, energy and momentum between land and atmosphere (Miralles et al., 2025; Liu et al., 2025). The future greening is expected to enhance terrestrial carbon uptake. However, the translation of vegetation structure (greenness) to functioning (carbon uptake) is very intricate (Kashyap and Kuttippurath, 2025b). The global vegetation exhibits disproportionate conversion of greening to increased carbon uptake in recent decades, as greening is mostly observed in sparse canopies (croplands and drylands) of low carbon sink potential and browning in dense canopies (tropical forests) due to warming-induced moisture stress and deforestation (Zhang et al., 2019; Feng et al., 2024). Interestingly, there is a decoupling of global greening and carbon sequestration in the future climate scenarios, which is predominant in grasslands and boreal biomes. Thus, the link between greening and carbon uptake is highly uncertain in the future due to changing climate and human interventions (Bian and Xia, 2024). Future greening will potentially expedite the hydrological cycle as it will enhance both ET and P, where the spatial disparity in their response to SM causes a hydrological response known as the "dry gets drier, wet gets wetter" (DDWW) paradigm (Wu et al., 2022). The future greening can potentially deplete SM in some semi-arid and arid regions due to

enhanced atmospheric aridity (Lian et al., 2020; Deng et al., 2020) and strengthened land-atmosphere coupling (Liu et al., 2025). In mesic ecosystems such as the tropical moist forests in Amazonia and Congo, greening-induced enhanced ET will promote more convective rains that boosts SM due to highly efficient moisture recycling in the atmospherically closed ecosystems. Therefore, the overall balance between the DDWW paradigm and moisture recycling of tropical ecosystems can maintain the future SM levels (Feng et al., 2021). The future greening-induced enhanced ET will lead to evaporative cooling, but greener canopies have a lower albedo than bare ground and absorb more sunlight, resulting in a higher sensible heat flux that causes albedo warming. The equilibrium between evaporative cooling and albedo warming determines the impact of greening on temperature (Piao et al., 2020). In warmer regions such as the tropics and temperate, the evaporative cooling counters albedo warming, resulting in net cooling (Forzieri et al., 2017). In recent decade, the enhancement in greening heterogeneity and amplified drying-induced browning led to greater SM limitations (Pan et al., 2018; Feng et al., 2021). The influence of drying outweighed the effects of temperature (Zhang et al., 2021) and energy (Denissen et al., 2022) on global photosynthesis.

4.7. Limitations

The existing remote sensing measurements exhibit limitations, including saturation and inadequate sensitivity in dense canopies, atmospheric and soil background noise, satellite orbital drifts, and sensor replacements. The MODIS MOD13A1 NDV and EVI data have an uncertainty of approximately ±0.02–0.05 (Huete et al., 2002; Didan et al., 2015). Additionally, the photosynthesis proxies derived from MODIS and MODIS-derived data do not accurately account for CFE. Therefore, to study the effects of CFE on global photosynthesis, ground-based measurements or high-resolution remote sensing data that efficiently accounts for CFE are required. Optical remote sensing data have limited applications in quantifying tropical disturbances such as deforestation, degradation and fires (Wigneron et al., 2024; Bar-On et al., 2025). Despite improvements, simulating accurate LAI is still a big challenge for CMIP6 models as they overestimate it (Gier et al., 2024). Furthermore, the CMIP6 model results are not very efficient in simulating the effect of SM-dryness on photosynthesis and they generally overestimate the future greening. Additionally, these models might not accurately simulate conditions of mega-droughts, intense wildfires, human mismanagements, destructive logging, insect and disease outbreaks, and forest diebacks that lead to browning (Zhao et al., 2020; Wu et al., 2022). Furthermore, these climate projections mostly underestimate the impacts of compound soil and atmospheric dryness stress on vegetation (Liu et al., 2023; Song et al., 2024). In a warmer future Earth, the stress arising from plant hydraulics and low atmospheric humidity can also impact global photosynthesis, which is highly underestimated by these climate projections (Feng et al., 2021; Liu et al., 2023). Also, these models fail to efficiently account for the impact of climatic oscillations like El Niño Southern Oscillation (ENSO) that can impact photosynthesis, particularly in the tropical regions of higher carbon uptake (Wigneron et al., 2020). The uncertainties in the data or measurements used in this study could induce some uncertainties in the derived results. The statistical and ML techniques employed in the study are also subject to certain limitations. The first order linear sensitivity analysis is subject to constraints in response to saturation and threshold behaviour. Granger causality works effectively for longer time series that are stationary and detects linear causal links. In this regard, the nonlinear causal inference approaches, such as Peter and Clarke's Momentary Conditional Independence (PCMCI) and Convergent Cross Mapping (CCM) could add more insights in the causal relationships. However, at times these causal approaches can also give spurious links that are not mechanistically feasible. ML based approaches are largely data-driven and require large volume of data to yield robust results.

4.8. Recommendations and policy relevance

There is a need to enhance the capability of remote sensing measurements and their validation with ground-based observations in quantifying global photosynthesis. However, the in-situ observations are available only in some regions, and very few in the tropical and mid-latitude regions of higher photosynthesis. Therefore, expansion of the current ground observational networks is of paramount significance for efficiently capturing the changing global vegetation-climate interactions. Recently launched satellites, geostationary satellites (Xiao et al., 2021) and global navigation satellites systems (GNSS) (Yao et al., 2024) can provide relatively high frequency spatio-temporal photosynthesis measurements. The uncertainties in the future of global photosynthesis call for better future projections for robust understanding of vegetation state and functioning. There is an urgent need for sustainable climate policies with a focus on effective terrestrial carbon sink management through the prevention of deforestation and forest degradation, particularly in the tropical and boreal forests of higher carbon uptake potential. Efforts should be directed towards preservation of indigenous forests, particularly in the tropical and sub-tropical regions, and enhance their resilience to climate change and climatic extremes (Feng et al., 2024; Kashyap and Kuttippurath, 2025b). Scientific afforestation should be promoted in mesic ecosystems (e.g. tropical forests) and should refrain from planting trees in xeric regions (e.g. arid lands) to maintain the energy balance and biogeochemical cycles. The indigenous xerophytes can be planted in drylands rather than invasive species that eventually degrade the regional flora and fauna (Hardy et al., 2025; Kashyap et al., 2025a).

Efficient and sustained carbon sink management should be one of the major agendas of climate policies. Additionally, targeted actions should be taken towards the restoration of degraded landscapes to preserve the indigenous biodiversity, socio-economic fabric and strengthen terrestrial carbon sinks. Focused attention should be drawn towards ecologically sensitive ecosystems such as the grasses, drylands and tropical forests. Furthermore, there is a need to check on anthropogenic disturbances of natural vegetation and better land management for croplands to attain sustainability. Additionally, there is a necessity to employ climate-smart agriculture (CSA) practices focussing on enhanced crop yields and improved climate resilience along with reduced emissions from land based sources. There is an urgent need to reduce carbon emissions in synergy with initiatives like REDD+ (Reducing Emissions from Deforestation and Forest Degradation, 2008), the Bonn Challenge (2011) and the Trillion Trees Initiative (2020) to ensure sustained terrestrial carbon sinks in the future, particularly in the tropical biome that exhibit slowdown in greening under dryness stress. The Land Degradation Neutrality (LDN, 2015) goals should be focused towards the vulnerable grasslands that are degrading due to moisture stress. Also, there is a need for sustainable policies for grazing such as rotational grazing and plantation of forage crops in the grasses and drylands. Adoption of Nature based Solutions (NbS) like Ecosystem-based Adaptation (EbA) is a way forward to effective green cover management in vulnerable tropical forests and grasslands and are of paramount significance to the future climate adaptation frameworks. The boreal biome exhibits saturation of warming-induced greening and there is a need for

control on the logging of fuel woods and promote bioeconomic strategies for climate-smart use of woods.

In a scenario of unprecedented population growth, there is a need for climate policies that promote agroforestry and other sustainable farming systems to reduce the pressure on natural forests in tropical and subtropical regions. Planting climate resilient and water-efficient crops, drought-resilient plant species and conservative agricultural practices are required to ensure global food security. These efforts would support United Nations (UN) Sustainable Development Goals (SDGs) 15.3 (combat desertification) and 13.1 (resilience to climate hazards). Conservative agricultural practices such as crop row spacing and mulching can reduce ET and promote SM retention in croplands, drylands and grasses under moisture stress. These approaches support UN SDGs 2.4 (sustainable food production) and 6.4 (increase water use efficiency). Additionally, plantation-based carbon sequestration targets should be revisited in the changing vegetation-climate interaction in the rising dryness scenario in accordance with SDG 15.2 (sustainable forest management). Furthermore, there is an urgent need to ensure sustainable agricultural practices in tune with the preservation of indigenous natural vegetation. Regional and global level detection, and forecast of climatic stress on vegetation should be established with the support of robust governance and policy-making. This calls for attention for climate adaption and mitigation policies in accordance with the broad UN SDGs 13 (climate action), 15 (life on land), 1 (no poverty) and 2 (zero hunger) to attain global food security and global sustainability. A brief summary of key results from this study is also provided in Table 3.

Table 3
Summary of the results from the study.

Discussion Paragraphs	Brief Summary
Shifting Climatic controls of Global Photosynthesis	The climatic control on global photosynthesis has shifted from warmth and energy to water availability in recent decades.
Greening Earth	Global greening continues across the land cover types, biomes and seasons (except DJF) in recent decades.
Slowdown of Global Greening	There is slowdown/reversal of global greening due to shift in climatic control to water availability and enhanced dryness.
Non-Climatic Drivers of Vegetation Dynamics	Apart from the climate drivers there are other drivers such as land management, afforestation, or deforestation, CO_2 fertilization effect (CFE) and nitrogen deposition (ND), which also drive regional vegetation dynamics and their influence largely remain stable over a long period.
Future of Global Photosynthesis	Greening is expected to continue in the future, and stronger in cold and arid biomes.
Biophysical implications of Changes in Global Photosynthesis	The future greening can expedite the hydrological cycle and intensify the land-atmosphere feedback and strengthened terrestrial carbon sink.
Constraints	The remote sensing data, climate projections, statistical and ML techniques have their own limitations.
Recommendations and Policy relevance	Need to improve the global vegetation monitoring by synergetic use of remote sensing, field and ground-based measurements. Focus should be drawn towards climate adaption and mitigation policies centered around the United Nations (UN) Sustainable Development Goals (SDGs) 13 (climate action), 15 (life on land) and 2 (zero hunger) to attain global food security and sustainability.

5. Conclusions

Global vegetation dynamics has garnered substantial attention due to its potential impact on food security, water cycle and terrestrial carbon sinks. Non-climatic factors have a rather straightforward and regional impact on vegetation. However, there remains large uncertainties regarding the response of terrestrial ecosystems to climate change as vegetation-climate interactions are very complex. The study finds high photosynthetic variability in the arid and cold biomes, grasses and forests during the JJA and SON seasons, and thus are the most sensitive to the changing climate**.** Warmth controls photosynthesis in temperate and cold biomes, but moisture availability in the tropical and arid biomes. Interestingly, the climatic control on global photosynthesis is shifting from warmth and energy to water availability in the drying world. "Greening Earth" is evident in recent decades, with India and China exhibiting the largest magnitudes of its increase. However, there is a decline in global photosynthetic growth rates in recent decade. There is widespread greening in the cold (warming-induced) and arid (moisture-induced) biomes and croplands (agricultural intensification and improved land management), but its slowdown/reversal in the tropical forests and temperate grasses (warming and drying-induced). The shifting climatic control constrains the intensified global photosynthesis. Greening is projected to continue until the 21st century, most intense in the cold and arid biomes. The future greening can expedite the hydrological cycle and intensify the land-atmosphere feedbacks and strengthened terrestrial carbon sink. In addition, the regime shift, deforestation and forest diebacks can alter vulnerable ecosystems such as those in boreal, drylands and tropical moist forests. This calls for policies on the conservation of natural ecosystems, land management and restoration programmes, prevention of destructive logging, judicial utilisation of forest resources, and effective agronomic planning to achieve global food security and sustainability. This study thus provides new insights into drafting appropriate climate policies to solve the challenges of global sustainability and food security in the rapidly changing climate with unprecedented population growth.

CRediT authorship contribution statement

Rahul Kashyap: Writing – review & editing, Writing – original draft, Visualization, Validation, Software, Methodology, Investigation, Formal analysis, Data curation, Conceptualization. **Jayanarayanan Kuttippurath:** Writing – review & editing, Visualization, Supervision, Methodology, Investigation, Conceptualization.

Funding

This study received no funding

Declaration of competing interest

The authors declare that they have no known competing financial interests or personal relationships that could have appeared to influence the work reported in this paper.

Acknowledgements

We thank the Director, Indian Institute of Technology Kharagpur (IIT Kgp), Chairman of CORAL IIT Kgp and the Ministry of Education (MoE) for facilitating the study. RK acknowledges the support from Prime Minister' s Research Fellowship (PMRF), MoE. We thank the NASA's LPDAAC team for providing the MODIS landcover, NDVI and EVI products. Giovanni's online data system developed and maintained by the NASA GES DISC for providing the GPM level–3 precipitation data; GLDAS for providing land temperature, soil moisture content, and downward surface radiation flux datasets; CMIP6 for providing future projection of LAI. Special thanks to Jingfeng Xiao for making the GOSIF

SIF dataset publicly accessible.

Appendix A. Supplementary data

Supplementary data to this article can be found online at https://doi.org/10.1016/j.jclepro.2025.147402.

Data availability

All data are publicly available and are listed in Table 2. The data are also available at: 10.6084/m9.figshare.28590770. Data processing is performed in R Studio (version 4.2.1) and ArcGIS (version 10.4). The plots and charts are created in and ArcGIS (version 10.4) and OriginPro (version 9). The R codes for RF and GC can be obtained from https://github.com/RahulKashyap1803

References

Abatzoglou, J.T., Williams, A.P., 2016. Impact of anthropogenic climate change on wildfire across western US forests. Proc. Natl. Acad. Sci. U.S.A 113 (42), 11770–11775. https://doi.org/10.1073/pnas.1607171113.

Baldocchi, D.D., 2020. How eddy covariance flux measurements have contributed to our understanding of Global Change Biology. Glob. Change Biol. 26 (1), 242–260. https://doi.org/10.1111/gcb.14807.

Bar-On, Y.M., Li, X., O'sullivan, M., Wigneron, J.P., Sitch, S., Ciais, P., Fischer, W.W., et al., 2025. Recent gains in global terrestrial carbon stocks are mostly stored in nonliving pools. Science 387 (6740), 1291–1295. https://doi.org/10.1126/science.adk1637.

Bastos, A., Ciais, P., Friedlingstein, P., Sitch, S., Pongratz, J., Fan, L., Zaehle, S., et al., 2020. Direct and seasonal legacy effects of the 2018 heat wave and drought on European ecosystem productivity. Sci. Adv. 6 (24). https://doi.org/10.1126/sciadv.aba2724 eaba2724.

Beck, H.E., McVicar, T.R., Vergopolan, N., Berg, A., Lutsko, N.J., Dufour, A., Miralles, D. G., et al., 2023. High-resolution (1 km) Köppen-Geiger maps for 1901–2099 based on constrained CMIP6 projections. Sci. Data 10 (1), 724. https://doi.org/10.1038/s41597-023-02549-6.

Bian, C., Xia, J., 2024. Divergent future trends in global land greening and carbon sequestration under climate change scenarios. Environ. Res. Lett. 19 (11), 114069. https://doi.org/10.1088/1748-9326/ad8508.

Brandt, M., Wigneron, J.P., Chave, J., Tagesson, T., Penuelas, J., Ciais, P., Fensholt, R., et al., 2018. Satellite passive microwaves reveal recent climate-induced carbon losses in African drylands. Nat. Ecol. Evol. 2 (5), 827–835. https://doi.org/10.1038/s41559-018-0530-6.

Breiman, L., 2001. Random forests. Mach. Learn. 45 (1), 5–32. https://doi.org/10.1023/A:1010933404324.

Bueso, D., Piles, M., Ciais, P., Wigneron, J.P., Moreno-Martínez, Á., Camps-Valls, G., 2023. Soil and vegetation water content identify the main terrestrial ecosystem changes. Natl. Sci. Rev. 10 (5), nwad026. https://doi.org/10.1093/nsr/nwad026.

Buitenwerf, R., Sandel, B., Normand, S., Mimet, A., Svenning, J.C., 2018. Land surface greening suggests vigorous woody regrowth throughout European semi-natural vegetation. Glob. Chang. Biol. 24 (12), 5789–5801. https://doi.org/10.1111/gcb.14451.

Chai, Y., Miao, C., Slater, L., Ciais, P., Berghuijs, W.R., Chen, T., Huntingford, C., 2025. Underestimating global land greening: future vegetation changes and their impacts on terrestrial water loss. One Earth 8 (2), 101176. https://doi.org/10.1016/j.oneear.2025.101176.

Chen, C., Park, T., Wang, X., Piao, S., Xu, B., Chaturvedi, R.K., Myneni, R.B., et al., 2019. China and India lead in greening of the world through land–use management. Nat. Sustain. 2 (2), 122–129. https://doi.org/10.1038/s41893-019-0220-7.

Chen, X., Chen, T., He, B., Liu, S., Zhou, S., Shi, T., 2024. The global greening continues despite increased drought stress since 2000. Glob. Ecol. Conserv. 49, e02791. https://doi.org/10.1016/j.gecco.2023.e02791.

Chen, Z., Wang, W., Forzieri, G., Cescatti, A., 2024. Transition from positive to negative indirect CO2 effects on the vegetation carbon uptake. Nat. Commun. 15 (1), 1500. https://doi.org/10.1038/s41467-024-45957-x.

Cooper, G.S., Willcock, S., Dearing, J.A., 2020. Regime shifts occur disproportionately faster in larger ecosystems. Nat. Commun. 11 (1), 1175. https://doi.org/10.1038/s41467-020-15029-x.

Cortés, J., Mahecha, M.D., Reichstein, M., Myneni, R.B., Chen, C., Brenning, A., 2021. Where are global vegetation greening and browning trends significant? Geophys. Res. Lett. 48 (6). https://doi.org/10.1029/2020GL091496 e2020GL091496.

Crowther, T.W., Glick, H.B., Covey, K.R., Bettigole, C., Maynard, D.S., Thomas, S.M., Bradford, M.A., et al., 2015. Mapping tree density at a global scale. Nature 525 (7568), 201–205. https://doi.org/10.1038/nature14967.

Deng, Y., Wang, S., Bai, X., Luo, G., Wu, L., Chen, F., Lu, Q., et al., 2020. Vegetation greening intensified soil drying in some semi-arid and arid areas of the world. Agric. For. Meteorol. 292, 108103. https://doi.org/10.1016/j.agrformet.2020.108103.

Denissen, J.M., Teuling, A.J., Pitman, A.J., Koirala, S., Migliavacca, M., Li, W., Orth, R., et al., 2022. Widespread shift from ecosystem energy to water limitation with climate change. Nat. Clim. Change 12 (7), 677–684. https://doi.org/10.1038/s41558-022-01403-8.

Deutsch, C.A., Tewksbury, J.J., Tigchelaar, M., Battisti, D.S., Merrill, S.C., Huey, R.B., Naylor, R.L., 2018. Increase in crop losses to insect pests in a warming climate. Science 361 (6405), 916–919. https://doi.org/10.1126/science.aat3466.

Didan, K., Munoz, A.B., Solano, R., Huete, A., 2015. MODIS Vegetation Index User's Guide (MOD13 Series), vol. 35. *University of Arizona:* Vegetation Index and Phenology Lab, pp. 2–33. https://modis-land.gsfc.nasa.gov/pdf/MOD13_User_Guide_V61.pdf.

Feng, X., Fu, B., Zhang, Y., Pan, N., Zeng, Z., Tian, H., Penuelas, J., et al., 2021. Recent leveling off of vegetation greenness and primary production reveals the increasing soil water limitations on the greening Earth. Sci. Bull. 66 (14), 1462–1471. https://doi.org/10.1016/j.scib.2021.02.023.

Feng, Y., Ciais, P., Wigneron, J.P., Xu, Y., Ziegler, A.D., van Wees, D., Zeng, Z., et al., 2024. Global patterns and drivers of tropical aboveground carbon changes. Nat. Clim. Change 14 (10), 1064–1070. https://doi.org/10.1038/s41558-024-02115-x.

Forzieri, G., Alkama, R., Miralles, D.G., Cescatti, A., 2017. Satellites reveal contrasting responses of regional climate to the widespread greening of Earth. Science 356 (6343), 1180–1184. https://doi.org/10.1126/science.aal1727.

Frieler, K., Lange, S., Piontek, F., Reyer, C.P., Schewe, J., Warszawski, L., Yamagata, Y., 2017. Assessing the impacts of 1.5 C global warming–simulation protocol of the Inter-Sectoral Impact Model Intercomparison Project (ISIMIP2b). Geosci. Model Dev. (GMD) 10 (12), 4321–4345. https://doi.org/10.5194/gmd-10-4321-2017.

Gampe, D., Zscheischler, J., Reichstein, M., O'Sullivan, M., Smith, W.K., Sitch, S., Buermann, W., 2021. Increasing impact of warm droughts on northern ecosystem productivity over recent decades. Nat. Clim. Change 11 (9), 772–779. https://doi.org/10.1038/s41558-021-01112-8.

Gier, B.K., Schlund, M., Friedlingstein, P., Jones, C.D., Jones, C., Zaehle, S., Eyring, V., 2024. Representation of the terrestrial carbon cycle in CMIP6. Biogeosci 21 (22), 5321–5360. https://doi.org/10.5194/bg-21-5321-2024.

Granger, C.W., 1969. Investigating causal relations by econometric models and cross–spectral methods. Econometrica 424–438. https://doi.org/10.2307/1912791.

Guillaume, T., Kotowska, M.M., Hertel, D., Knohl, A., Krashevska, V., Murtilaksono, K., Kuzyakov, Y., et al., 2018. Carbon costs and benefits of Indonesian rainforest conversion to plantations. Nat. Commun. 9 (1), 2388. https://doi.org/10.1038/s41467-018-04755-y.

Gutiérrez-Hernández, O., García, L.V., 2025. Uncovering true significant trends in global greening. Remote Sens. Appl.: Soci. Environ. 37, 101377. https://doi.org/10.1016/j.rsase.2024.101377.

Hardy, N.G., Kuebbing, S.E., Duguid, M.C., Ashton, M.S., Sheban, K.C., Inman, S.E., Martin, M.P., 2025. Non-native invasive plants in tropical dry forests: a global review of presence, impacts, and management. Restor. Ecol. 33 (1), e14288. https://doi.org/10.1111/rec.14288.

Heagney, E.C., Falster, D.S., Kovač, M., 2021. Land clearing in south-eastern Australia: drivers, policy effects and implications for the future. Land Use Policy 102, 105243. https://doi.org/10.1016/j.landusepol.2020.105243.

Higgins, S.I., Conradi, T., Muhoko, E., 2023. Shifts in vegetation activity of terrestrial ecosystems attributable to climate trends. Nat. Geosci. 16 (2), 147–153. https://doi.org/10.1038/s41561-022-01114-x.

Huang, M., Piao, S., Ciais, P., Peñuelas, J., Wang, X., Keenan, T.F., Janssens, I.A., et al., 2019. Air temperature optima of vegetation productivity across global biomes. Nat. Ecol. Evol. 3 (5), 772–779. https://doi.org/10.1038/s41559-019-0838-x.

Huete, A., Didan, K., Miura, T., Rodriguez, E.P., Gao, X., Ferreira, L.G., 2002. Overview of the radiometric and biophysical performance of the MODIS vegetation indices. Remote Sens. Environ. 83 (1–2), 195–213. https://doi.org/10.1016/S0034-4257(02)00096-2.

Humphrey, V., Berg, A., Ciais, P., Gentine, P., Jung, M., Reichstein, M., Frankenberg, C., et al., 2021. Soil moisture-atmosphere feedback dominates land carbon uptake variability. Nature 592 (7852), 65–69. https://doi.org/10.1038/s41586-021-03325-5.

Kashyap, R., Kuttippurath, J., 2024a. Unraveling the sensitivity and response of ecosystems to rising moisture stress in India. Ecosys. Health Sustain. 10, 180. https://doi.org/10.34133/ehs.0180.

Kashyap, R., Kuttippurath, J., 2024b. Warming-induced soil moisture stress threatens food security in India. Environ. Sci. Pollunt. Res. 31 (49), 59202–59218. https://doi.org/10.1007/s11356-024-35107-7.

Kashyap, R., Kuttippurath, J., 2025a. Tropical cyclones enhance photosynthesis in moisture-stressed regions of India. npj Clim. Atmos. Sci. 8 (1), 115. https://doi.org/10.1038/s41612-025-00988-z.

Kashyap, R., Kuttippurath, J., 2025b. Weakening of forest carbon stocks due to declining Ecosystem Photosynthetic Efficiency under the current and future climate change scenarios in India. India. Resour. Conserv. Recycl. 222, 108478. https://doi.org/10.1016/j.resconrec.2025.108478.

Kashyap, R., Pandey, A.C., Kuttippurath, J., 2022. Photosynthetic trends in India derived from remote sensing measurements during 2000–2019: vegetation dynamics and key climate drivers. Geocarto Int. 37 (26), 11813–11829. https://doi.org/10.1080/10106049.2022.2060325.

Kashyap, R., Kuttippurath, J., Kumar, P., 2023a. Browning of vegetation in efficient carbon sink regions of India during the past two decades is driven by climate change and anthropogenic intrusions. J. Environ. Manage. 336, 117655. https://doi.org/10.1016/j.jenvman.2023.117655.

Kashyap, R., Kuttippurath, J., Patel, V.K., 2023b. Improved air quality leads to enhanced vegetation growth during the COVID–19 lockdown in India. Appl. Geogr. 151, 102869. https://doi.org/10.1016/j.apgeog.2022.102869.

Kashyap, R., Kuttippurath, J., Patel, V.K., 2025a. Agriculture intensification and moisture-induced Thar desert greening: implications for energy balance, socio-economy, and biodiversity. GISci. Remote Sens. 62 (1), 2483458. https://doi.org/10.1080/15481603.2025.2483458.

Kashyap, R., Kuttippurath, J., Patel, V.K., 2025b. Ecological droughts increased in India with changing Indian summer monsoon and human interventions. Commun. Earth Environ. 6 (1), 853. https://doi.org/10.1038/s43247-025-02694-3.
Keenan, T.F., Prentice, I.C., Canadell, J.G., Williams, C.A., Wang, H., Raupach, M., Collatz, G.J., 2016. Recent pause in the growth rate of atmospheric CO2 due to enhanced terrestrial carbon uptake. Nat. Commun. 7 (1), 13428. https://doi.org/10.1038/ncomms13428.
Keenan, T.F., Luo, X., Stocker, B.D., De Kauwe, M.G., Medlyn, B.E., Prentice, I.C., Zhou, S., et al., 2023. A constraint on historic growth in global photosynthesis due to rising CO2. Nat. Clim. Change 13 (12), 1376–1381. https://doi.org/10.1038/s41558-023-01867-2.
Krich, C., Runge, J., Miralles, D.G., Migliavacca, M., Perez-Priego, O., El-Madany, T., Mahecha, M.D., et al., 2020. Estimating causal networks in biosphere–atmosphere interaction with the PCMCI approach. Biogeosci 17 (4), 1033–1061. https://doi.org/10.5194/bg-17-1033-2020.
Kuttippurath, J., Kashyap, R., 2023. Greening of India: forests or croplands? Appl. Geogr. 161, 103115. https://doi.org/10.1016/j.apgeog.2023.103115.
Lal, P., Shekhar, A., Gharun, M., Das, N.N., 2023. Spatiotemporal evolution of global long-term patterns of soil moisture. Sci. Total Environ. 867, 161470. https://doi.org/10.1016/j.scitotenv.2023.161470.
Li, X., Xiao, J., 2019. Mapping photosynthesis solely from solar–induced chlorophyll fluorescence: a global, fine-resolution dataset of gross primary production derived from OCO–2. Remote Sens. 11 (21), 2563. https://doi.org/10.3390/rs11212563.
Lian, X., Piao, S., Li, L.Z., Li, Y., Huntingford, C., Ciais, P., McVicar, T.R., et al., 2020. Summer soil drying exacerbated by earlier spring greening of northern vegetation. Sci. Adv. 6 (1). https://doi.org/10.1126/sciadv.aax0255 eaax0255.
Liu, Y., Liu, Y., Wang, W., 2019. Inter-comparison of satellite-retrieved and Global Land Data Assimilation System–simulated soil moisture datasets for global drought analysis. Remote Sens. Environ. 220, 1–18. https://doi.org/10.1016/j.rse.2018.10.026.
Liu, L., Gudmundsson, L., Hauser, M., Qin, D., Li, S., Seneviratne, S.I., 2020. Soil moisture dominates dryness stress on ecosystem production globally. Nat. Commun. 11 (1), 4892. https://doi.org/10.1038/s41467-020-18631-1.
Liu, Q., Peng, C., Schneider, R., Cyr, D., Liu, Z., Zhou, X., Kneeshaw, D., et al., 2023a. Vegetation browning: global drivers, impacts, and feedbacks. Trends Plant Sci. 28 (9), 1014–1032. https://doi.org/10.1016/j.tplants.2023.03.024.
Liu, X., Sun, G., Fu, Z., Ciais, P., Feng, X., Li, J., Fu, B., 2023b. Compound droughts slow down the greening of the Earth. Glob. Change Biol. 29 (11), 3072–3084. https://doi.org/10.1111/gcb.16657.
Liu, Y., Li, Z., Chen, Y., Jin, L., Li, F., Wang, X., Kayumba, P.M., et al., 2025. Global greening drives significant soil moisture loss. Commun. Earth Environ. 6 (1), 600. https://doi.org/10.1038/s43247-025-02470-3.
Miralles, D.G., Vilà-Guerau de Arellano, J., McVicar, T.R., Mahecha, M.D., 2025. Vegetation–climate feedbacks across scales. Ann. N. Y. Acad. Sci. 1554 (1), 27–41. https://doi.org/10.1111/nyas.15286.
MODIS Land Team, 2014. Status for: land cover/dynamics (MCD12), validation. http://landval.gsfc.nasa.gov/ProductStatus.php?ProductID=MOD12. (Accessed 18 March 2023).
Molina Bacca, E.J., Stevanović, M., Bodirsky, B.L., Doelman, J.C., Parsons Chini, L., Volkholz, J., Popp, A., et al., 2025. Future land-use pattern projections and their differences within the ISIMIP3b framework. Earth Syst. Dyn. 16 (3), 753–801. https://doi.org/10.5194/esd-16-753-2025.
Myers-Smith, I.H., Kerby, J.T., Phoenix, G.K., Bjerke, J.W., Epstein, H.E., Assmann, J.J., Wipf, S., et al., 2020. Complexity revealed in the greening of the Arctic. Nat. Clim. Change 10 (2), 106–117. https://doi.org/10.1038/s41558-019-0688-1.
Nemani, R.R., Keeling, C.D., Hashimoto, H., Jolly, W.M., Piper, S.C., Tucker, C.J., Running, S.W., et al., 2003. Climate–driven increases in global terrestrial net primary production from 1982 to 1999. Science 300 (5625), 1560–1563. https://doi.org/10.1126/science.1082750.
Pan, N., Feng, X., Fu, B., Wang, S., Ji, F., Pan, S., 2018. Increasing global vegetation browning hidden in overall vegetation greening: insights from time–varying trends. Remote Sens. Environ. 214, 59–72. https://doi.org/10.1016/j.rse.2018.05.018.
Patel, V.K., Kuttippurath, J., Kashyap, R., 2024a. Increased global cropland greening as a response to the unusual reduction in atmospheric $PM_{2.5}$ concentrations during the COVID–19 lockdown period. Chemosphere 358, 142147. https://doi.org/10.1016/j.chemosphere.2024.142147.
Patel, V.K., Kuttippurath, J., Kashyap, R., 2024b. Rise in water vapour driven by moisture transport facilitates water availability for the greening of global deserts. Sci. Total Environ. 946, 174111. https://doi.org/10.1016/j.scitotenv.2024.174111.
Peñuelas, J., Ciais, P., Canadell, J.G., Janssens, I.A., Fernández-Martínez, M., Carnicer, J., Sardans, J., et al., 2017. Shifting from a fertilization-dominated to a warming-dominated period. Nat. Ecol. Evol. 1 (10), 1438–1445. https://doi.org/10.1038/s41559-017-0274-8.
Piao, S., Liu, Z., Wang, T., Peng, S., Ciais, P., Huang, M., Tans, P.P., et al., 2017. Weakening temperature control on the interannual variations of spring carbon uptake across northern lands. Nat. Clim. Change 7 (5), 359–363. https://doi.org/10.1038/nclimate3277.
Piao, S., Wang, X., Park, T., Chen, C., Lian, X.U., He, Y., Myneni, R.B., et al., 2020. Characteristics, drivers and feedbacks of global greening. Nat. Rev. Earth Environ. 1 (1), 14–27. https://doi.org/10.1038/s43017-019-0001-x.
Qin, Y., Xiao, X., Wigneron, J.P., Ciais, P., Brandt, M., Fan, L., Moore, I.I.I.B., et al., 2021. Carbon loss from forest degradation exceeds that from deforestation in the Brazilian Amazon. Nat. Clim. Change 11 (5), 442–448. https://doi.org/10.1038/s41558-021-01026-5.
Qiu, B., Ye, Z., Chen, C., Tang, Z., Chen, Z., Huang, H., Berry, J., et al., 2022. Dense canopies browning overshadowed by global greening dominant in sparse canopies. Sci. Total Environ. 826, 154222. https://doi.org/10.1016/j.scitotenv.2022.154222.
Rascher, U., Alonso, L., Burkart, A., Cilia, C., Cogliati, S., Colombo, R., Zemek, F., et al., 2015. Sun-induced fluorescence–a new probe of photosynthesis: first maps from the imaging spectrometer HyPlant. Glob. Change Biol. 21 (12), 4673–4684. https://doi.org/10.1111/gcb.13017.
Rogers, A., Medlyn, B.E., Dukes, J.S., Bonan, G., Von Caemmerer, S., Dietze, M.C., Zaehle, S., et al., 2017. A roadmap for improving the representation of photosynthesis in Earth system models. New Phytol. 213 (1), 22–42. https://doi.org/10.1111/nph.14283.
Rosenzweig, C., Arnell, N.W., Ebi, K.L., Lotze-Campen, H., Raes, F., Rapley, C., Warszawski, L., 2017. Assessing inter-sectoral climate change risks: the role of ISIMIP. Environ. Res. Lett. 12 (1), 010301. https://doi.org/10.1088/1748-9326/12/1/010301.
Ruehr, S., Keenan, T.F., Williams, C., Zhou, Y., Lu, X., Bastos, A., Terrer, C., et al., 2023. Evidence and attribution of the enhanced land carbon sink. Nat. Rev. Earth Environ. 4 (8), 518–534. https://doi.org/10.1038/s43017-023-00456-3.
Ryu, Y., Berry, J.A., Baldocchi, D.D., 2019. What is global photosynthesis? History, uncertainties and opportunities. Remote Sens. Environ. 223, 95–114. https://doi.org/10.1016/j.rse.2019.01.016.
Schimel, D., Pavlick, R., Fisher, J.B., Asner, G.P., Saatchi, S., Townsend, P., Cox, P., et al., 2015. Observing terrestrial ecosystems and the carbon cycle from space. Glob. Change Biol. 21 (5), 1762–1776. https://doi.org/10.1111/gcb.12822.
Sellers, P.J., Tucker, C.J., Collatz, G.J., Los, S.O., Justice, C.O., Dazlich, D.A., Randall, D. A., 1996. A revised land surface parameterization (SiB2) for atmospheric GCMs. Part II: the generation of global fields of terrestrial biophysical parameters from satellite data. J. Clim. 9 (4), 706–737. https://doi.org/10.1175/1520-0442(1996)009<0706:ARLSPF>2.0.CO;2.
Sellers, P.J., Schimel, D.S., Moore III, B., Liu, J., Eldering, A., 2018. Observing carbon cycle–climate feedbacks from space. Proc. Natl. Acad. Sci. U.S.A 115 (31), 7860–7868. https://doi.org/10.1073/pnas.1716613115.
Shekhar, A., Buchmann, N., Gharun, M., 2022. How well do recently reconstructed solar-induced fluorescence datasets model gross primary productivity? Remote Sens. Environ. 283, 113282. https://doi.org/10.1016/j.rse.2022.113282.
Skofronick-Jackson, G., Kirschbaum, D., Petersen, W., Huffman, G., Kidd, C., Stocker, E., Kakar, R., et al., 2018. The Global Precipitation Measurement (GPM) mission's scientific achievements and societal contributions: reviewing four years of advanced rain and snow observations. Q. J. R. Meteorol. Soc. 144, 27–48. https://doi.org/10.1002/qj.3313.
Song, J., Zhou, S., Yu, B., Li, Y., Liu, Y., Yao, Y., Fu, B., et al., 2024. Serious underestimation of reduced carbon uptake due to vegetation compound droughts. npj Clim. Atmos. Sci. 7 (1), 23. https://doi.org/10.1038/s41612-024-00571-y.
Southworth, J., Ryan, S.J., Herrero, H.V., Khatami, R., Bunting, E.L., Hassan, M., Waylen, P., et al., 2023. Latitudes and land use: global biome shifts in vegetation persistence across three decades. Front. Remote Sens. 4, 1063188. https://doi.org/10.3389/frsen.2023.1063188.
Tagesson, T., Schurgers, G., Horion, S., Ciais, P., Tian, F., Brandt, M., Fensholt, R., et al., 2020. Recent divergence in the contributions of tropical and boreal forests to the terrestrial carbon sink. Nat. Ecol. Evol. 4 (2), 202–209. https://doi.org/10.1038/s41559-019-1090-0.
Tao, S., Chave, J., Frison, P.L., Le Toan, T., Ciais, P., Fang, J., Saatchi, S., et al., 2022. Increasing and widespread vulnerability of intact tropical rainforests to repeated droughts. Proc. Natl. Acad. Sci. U.S.A 119 (37), e2116626119. https://doi.org/10.1073/pnas.2116626119.
Teng, H., Chen, S., Hu, B., Shi, Z., 2023. Future changes and driving factors of global peak vegetation growth based on CMIP6 simulations. Ecol. Inform. 75, 102031. https://doi.org/10.1016/j.ecoinf.2023.102031.
Tong, X., Brandt, M., Yue, Y., Ciais, P., Rudbeck Jepsen, M., Penuelas, J., Fensholt, R., et al., 2020. Forest management in southern China generates short term extensive carbon sequestration. Nat. Commun. 11 (1), 129. https://doi.org/10.1038/s41467-019-13798-8.
Trenberth, K.E., 2015. Has there been a hiatus? Science 349 (6249), 691–692. https://doi.org/10.1126/science.aac9225.
Wang, L., Li, X., Chen, Y., Yang, K., Chen, D., Zhou, J., Huang, J., et al., 2016. Validation of the global land data assimilation system based on measurements of soil temperature profiles. Agric. For. Meteorol. 218, 288–297. https://doi.org/10.1016/j.agrformet.2016.01.003.
Wang, S., Zhang, Y., Ju, W., Chen, J.M., Ciais, P., Cescatti, A., Peñuelas, J., et al., 2020. Recent global decline of CO2 fertilization effects on vegetation photosynthesis. Science. 370 (6522), 1295–1300. https://doi.org/10.1126/science.abb7772.
Warszawski, L., Frieler, K., Huber, V., Piontek, F., Serdeczny, O., Schewe, J., 2014. The inter-sectoral impact model intercomparison project (ISI–MIP): project framework. Proc. Natl. Acad. Sci. 111 (9), 3228–3232. https://doi.org/10.1073/pnas.1312330110.
Wei, N., Xia, J., Zhou, J., Jiang, L., Cui, E., Ping, J., Luo, Y., 2022. Evolution of uncertainty in terrestrial carbon storage in earth system models from CMIP5 to CMIP6. J. Clim. 35 (17), 5483–5499. https://doi.org/10.1175/JCLI-D-21-0763.1.
Wigneron, J.P., Fan, L., Ciais, P., Bastos, A., Brandt, M., Chave, J., Fensholt, R., et al., 2020. Tropical forests did not recover from the strong 2015–2016 El Niño event. Sci. Adv. 6 (6). https://doi.org/10.1126/sciadv.aay4603 eaay4603.
Wigneron, J.P., Ciais, P., Li, X., Brandt, M., Canadell, J.G., Tian, F., Fensholt, R., et al., 2024. Global carbon balance of the forest: satellite-based L-VOD results over the last decade. Front. Remote Sens. 5, 1338618. https://doi.org/10.3389/frsen.2024.1338618.

Wild, M., 2016. Decadal changes in radiative fluxes at land and ocean surfaces and their relevance for global warming. Wiley Interdiscip. Rev. Clim. Change. 7 (1), 91–107. https://doi.org/10.1002/wcc.372.

Winkler, A.J., Myneni, R.B., Hannart, A., Sitch, S., Haverd, V., Lombardozzi, D., Brovkin, V., et al., 2021. Slowdown of the greening trend in natural vegetation with further rise in atmospheric CO 2. Biogeosci 18 (17), 4985–5010. https://doi.org/10.5194/bg-18-4985-2021.

Wu, J., Wang, D., Li, L.Z., Zeng, Z., 2022. Hydrological feedback from projected Earth greening in the 21st century. Sustain. Horiz. 1, 100007. https://doi.org/10.1016/j.horiz.2022.100007.

Xiao, J., Fisher, J.B., Hashimoto, H., Ichii, K., Parazoo, N.C., 2021. Emerging satellite observations for diurnal cycling of ecosystem processes. Nat. Plants 7 (7), 877–887. https://doi.org/10.1038/s41477-021-00952-8.

Yao, Y., Humphrey, V., Konings, A.G., Wang, Y., Yin, Y., Holtzman, N., Frankenberg, C., 2024. Investigating diurnal and seasonal cycles of vegetation optical depth retrieved from GNSS signals in a broadleaf forest. Geophys. Res. Lett. 51 (6). https://doi.org/10.1029/2023GL107121 e2023GL107121.

Zhang, Y., Song, C., Band, L.E., Sun, G., 2019. No proportional increase of terrestrial gross carbon sequestration from the greening Earth. J. Geophys. Res. Biogeosci. 124 (8), 2540–2553. https://doi.org/10.1029/2018JG004917.

Zhang, A., Jia, G., Ustin, S.L., 2021. Water availability surpasses warmth in controlling global vegetation trends in recent decade: revealed by satellite time series. Environ. Res. Lett. 16 (7), 074028. https://doi.org/10.1088/1748-9326/ac0b68.

Zhang, H., Hu, Z., Chen, X., Li, J., Zhang, Q., Zheng, X., 2025. Global greening major contributed by climate change with more than two times rate against the history period during the 21th century. Glob. Change Biol. 31 (3), e70126. https://doi.org/10.1111/gcb.70126.

Zhao, Q., Zhu, Z., Zeng, H., Zhao, W., Myneni, R.B., 2020. Future greening of the Earth may not be as large as previously predicted. Agric. For. Meteorol. 292, 108111. https://doi.org/10.1016/j.agrformet.2020.108111.

Zhao, Z., Ciais, P., Wigneron, J.P., Santoro, M., Brandt, M., Kleinschroth, F., Li, W., et al., 2024. Central African biomass carbon losses and gains during 2010–2019. One Earth 7 (3), 506–519. https://doi.org/10.1016/j.oneear.2024.01.02101.

Zhu, Z., Piao, S., Myneni, R.B., Huang, M., Zeng, Z., Canadell, J.G., Zeng, N., et al., 2016. Greening of the Earth and its drivers. Nat. Clim. Change 6 (8), 791–795. https://doi.org/10.1038/nclimate3004.

Science of the Total Environment 1015 (2026) 181416

Contents lists available at ScienceDirect

Science of the Total Environment

journal homepage: www.elsevier.com/locate/scitotenv

Increased moisture stress and weakened resilience to aridity limit global greening

Rahul Kashyap, Jayanarayanan Kuttippurath *

CORAL, Indian Institute of Technology Kharagpur, Kharagpur, 721302, India

HIGHLIGHTS

- The response of global photosynthesis to rising moisture stress is examined for biomes and land covers.
- VPD (39.8%) has greater control on global photosynthesis than SM (31.4%) and CWD (28.8%).
- SM and CWD influences photosynthesis through VPD in biomes and land covers where they lack direct causality.
- Moisture-stressed ecosystems, non-resilient to dryness exhibit slowdown of greening.
- Sparse canopy greening and dense canopy browning are projected in 21st century driven by moisture.

GRAPHICAL ABSTRACT

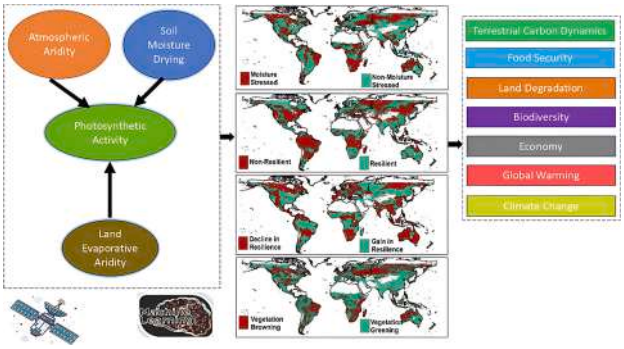

ARTICLE INFO

Keywords:
Greening
Browning
Soil moisture
Vapour pressure deficit
Carbon-water coupling
Land-atmosphere interactions
Machine learning
Resilience

ABSTRACT

The "Greening Earth" and rising aridity are both climate change signatures. We investigate the response of global photosynthesis to moisture stress (higher demand and lower availability of moisture) in current (2000–2021) and future climate scenarios (until 2100). We employ a suite of statistical and machine learning (ML) techniques on satellite remote sensing, reanalyses and climate projection data for robust findings. Remote sensing based high resolution indicators of global photosynthesis in Fraction of Photosynthetically Active Radiation (FPAR), Enhanced Vegetation Index (EVI) and Solar-Induced Fluorescence (SIF) are utilised. Vapour Pressure Deficit (VPD, 39.76%) influences global photosynthesis more than Soil Moisture (SM, 31.44%) and Climatic Water Deficit (CWD, 28.8%), reveals Random Forest (RF). VPD exhibits a direct causal relationship with photosynthesis across biomes and land cover types, unlike SM and CWD. In absence of direct causal association, SM and CWD influence photosynthesis through VPD. Enhanced land (CWD, 16.7%) and atmospheric (VPD, 4.3%) evaporative demands reduce SM (−2.2%) in recent decade (2010–2019) from the previous (2000–2009). Concurrently, global photosynthesis exhibits enhanced cumulative growth rates (CGR), with a slowdown/reversal of global greening (−2.8% CGR), notably in grasses and tropical biomes due to rising moisture stress. Cropland, and temperate and arid biomes exhibit high sensitivity and low resilience to dryness stress. Global photosynthesis has gained resilience against land evaporative (CWD, 6.7%) and atmospheric aridity (VPD, 4.1%), conversely lost resilience against SM drying (−0.5%) in recent decade from previous. In moisture-stressed ecosystems, gain in resilience facilitates photosynthesis and decline in resilience results in slowdown or reversal of greening. This

* Corresponding author.
E-mail addresses: rahulkashyaprsm@gmail.com (R. Kashyap), jayan@coral.iitkgp.ac.in (J. Kuttippurath).

https://doi.org/10.1016/j.scitotenv.2026.181416
Received 10 October 2025; Received in revised form 9 December 2025; Accepted 14 January 2026
Available online 23 January 2026

calls for effective land management to enhance the resilience of vulnerable ecosystems to rising moisture stress for ensuring food security and sustainability.

1. Introduction

Vegetation is an essential component of the earth, and climate systems that significantly influence the carbon and water cycles by regulating their fluxes between the atmosphere and biosphere through processes such as photosynthesis and transpiration (Piao et al., 2020; Humphrey et al., 2021). Comprehending the changes in global photosynthesis is of paramount significance to unveil the changes in carbon-climate feedbacks, and to sustain the unprecedented growth in population through crop and wood production (Piao et al., 2020; Keenan et al., 2023). In the warming world, enhanced atmospheric moisture demand (vapour pressure deficit [VPD]) and lower soil moisture (SM) can have detrimental effects on photosynthesis (Fu et al., 2022; Liu et al., 2024). SM serves as the primary water source for vegetation, that influences moisture readily accessible to plant roots. Consequently, decline in SM is the prime indicator of moisture stress experienced by vegetation (Liu et al., 2020; Feng et al., 2021). Elevated VPD can prompt vegetation to close stomata to minimise water loss at the leaf surface level, and thus restrict plant photosynthesis and growth (Yuan et al., 2019, 2025; Fu et al., 2022).

In the global warming scenario, moisture stress is expected to become more intense and frequent, thereby adversely affect terrestrial ecosystems worldwide (Reichstein et al., 2013; Green, 2024). Moisture stress can cause severe threats to crop productivity and trigger tree mortality (Yuan et al., 2019, 2025; Bauman et al., 2022) through two mechanisms i.e., carbon starvation and hydraulic failure (McDowell and Sevanto, 2010; Hartmann, 2015). The carbon starvation hypothesis attributes the tree mortality events to deficits in carbohydrate reserves due to a reduction in photosynthesis driven by prolonged drought. The plant carbon reserve is exhausted due to stomatal closure and inadequate carbon assimilation to satisfy tissue maintenance requirements during carbon starvation. The hydraulic failure hypothesis suggests that during moisture stress, tree dies primarily from impaired water transport due to xylem embolism. Inability to sustain xylem water tension below its cavitation threshold leads to embolisms, which if unresolved, can ultimately result in extensive desiccation to lead to plant mortality (McDowell et al., 2022).

A robust understanding of the impact of moisture stress on ecosystems is crucial for managing ecological implications of drought risks and reducing uncertainties in predicting future land carbon sink potential and climate change (Liu et al., 2020; Liu et al., 2023a). It also enables to test the capacity of terrestrial ecosystems to serve as future carbon sinks in a warmer and drier world (Kashyap and Kuttippurath, 2024a, 2024b, 2025a). Satellite based photosynthetic proxies reveal that the overall global vegetation greenness has increased (i.e. greening) over the years (Zhu et al., 2016; Chen et al., 2019; Cortés et al., 2021; Chen et al., 2024; Kashyap and Kuttippurath, 2026). However, there is a rise in decline of vegetation greenness (i.e. browning) on regional scales in recent decades (Brandt et al., 2018; Pan et al., 2018; Liu et al., 2023a; Kashyap and Kuttippurath, 2026). Concurrently, reduction in precipitation (P) and increase in evapotranspiration (ET) have led to SM drying in recent decades, where 40% of the global vegetated land experiences a decline in SM (Lal et al., 2023; Peng et al., 2023). This SM drying limits photosynthesis and reduces terrestrial carbon uptake (Liu et al., 2020; Feng et al., 2021; Liu et al., 2025a). Furthermore, recent studies suggest that elevated atmospheric dryness (VPD) adversely affects global vegetation growth and terrestrial productivity (Yuan et al., 2019, 2025; Fu et al., 2022). Studies also suggest that the concurrent events of reduction in SM accompanied by enhanced VPD are more detrimental to vegetation health (Liu et al., 2023b; Song et al., 2024).

The sensitivity of global photosynthesis to SM has increased in recent decades (Li et al., 2022; Kashyap and Kuttippurath, 2026) and future climate scenario (Denissen et al., 2022). Since, both global photosynthesis and moisture stress are increasing in the changing climate, it is of paramount significance to extensively investigate the relationship between the two. We hypothesise that in the rising moisture stress scenario, there can be a slowdown/reversal of the global greening particularly in the dense canopies. The ecosystems that are resilient to moisture stress would continue greening in the future climate change scenario. Since we want to examine extreme climate cases, we select high emissions scenarios (Shared Socioeconomic Pathways, SSP585) in the study.

However, still uncertainties exist in terms of the response of global photosynthesis to moisture stress across land cover types and biomes. Therefore, we comprehensively investigate the following science questions: (i) What is the relationship between global moisture availability/demand and photosynthesis in current and future climate? (ii) How does the changes in moisture availability/demand influence global photosynthesis? (iii) Which are the vegetated regions where photosynthesis is resilient/non-resilient to moisture stress and how does it evolve with time? We employ a suite of statistical techniques that includes correlation, Partial Correlation (PC), Multiple Linear Regression (MLR), Machine Learning (ML) based Random Forest (RF) model, Granger Causality, Sensitivity analysis, Resilience method and Growth Rate Analysis on remote sensing measurements and reanalyses data for this assessment. The findings would enable new insights on the intricacies of the global carbon-water cycle interactions and feedbacks that are of paramount significance for ecosystem management for a sustainable world.

2. Data and methods

2.1. Data

2.1.1. Land covers and biomes

We categorise different land cover types according to Moderate Resolution Imaging Spectroradiometer (MODIS) land cover data following the International Geosphere and Biosphere Programme (IGBP) classification that has an overall accuracy of 74.8% (MODIS Land Team, 2014). We reclassify land covers, where the various forest type classes are grouped as a common or broad forest class, croplands and all other forms of natural vegetation, such as grasslands, shrublands, and savannahs. All other natural land cover types are referred to as grasses for clear understanding (Fig. S1a). We conduct an analysis of the four principal biomes globally—tropical, temperate, cold, and arid, but the polar biome is left out as it is largely non-vegetated (Fig. S1b). We utilise the most recent high-resolution version of the Köppen-Geiger (KG) climate classification data which inherently integrates elevation effects through temperature (T) and P patterns (Beck et al., 2023).

2.1.2. Proxies of photosynthesis

All the data with their resolution, purpose and sources are listed in Table 1. Earth observations provide a comprehensive perspective of global terrestrial biosphere and are essential for their timely monitoring (Nemani et al., 2003; Piao et al., 2020). The efficacy of the MODIS in monitoring the terrestrial biosphere is well documented (Chen et al., 2019; Kashyap et al., 2023a). Fraction of Photosynthetically Active Radiation (FPAR) is an essential climate variable (ECV) that serves as a vital metric for photosynthesis and terrestrial carbon cycle. FPAR is also crucial for comprehending carbon-climate and carbon-water interactions, as well as the biogeochemical cycles of terrestrial ecosystems (Sellers et al., 1996; Cai et al., 2025). The Normalised Difference

Table 1
The datasets, their resolution, purpose and the sources are listed.

Data	Resolution	Purpose/Use	Source
MODIS LULC (MCD12Q1)	500 m	LULC data to extract vegetated land covers	(https://lpdaacsvc.cr.usgs.gov/)
MODIS NDVI (MOD13A1)	500 m	calculation of FPAR of change in photosynthesis	(https://lpdaacsvc.cr.usgs.gov/)
MODIS EVI (MOD13A1)	500 m	EVI & calculation of change in photosynthesis	(https://lpdaacsvc.cr.usgs.gov/)
GOSIF SIF	0.05° × 0.05°	SIF & calculation of change in photosynthetic activity and productivity	(http://data.globalecology.unh.edu/)
GLDAS Soil Moisture	0.25° × 0.25°	Soil Moisture, relationship with photosynthesis and changes	(https://daac.gsfc.nasa.gov/)
TerraClimate CWD	4 km	Land evaporative aridity (CWD), relationship with photosynthesis and changes	(https://www.climatologylab.org/terraclimate.html)
TerraClimate VPD	4 km	Atmospheric aridity (VPD), relationship with photosynthesis and changes	(https://www.climatologylab.org/terraclimate.html)
Köppen-Geiger classification	1 km	Biome delineation	(https://www.gloh2o.org/koppen/)
CESM2 LAI	1° × 1°	Future LAI and changes	(https://esgf-node.llnl.gov/projects/cmip6/)
CSM-2 MR LAI	1.25° × 1.25°	Future LAI and changes	(https://esgf-node.llnl.gov/projects/cmip6/)
CNRM LAI	1.40° × 1.40°	Future LAI and changes	(https://esgf-node.llnl.gov/projects/cmip6/
ACCESS LAI	1.875° × 1.25°	Future LAI and changes	(https://esgf-node.llnl.gov/projects/cmip6/)
MPI-ESM LAI	1.88° × 1.86°	Future LAI and changes	(https://esgf-node.llnl.gov/projects/cmip6/)
GFDL SM	1° × 1°	Future SM and changes	(https://esgf- node.llnl.gov/projects/cmip6/)
CNRM SM	0.5° × 0.5°	Future SM and changes	(https://esgf-node.llnl.gov/projects/cmip6/)
HadGEM SM	1.875° × 1.25°	Future SM and changes	(https://esgf-node.llnl.gov/projects/cmip6/)
CanESM SM	2.81° × 2.77°	Future SM and changes	(https://esgf- node.llnl.gov/projects/cmip6/)

Vegetation Index (NDVI) and FPAR exhibit a linear relation, allowing for more accurate computation of FPAR through the application of NDVI (Sellers et al., 1996). We employ MODIS NDVI to calculate FPAR using the Linear Scaling technique (as detailed in the Supplementary material). We also employ the Enhanced Vegetation Index (EVI) from MODIS, as a surrogate for photosynthesis as it accounts for the impact of canopy background and atmospheric effects through the application of a correction factor (Huete et al., 2002; Patel et al., 2024a). Also, EVI exhibits greater sensitivity to alterations in canopy structure and does not reach saturation in high biomass areas such as Amazon (Zeng et al., 2023; Kashyap et al., 2023b). Additionally, we also consider Solar-induced Fluorescence (SIF) as a photosynthetic proxy, which is widely regarded as a highly effective indicator of photosynthesis and productivity (Shekhar et al., 2022). SIF is more closely associated with plant physiological processes than traditional reflectance-based indices NDVI and EVI (Li et al., 2018; Li and Xiao, 2019). The global Orbiting Carbon Observatory (OCO-2) SIF (GOSIF v2) data are utilised for measuring plant photosynthetic activity and terrestrial productivity (Li and Xiao, 2019; Kashyap et al., 2023b). The temporal framework of the study spans from 2000 to 2021, to keep the data quality intact and consistent across the metrics, and the climatology and variability are centered around it. However, for the long-term decadal change analysis, we have restricted our study for the time period of 2000 to 2019 (Kashyap and Kuttippurath, 2026). This is due to the anomalous vegetation response due to COVID-19 in the years 2020 and 2021 that would eventually corrupt the long-term data and analysis (Patel et al., 2024a; Kashyap et al., 2023b; Su et al., 2021).

2.1.3. Soil moisture and aridity metrics

Moisture availability greatly impacts the health and functioning of terrestrial ecosystems (Higgins et al., 2023; Liu et al., 2023b; Kashyap and Kuttippurath, 2024a, 2024b, 2025a, 2025b). SM is the plant available moisture in the soil that is readily utilised for photosynthesis (Green et al., 2019; Humphrey et al., 2021). Here, we employ the SM data from the Global Land Data Assimilation System (GLDAS) that incorporates both satellite and ground observations to generate depictions of land surface conditions. This is accomplished through the utilisation of advanced land surface modelling and data assimilation techniques (Liu et al., 2019). We consider two aridity metrics, Climatic Water Deficit (CWD) and VPD, derived from the TerraClimate data as they have better spatial resolution (Abatzoglou et al., 2018). CWD quantifies the water that would have been utilised by plants or evaporated from soil, and it serves as a prevalent indicator of moisture stress (Huang et al., 2021). Potential evapotranspiration (PET) refers to the adequate moisture in optimal conditions for healthy crops that can be evaporated, whereas actual evapotranspiration (AET) denotes the moisture available to plants for evaporation, influenced by weather conditions, water availability, and crop health (Otkin et al., 2013). CWD is measured as the hydrological deficit between PET and AET, as demonstrated in Eq. (1):

$$CWD = PET - AET \quad (1)$$

VPD is regarded as a metric for atmospheric aridity or atmospheric moisture or evaporative demand, which is a crucial environmental factor that influences ET, latent heat exchange, surface energy budget, and vegetation water stress (Yuan et al., 2019; Grossiord et al., 2020). VPD influences vegetation water stress, canopy photosynthesis, and global carbon and climate feedbacks by regulating vegetation stomatal opening (Fu et al., 2022; Yuan et al., 2025). VPD as the estimate of atmospheric moisture demand is calculated as the difference between saturated (SVP) and actual ambient atmospheric vapour pressures (AVP) at a given temperature (Grossiord et al., 2020; Liu et al., 2020), as demonstrated in Eq. (2):

$$VPD = SVP - AVP \quad (2)$$

2.1.4. Future projections

The future response of photosynthesis to moisture availability is investigated through the Coupled Model Intercomparison Project Phase 6 (CMIP6) based future projection data of Leaf Area Index (LAI) and SM. The LAI data from six CMIP6 models in CESM2, CSM-2 MR, CNRM, ACCESS, MPI-ESM and Can-ESM are employed (Zhao et al., 2020) as detailed in Table S1. The SM data from CMIP6 models in GFDL, CNRM, CanESM and HadGEM are utilised. To ensure the consistency across LAI and SM datasets we harmonise them by employing the ensemble of multi-model mean of both datasets and ensuring the same spatio-temporal resolution. Also, we have the analysis and comparison of LAI and SM data across various land cover types and biomes for various time periods. All future projection data are considered for the high emissions scenario (Shared Socioeconomic Pathways, SSP585) as we want to examine the changes during the most extreme climate context (Eyring et al., 2016). Three time periods are selected for comparison: (a) historical (P1, 2015–2019), (b) mid-century (P2, 2040–2050) and (c) end-century (P3, 2090–2100).

2.2. Methods

This study explores the response of terrestrial ecosystems in terms of photosynthesis to the changing moisture availability and aridity. We employ effective indicators of moisture stress in SM, CWD and VPD (Kashyap and Kuttippurath, 2024a, 2025a) and recent high resolution remote sensing data (FPAR, SIF and EVI) as plant photosynthesis proxies with FPAR being the key proxy for simplicity and novelty with EVI and SIF as supporting indicators. These are highly responsive indicators of plant photosynthesis that rely on radiometrically and geometrically corrected satellite data with high accuracy in interpreting biophysical proxies (e.g. Leaf Area Index: LAI, Gross Primary Productivity: GPP, and Net Primary Productivity: NPP) (Higgins et al., 2023). The response of terrestrial ecosystems to change in moisture is very intricate and non-linear (Kashyap et al., 2025a, 2025b). Droughts provoke varied ecosystem responses shaped by their duration, distribution, trends, severity, and intricate interactions. Additionally, it depends on the biome, prevailing climate, topography, river basin, and regional carbon-water coupling (Sharma and Goyal, 2018; Green, 2024). Henceforth, to make robust conclusions we apply on a suite of statistical techniques such as partial correlation, MLR, ML based RF, Granger Causality, sensitivity analysis and Resilience method. The key methods are detailed below.

2.2.1. Spatio-temporal variability

We compute the spatio-temporal patterns of SM, CWD, VPD and FPAR for seasonal, interannual and decadal variability. The four seasons considered are, winter (DJF: December, January and February), spring (MAM: March, April and May), summer (JJA: June, July and August) and autumn (SON: September, October and November). This reverses in the southern hemisphere, wherein DJF is summer, MAM is autumn, JJA is winter and SON is spring. We estimate the normalised regional anomaly (NRA) in SM, CWD, VPD and FPAR for various land cover types and biomes as per Eq. (3):

$$\mathrm{NRAI} = (\mathrm{I_m}–\mathrm{X_m})/\mathrm{X_m} \tag{3}$$

Here, $\mathrm{I_m}$ = mean value for any region as land cover type or biome sand $\mathrm{X_m}$ = mean value for the global vegetated land.

Likewise, we also estimate the normalised seasonal anomaly (NSA) in SM, CWD, VPD and FPAR for various land cover types and biomes as per Eq. (4):

$$\mathrm{NSAI} = (\mathrm{I_m}–\mathrm{X_m})/\mathrm{X_m} \tag{4}$$

Here, $\mathrm{I_m}$ = mean value for any season as DJF, MAM, JJA or SON and $\mathrm{X_m}$ = mean value for the yearly average for the study period.

The change in different parameters during the period (2000–2019) is quantified in terms of percentage as per Eq. (5):

$$\%X_{R-P} = \frac{X_R - X_P}{X_P} \times 100 \tag{5}$$

Here, X is any variable, R is the mean of X in recent decade (2010–2019) and P is the mean of X in the previous decade (2000–2009).

2.2.2. Correlation and partial correlation

To understand the relation of photosynthesis (FPAR) with moisture (SM, CWD and VPD) we employ Pearsons's correlation analysis. We also employ partial correlation (PC) to investigate the link between two variables limiting the influence of the third variable (covariate) using Eq. (6):

$$r_{xy.z} = \left(\frac{r_{xy} - r_{xz}.r_{yz}}{\sqrt{1 - r_{xz}^2} \cdot \sqrt{1 - r_{yz}^2}} \right) \tag{6}$$

Here,

r_{xy} = correlation coefficient of between variable x and variable y.

$r_{xy.z}$ = first order partial correlation between variable x and y by the elimination of covariate (z) from the other variables (x and y).

2.2.3. Change in coupling

To investigate the change in relation of moisture availability/demand (SM, CWD and VPD) with global photosynthesis (FPAR), we compute the change in coupling (correlation) between them among the two decades converted to percentage values using Eq. (7):

$$\%C_{R-P} = \frac{C_R - C_P}{C_P} \times 100 \tag{7}$$

Here, C is the coupling (correlation) between FPAR and moisture availability/demand indicators in recent decade (2010–2019) and P is C in the previous decade (2000–2009).

2.2.4. Causal relations

Correlation analysis generally suggests the relation between two variables and does not imply causation. Therefore, to investigate the existence of causal relationships among photosynthesis (FPAR) and moisture availability/demand(SM, CWD and VPD), we employ Granger Causality (GC) test. GC explores causal connection between two variables based on the concepts of "cause" and "effect". A causal relationship is said to be Granger if the ability to predict future responses of variable Y improves by incorporating all pertinent information, excluding the present value of variable X (Granger, 1969). To conduct a Granger causality test, a bivariate model is established between the time series (X and Y) that are stationary per Eqs. (8) and (9):

$$Y_t = \sum_{i=1}^{n} a_i Y_{t-i} + \sum_{i=1}^{n} b_i X_{t-i} + \varepsilon_t \tag{8}$$

$$X_t = \sum_{i=1}^{n} c_i X_{t-i} + \sum_{i=1}^{n} d_i Y_{t-i} + \delta_t \tag{9}$$

where, X and Y are two stationary time series; a, b, c and d are coefficients; and ε and δ are white noise. For X to Granger cause Y, $b_i \neq 0$; for feedback between X and Y, $d_i \neq 0$.

The stationarity of the data is validated through the Augmented Dickey-Fuller (ADF) test. The maximum allowable lag between photosynthesis (FPAR) and moisture availability/demand is assigned as 3 months and its statistical significance is considered at the 95% confidence interval based on multiple iterations and previous studies for similar bioclimatic regions (Krich et al., 2020; Winkler et al., 2021; Kashyap et al., 2023a; Kashyap and Kuttippurath, 2024b, 2026). This specific lag is chosen to preserve the causal effects of drivers on FPAR in the same season, thereby reducing their seasonal influence (Winkler et al., 2021; Kashyap and Kuttippurath, 2025b, 2026).

2.2.5. Relative contribution

Machine learning (ML) is a highly effective in managing multidimensional data, making it invaluable for modelling systems with complex nonlinear structures. A model known as Random Forest (RF) integrates boosting and regression trees to generate multiple individual tree models. We utilise the RF model in R Studio version 4.2.1, employing the "randomForest" and "caret" packages to assess the relative influence of moisture availability/demand (SM, CWD, and VPD) on photosynthesis (FPAR) (Kashyap and Kuttippurath, 2024a, 2024b, 2025a). The RF model generates a total of 500 decision trees, permitting two variable splits in each tree. Seventy percent of the data is allocated for training, and 30% is designated for testing. Each tree possesses its own independent out-of-bag data sample that was excluded from the initial construction. The significance of a variable quantifies the extent to which its exclusion leads to a reduction in precision. The significance of a variable quantifies the extent to which its exclusion leads to a reduction in precision, as detailed in Supplementary material.

Additionally, we also incorporate the multiple linear regression (MLR) to complement the RF based contribution analysis as detailed in the Supplementary material. The performance of ML models RF (Table S1) and MLR (Table S2) is assessed and presented in Supplementary material.

2.2.6. Sensitivity analysis

We compute the sensitivity of global photosynthesis (FPAR) to moisture availability/demand (SM, CWD and VPD) as per Eq. (10):

$$Sx = \frac{\Delta S}{\Delta X} \tag{10}$$

Here, Sx is the sensitivity of S to X, and S is FPAR and X is moisture availability/demand (SM, CWD and VPD). The change in S (ΔS) and X (ΔX) are the percentage change in recent decade (2010–2019) from the previous decade (2000–2009). Furthermore, we have also normalised Sx for better understanding and easier comparison.

2.2.7. Growth rate analysis

Growth Rate (GR) concept is extensively employed in economics and finance to identify intermediate variations and overall cumulative changes over time. This method is also extensively employed in assessing the variability of atmospheric CO_2 concentration (Keenan et al., 2016). It is the difference in the value (X) in the current period (t) from the previous period (t-1) based on the Eq. (11):

$$X_{GR} = X_t - X_{t-1} \tag{11}$$

Here, XGR is the growth rate (GR) in X (photosynthesis: FPAR and moisture availability/demand) among time periods t and t-1. We also estimate the cumulative growth rate (CGR, Eq. (12)) and mean growth rate (MGR, Eq. (13)) in FPAR and moisture availability/demand for three time periods: (i) Study period (2000–2019); (ii) previous decade (P, 2000–2009) and (iii) recent decade (R, 2010–2019).

$$CGR = \sum_{i=1}^{n} X_{GR} \tag{12}$$

$$MGR = \left(\sum_{i=1}^{n} X_{GR}\right) \Big/ n \tag{13}$$

Here, n is the number of years of the study.

To understand the change in the MGR and CGR, we also estimate the change in them among the decades as converted to percentage values as per Eq. (14):

$$\%CGR \Big/ MGR_{R-P} = \frac{CGR/MGR_R - CGR/MGR_P}{CGR/MGR_P} \times 100 \tag{14}$$

2.2.8. Delineation of moisture stressed region

We delineate the moisture stressed regions as the areas where the moisture demand i.e. both atmospheric (VPD) and land evaporative (CWD) are increasing and concurrently, the moisture availability i.e. readily plant available soil water (SM) is decreasing. The changes in SM, VPD and CWD are estimated in recent decade (2010–2019) from the previous decade (2000–2009). The regions that exhibit increase in VPD and CWD, but a decline in SM is considered as "moisture stressed" region in the study.

2.2.9. Resilience analysis

The response of terrestrial ecosystems to moisture stress is intricate and contingent upon various factors, including season, drought intensity, current soil water availability, topography, climate, legacy effects, and plant functional types (Zhang et al., 2017; Kashyap and Kuttippurath, 2024a, 2025a). Here we employ Resilience method wherein the core concept is the its ability to absorb and recover from changes, which is a prevalent method for characterising ecosystem responses to climate disturbances (Holling, 1973; Sharma and Goyal, 2018). Here, we define resilience as the ability of an ecosystem to restore its equilibrium state under moisture stress. Since, this analysis spans two decades we cannot consider every event as it would be for a small period and on a regional scale, we rely on the worst affected year. Moisture stress exerts direct effects on ecosystems and can also induce delayed consequences in subsequent seasons and years. The enduring impacts on ecosystem structure and function following the cessation of moisture stress are referred to as legacy effects or drought legacies. The transitional period between peak and minimal carbon uptake seasons, known as the shoulder seasons, may result in a reduction of carbon uptake by ecosystems due to temperature variations, diminished sunlight, and alterations in vegetation dynamics (Zhang et al., 2017; Huang et al., 2021). Consequently, we consider the driest year to represent a singular drought event lasting one year. We assess the resilience of global photosynthesis to SM drying, land evaporative (CWD) and atmospheric (VPD) aridity. Initially, we identify the largest negative anomaly (SM) and the largest positive anomaly (CWD and VPD). Subsequently, we calculate the ratio (Ri) of the most adversely impacted year (Yx) to the overall mean of the period (Ym). The non-dimensional quantity Ri is referred to as the coefficient of resilience according to Eq. (15):

$$R_i = \frac{Y_x}{Y_m} \tag{15}$$

The Ri threshold of 0.8–0.9 is moderately resilient, while higher than that is resilient and lower is non-resilient (Sharma and Goyal, 2018; Kashyap and Kuttippurath, 2024a, 2025a).

We also perform the resilience analysis separately for the two decades i.e. previous decade (P, 2000–2009) and recent decade (R, 2010–2019). The difference in the two resilience scores gives the change in resilience, converted to percentage values as per Eq. (16).

$$\%Ri_{R-P} = \frac{Ri_R - Ri_P}{Ri_P} \times 100 \tag{16}$$

Here, Ri is the resilience score of FPAR to SM drying/ high CWD/high VPD in recent decade (2010–2019) and P is the resilience score in the previous decade (2000–2009).

3. Results

3.1. Global moisture availability/demand and photosynthesis: variability and relation

We employ three metrics of moisture in terms of readily plant available soil water (SM), land evaporative aridity (CWD), atmospheric aridity (VPD) and FPAR as photosynthetic proxy (Fig. 1a, b, c) and the normalised regional anomaly (NRA) in them (Fig. 1d). Croplands (0.52) and grasses (0.48) exhibit lower photosynthesis (FPAR) due to less SM, larger CWD and VPD. Contrarily, forests show larger FPAR (0.69) due to higher SM, lower CWD and smaller VPD. Tropical (0.7) and temperate (0.64) biomes show higher photosynthesis despite higher VPD and CWD due to high SM. Arid biome shows smaller FPAR (0.32) owing to very large aridity and less SM. Seasonally, In MAM, FPAR is small (0.49) despite higher SM and lower CWD due to large VPD. In SON, FPAR is high (0.55) due to low VPD, even with higher CWD and low SM and the normalised seasonal anomaly (NSA) results also exhibit the same (Fig. S2). The years of higher photosynthesis (FPAR) such as 2006, 2010, 2016 have lower CWD and VPD, and higher SM. Conversely, the years of higher CWD, FPAR and lower SM result in low FPAR such as in 2009, 2012 and 2015 (Fig. S3).

Next, we investigate the relation between photosynthesis (FPAR) and moisture availability/demand (SM, VPD and CWD) based on correlation analyses. SM has a variable relationship with photosynthesis (FPAR), for which it has a positive impact in regions like southern North America, northeastern South America, Africa, India and western China.

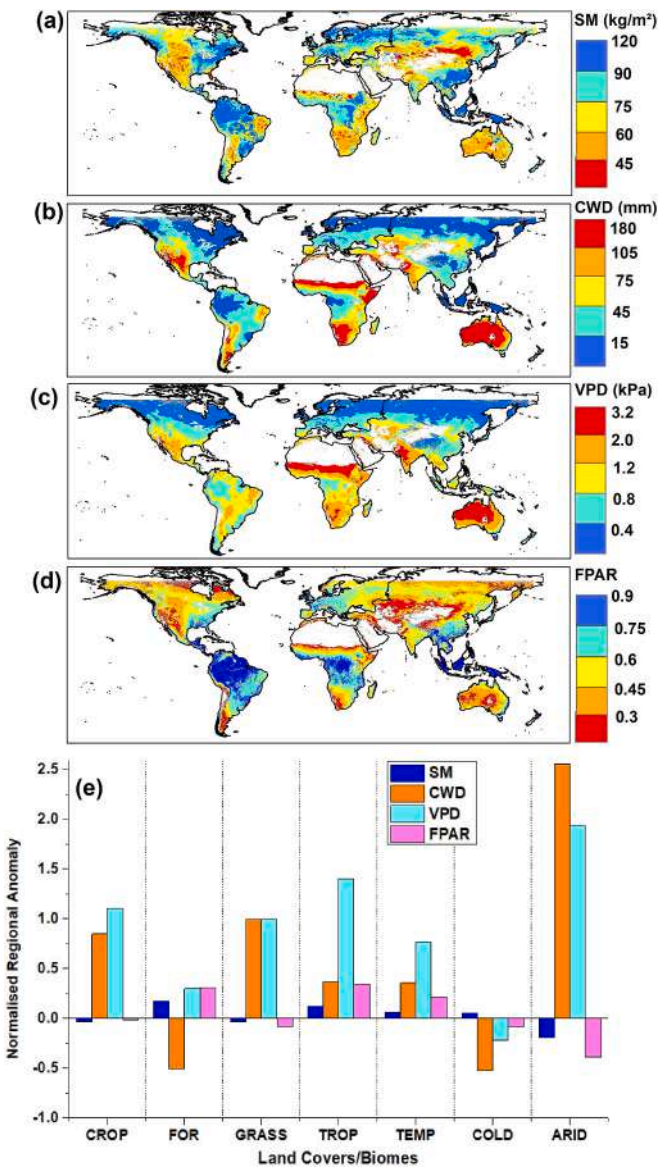

Fig. 1. Spatial variability in (a) Soil Moisture (SM), (b) Climatic Water Deficit (CWD), (c) Vapour Pressure Deficit (VPD) and (d) Fraction of Photosynthetically Active Radiation (FPAR), (e) Normalised Regional Anomaly (NRA) in SM, CWD, VPD and FPAR for land covers [Croplands (CROP), Forests (FOR), other natural vegetation (GRASS)] and biomes [Tropical (TROP), Temperate (T), Cold (COLD), and Arid (ARID)] averaged for the period 2000–2021.

Contrarily, negative relation in northern latitudes of North America, Europe and Eurasia (Fig. 2a). For biomes, SM has a strong positive relation with FPAR in tropical (0.53) and arid (0.46), but relatively weak connection in temperate (0.29) and negative (−0.51) in cold biomes (Fig. 2d). CWD has a positive relationship with FPAR in northeastern North America, Amazonia, Central Africa, Indonesia, western China and central Australia. Conversely, it is negative in western North America, northeastern South America, northeastern Africa, southern Africa, Eurasia, India and peripheries of Australia (Fig. 2b). The FPAR-CWD relationship is negative for all land cover types and biomes, which is relatively stronger in arid (−0.31) and temperate (−0.27), but weaker in tropical (−0.16) and cold (−0.14) biomes (Fig. 2d). VPD largely exhibits a negative relationship with photosynthesis, except for some regions such as northwestern North America, western boundaries of South America, southern Europe, eastern Eurasia, western China, and central Australia (Fig. 2c). FPAR-VPD relationship is negative for all land cover types and biomes, and is stronger in croplands (−0.31), arid (−0.38) and tropical (−0.34) biomes) (Fig. 2d).

To get a vivid understanding of the relationship between FPAR and moisture availability/demand (SM, VPD and CWD), we also employ the partial correlation analyses. Since, SM-CWD and SM-VPD are generally coupled, we employ partial correlation analyses to examine their intricate relationship with photosynthesis (FPAR). The FPAR-CWD relationship neglecting/limiting the influence of SM (Fig. 2e), is negative in northern latitudes of North America, Europe and Eurasia, central North America, Europe, Eurasia, some regions in Amazonia, southeastern South America, Central Africa, eastern Asia, eastern and southern India. However, the regions northeastern and central South America, northern and southern Africa and western China have a strong positive influence of CWD on FPAR, limiting the role of SM. Among the land cover types, all show a negative relation, which is relatively larger in forests (−0.3), strong negative (−0.71) in cold and large positive in tropical (0.75) biomes (Fig. 2h). Next, we investigate the FPAR-VPD relation limiting the influence of SM (Fig. 2f), and is negative in northeastern and northwestern North America, central and eastern Europe, western Eurasia eastern southeast Asia, eastern and southern India, northern and central Africa, northeastern, central and southern South America. In contrast, the relation is positive in northwestern and central North America, western Europe, eastern Asia, western China, northern, central east and southeastern Africa, eastern and western South America. All land cover types and biomes exhibit negative relation, which is stronger in cold biomes (−0.42), croplands (−0.34) and forests (−0.33) (Fig. 2h). Then, we examine the FPAR-SM relationship limiting the influence of VPD (Fig. 2g) and find a negative relation in northern latitudes in North America, Europe, Eurasia, eastern China, tropical forests in Indonesia, Amazonia, southeastern and southern South America. The relation is positive in other vegetated regions, and is stronger in northeastern South America, northern and southern Africa, and India. The relation is strong negative in cold biome (−0.79), forests (−0.3) and strongly positive in tropical (0.76), temperate (0.38) and arid (0.35) biomes (Fig. 2h).

3.2. *Contribution and causal connection of photosynthesis with moisture availability/demand*

The relationship between moisture availability/demand and photosynthesis is explored. However, the relative controls of SM, CWD and VPD on FPAR across land cover types and biomes are still not well known. Therefore, we employ ML based RF model (Fig. 3a) to estimate the same and find that VPD (39.76%) has a larger control on photosynthesis (FPAR) than SM (31.44%) and CWD (28.8%) in global vegetated lands. For land cover types, VPD has a greater influence on FPAR than SM and CWD, which is larger in sparse canopies (e.g.: croplands and grasses) than dense canopies (e.g.: forests). SM impacts FPAR more than CWD in forests (SM: 36.47% and CWD: 26.37%) and croplands (SM: 30.7% and CWD: 29.2%). For biomes, VPD has a greater control on photosynthesis in cold (39.1%) and tropical (37%) biomes. In temperate biome, SM (38.3%) has a stronger control on photosynthesis followed by VPD (33%) and CWD (28.7%). Likewise, in arid biomes, SM (35.67%) has a slightly greater control on photosynthesis than VPD (34.75%) followed by CWD (29.58%). CWD has a greater influence on FPAR than SM in grasses (CWD:32.16% and SM:28.63%) and cold (CWD: 34.1%, SM:26.8%) biomes (Table S3). The results from MLR also affirms the findings from RF model (Tables S4–S11). Both RF (Table S1) and MLR (Table S2) performs well across various land cover types and biomes.

We have investigated the relationship and relative control of moisture availability/demand (SM, CWD and VPD) over photosynthesis (FPAR). However, the causal connections are unknown, and thus, we employ Granger Causality with maximum allowable temporal lag between photosynthesis (FPAR) and moisture availability/demand as 3 months and significant at 95% confidence interval for the same (Fig. 3b–i). We find, for global vegetated land, FPAR has a causal link with VPD and CWD, but not with SM, and there is no feedback. SM has a

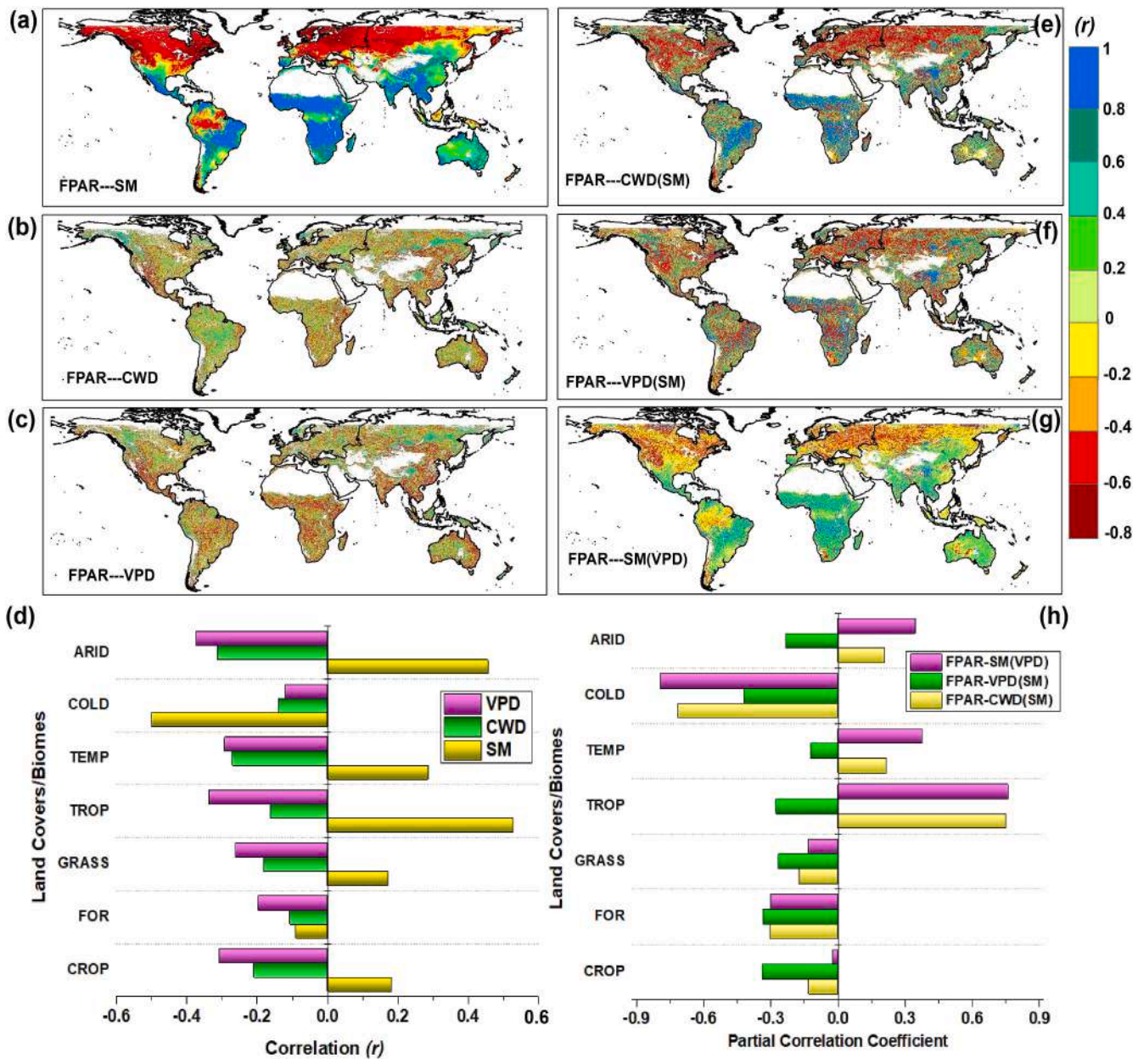

Fig. 2. The correlation of (a) Soil Moisture (SM), (b) Climatic Water Deficit (CWD), (c) Vapour Pressure Deficit (VPD) with Fraction of Photosynthetically Active Radiation (FPAR), (d) (a, b, c) for land covers [Croplands (CROP), Forests (FOR), other natural vegetation (GRASS)] and biomes [Tropical (TROP), Temperate (T), Cold (COLD), and Arid (ARID)], (e) partial correlation of FPAR with CWD limiting the influence of SM, (f) FPAR with VPD limiting the influence of SM, (g) FPAR with SM limiting the influence of VPD, (h) for various land cover types and biomes averaged for the period 2000–2021.

causal connection with both CWD and VPD (at no lag), and influence global vegetation through the two. Interestingly, SM and VPD also have causal feedbacks (Fig. 3b). For croplands, CWD, VPD and SM have causal relations with FPAR, and SM has causal feedback (Fig. 3c). In forests, except CWD, VPD and SM have causal connections with FPAR. VPD has a feedback relation with FPAR. CWD has a causal relation with both VPD and SM (at no lag), and influence FPAR through them (Fig. 3d). In grasses, CWD and VPD have causal links with FPAR. However, SM does not exhibit a direct causal connection with FPAR and affects it through CWD and VPD, as it has a causal link with them (at no lag). SM-VPD also have causal feedback relationships as well (Fig. 3e). For biomes, in tropical, CWD, VPD and SM exhibit causal relationships with FPAR, where both CWD and VPD have feedback relation (Fig. 3f). In temperate biome, SM and VPD exhibit causal connections with FPAR, and VPD has a feedback relation with FPAR. CWD does not have a direct causal link with FPAR, but influences photosynthesis through SM and VPD as it has causal relations with both (at no lag) (Fig. 3g). In cold biome, VPD has a causal link with FPAR, and both CWD and SM impact photosynthesis through VPD as they have causal connections with VPD (at no lag). Additionally, FPAR-VPD exhibits a causal feedback relationship (Fig. 3h). In arid biome, all CWD, VPD and SM have causal relationships with FPAR. Also, both SM and CWD have a causal relationship with VPD, and CWD has a causal link with SM (at no lag) (Fig. 3i).

3.3. *Changes in the relationship between moisture availability/demand and photosynthesis*

After extensively investigating the relationship between moisture availability/demand and photosynthesis, we examine the change in relationship between the two across land cover types and biomes in

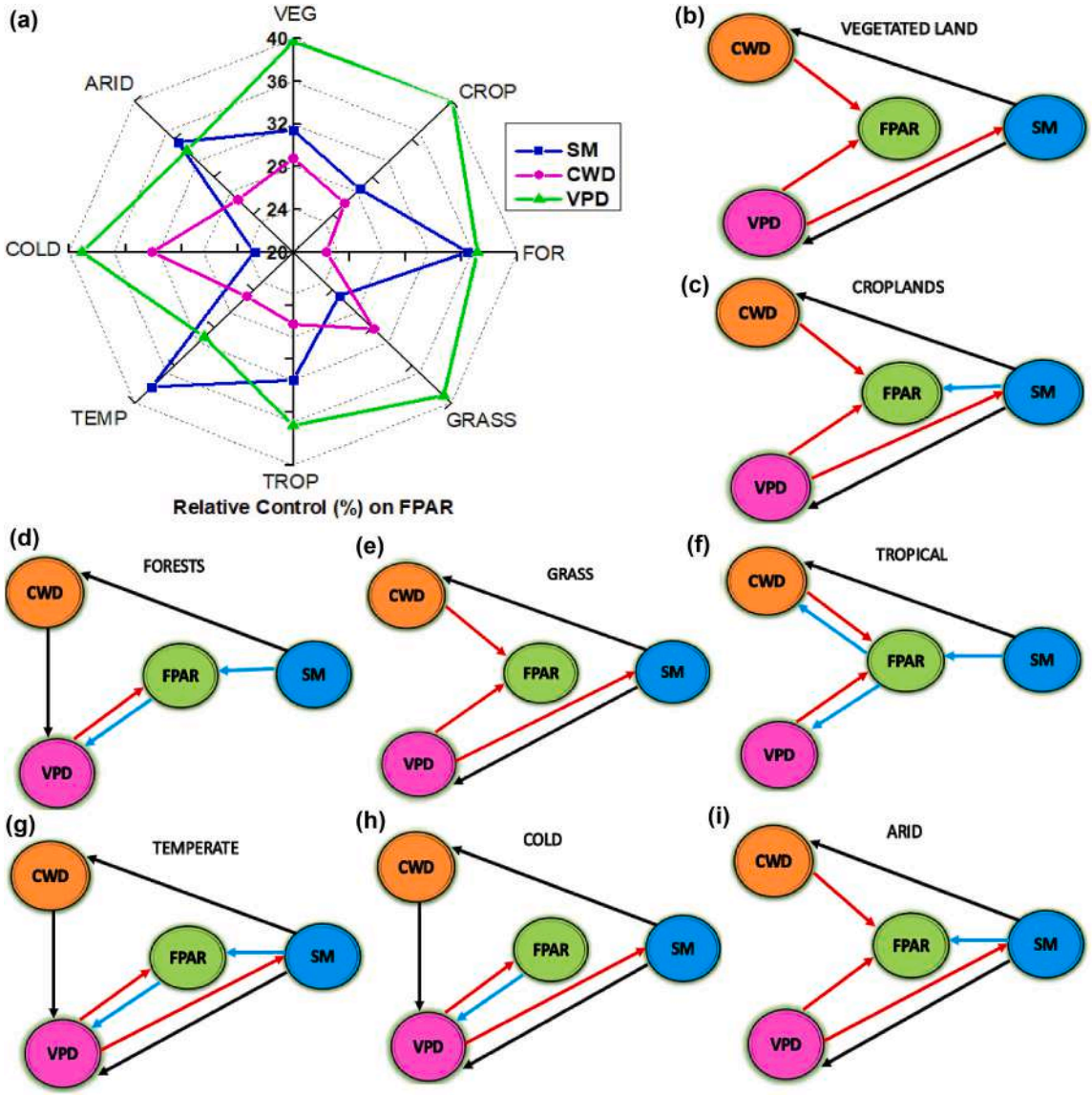

Fig. 3. (a) The relative control of Soil Moisture (SM), Climatic Water Deficit (CWD), Vapour Pressure Deficit (VPD) on Fraction of Photosynthetically Active Radiation (FPAR) variability across land cover types [net vegetated land (VEG), Croplands (CROP), Forests (FOR), other natural vegetation (GRASS)] and biomes [Tropical (TROP), Temperate (T), Cold (COLD), and Arid (ARID)] based on Random Forest model and (b-i) Causal associations among photosynthesis (FPAR) and moisture avilability/demand (SM, CWD and VPD) across land cover types and biomes averaged for the period 2000–2021 at lag of 0–3 months (red line: negative impact; blue line: positive impact) and no lag (black line).

recent decade (2010–2019) from the previous decade (2000–2009) (Fig. S4). The FPAR–SM coupling has intensified in northern and central North America, northwest and southern South America, sub-Saharan Africa, central and southern Africa, eastern and western Europe, eastern Asia, India, and Australia. The FPAR–SM relationship has greatly improved for croplands (20.9%), while it has declined for forests and grasses. All biomes have experienced an increase in FPAR-SM coupling, with the most substantial growth in temperate (3.3%) and arid (2.2%) biomes. The FPAR-CWD coupling exhibits an increase in most regions, but there is a decline in northern latitudes in North America, Europe, Eurasia and regions in tropical biome. FPAR-CWD relationship has strengthened in all land cover types, which is highest in grasses (11%), followed by forests and croplands (around 7.2%). For biomes, the FPAR-CWD coupling has strengthened for arid (6.9%) and temperate (3.1%), but weakened for cold and tropical types. The FPAR-VPD coupling has strengthened in most regions for vegetated land, strongest in the northern latitudes of North America, Europe and Eurasia. FPAR-VPD relationship has strengthened for grasses (7.1%) and croplands (4.2%) and weakened for forests (−5%). The FPAR-VPD coupling has strengthened in all biomes, which is highest in cold (38.8%), followed by arid (5.1%), tropical (4.4%) and temperate (2.5%) biomes (Fig. S4).

3.4. Change in moisture availability/demand and photosynthesis

We investigate the relation of moisture availability/demand and photosynthesis, but this carbon-water connection has been evolving with time. Henceforth, we explore the change in moisture availability/demand and response of photosynthesis to it in recent decade (2010–2019) from the previous decade (2000–2009). The global vegetated land exhibits a substantial increase in the land evaporative aridity (CWD) with higher increase (> 10%) in northeastern and northwestern North America, eastern and western Europe, Eurasia, western China, eastern south Asia, Indonesia, central and southwestern Africa, northwestern and northeastern South America (Fig. 4a). Interestingly, the atmospheric aridity (VPD) has also enhanced in most vegetated regions, which is predominant (>10%) in the regions of high increase in CWD

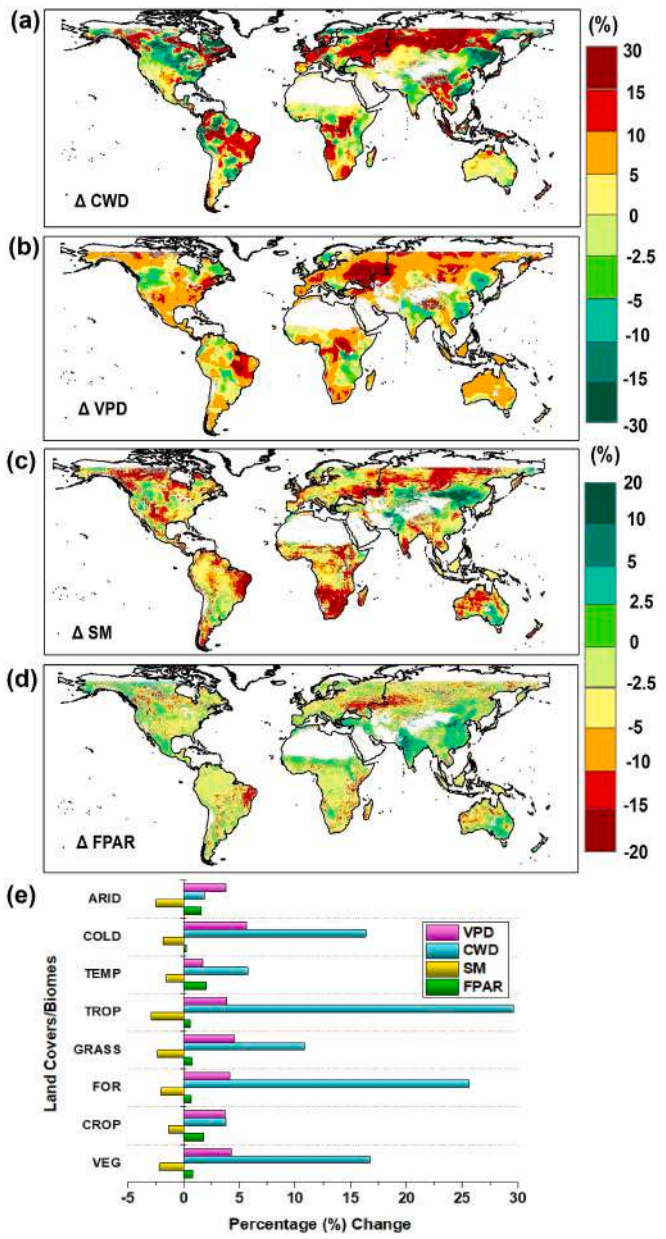

Fig. 4. Change (%) in (a) Climatic Water Deficit (CWD), (b) Vapour Pressure Deficit (VPD), (c) Soil Moisture (SM), (d) Fraction of Photosynthetically Active Radiation (FPAR) during recent decade (2010–2019) from previous decade (2000–2009); (d) (a, b, c) for land covers [net vegetated land (VEG), Croplands (CROP), Forests (FOR), other natural vegetation (GRASS)] and biomes [Tropical (TROP), Temperate (T), Cold (COLD), and Arid (ARID)].

(Fig. 4b). Concurrently, the global vegetated land exhibits a widespread reduction in readily plant available soil water (SM) with a substantial (> −10%) decline in northern and central North America, western Europe, eastern and central Eurasia, eastern and southern India, northern and western Australia, southern Africa and northeastern South America (Fig. 4c). The regions of substantial increase in land evaporative (CWD) and atmospheric aridity (VPD) greatly coincide with the SM drying in vegetated lands. In the warming world, there is more demand than availability of moisture for plants to utilise, and we call it as moisture stress in the long-term context.

Next, we investigate the changes in photosynthesis and find decrease in photosynthesis (hereafter referred to as browning) is severe (FPAR, −5 to −20%) in northwestern North America, southeastern Europe and western Eurasia and northeastern South America. Other regions such as central North America, central and southern South America, eastern and southern Africa, western and northern Australia also exhibit browning. It is evident that the vegetated regions that experience moisture stress exhibit browning (Fig. 4d). However, the global vegetated land largely exhibits increase in photosynthesis (greening). Greening is predominant (+FPAR, 10–20%) in northwest India and northeastern China. Other regions such as northern and southern North America, northern and western Europe, eastern Asia, India, China, southeastern Australia, sub-Sahara and some areas in South America show greening. Interestingly, most of these regions show either decline in land evaporative (CWD) or atmospheric (VPD) aridity and improved SM (Fig. 4a–d). Additionally, we also employ the SIF and EVI data to examine the change in global photosynthesis and complement the FPAR analysis. We find that the changes are homogeneous across the photosynthetic proxies. The greening is predominant in sparse canopy like croplands (1.8% FPAR, 7.3% SIF, and 4.6% EVI), and arid (1.6% FPAR, 5.7% SIF, and 2.4% EVI) and temperate (2% FPAR, 5% SIF, and 3.5% EVI) biomes than dense canopy like forests (0.68% FPAR, 3.2% SIF, and 2.3% EVI), tropical (0.6% FPAR, 2.9% SIF, and 1.5% EVI) and cold (0.25% FPAR, 5% SIF, and 3.8% EVI) biomes (Fig. S5). CWD is enhanced for all land cover types and biomes, and is dominant in dense canopy like forests (25.61%), and tropical (29.6%) and cold (16.36%) biomes. VPD is also increased for all land cover types and biomes, which is high in dense canopy like forests (4.16%), cold (5.63%) and tropical (3.84%) biomes. SM exhibits a decline in all land cover types and biomes with a marked decline in tropical (−2.9%) biome (Fig. 4e). Across the seasons, the land evaporative (CWD) and atmospheric (VPD) aridity are increased, but SM is decreased. Moisture stress peaks in JJA (CWD: +5.15%, VPD: +4.12%, SM: −3.04%) and DJF (CWD: +3.2%, VPD: +3.85%, SM: −2.14%) (Fig. S6).

3.5. Growth rate in moisture availability/demand and photosynthesis

We next investigate the cumulative growth rate (CGR) in moisture availability/demand (CWD, VPD and SM) and photosynthesis (FPAR) to get insights of their change in recent decades (Fig. 5). Both CWD (15.14%), VPD (11.85%) and global photosynthesis (FPAR) exhibit a positive (1.16%), and SM show a negative (−0.11%) growth rate for global vegetated land in 2000–2019. Both CWD and VPD exhibit a high positive growth in dense canopies as forests (CWD: 36.35%; VPD: 19.1%), and tropical (CWD: 26.69%; VPD:13.8%) and cold (CWD: 23.69%; VPD: 19.2%) biomes. Simultaneously, SM shows a high negative growth in grasses (−6.67%), and tropical (−7%) and temperate (−4.14%) biomes. Concurrently, global photosynthesis (FPAR) exhibits a high growth in sparse canopies like croplands (6.38%), and cold (6.45%) and temperate (5% CGR) biomes (Fig. 5c). Seasonally, VPD shows higher growth in SON (14.23%) and DJF (12%) than in MAM and JJA. SM has a high negative growth in JJA (−6.36%), MAM (−5.51%) and SON (−4.81%). Global photosynthesis (FPAR) exhibits a growth rate higher in DJF (5.84%) and SON (3.76%), lower in JJA (0.27%) in the same period. The high positive growth in moisture demand (CWD and VPD) and negative growth in moisture availability (SM) result in smaller positive growth in photosynthesis (Fig. 5a).

We now examine the change in CGR for moisture availability/demand and photosynthesis in recent decade (2010−2019) from the previous (2000−2009). The global vegetated land experiences substantial increase in CWD (9.85%) and VPD (5%), but a small increase in SM (2.6%) and a decline in photosynthesis (−2.8%, FPAR). Aridity (CWD and VPD) is enhanced in dense canopies like forests (VPD: 10.72%, CWD: 3%), tropical (CWD: 15.76%; VPD: 8.68%) and cold (CWD: 10.54%, VPD: 9.93%) biomes. SM shows an increase in CGR for croplands (7.78%) and forests (5.32%), and a decline in temperate (−5.45%) and tropical (−2.27%) biomes. In response, sparse canopies such as croplands (1.7%), and arid (1.6%) and temperate (1.4%) biomes exhibit intensified greening. Contrarily, grasses (−4.1%), and tropical (−1.8%) and cold (−0.2%) biomes show a slowdown/reversal in greening

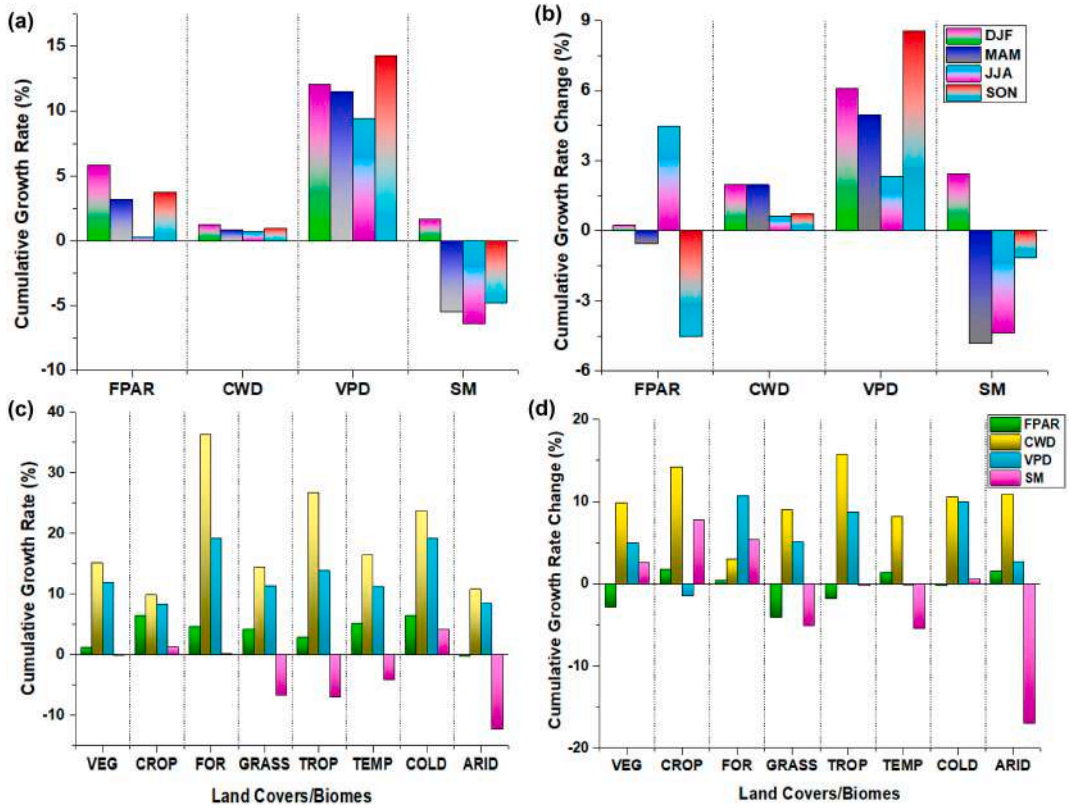

Fig. 5. (a) Cumulative Growth Rate (CGR, %) of Fraction of Photosynthetically Active Radiation (FPAR), Climatic Water Deficit (CWD), Vapour Pressure Deficit (VPD) and Soil Moisture (SM) for various seasons [(DJF: December, January and February), (MAM: March, April and May), (JJA: June, July and August), (SON: September, October and November)] during 2000–2019. (b) Change (%) in CGR for (a) during recent decade (2010–2019) from the previous decade (2000–2009). (c) CGR in FPAR, CWD, VPD and SM for land covers [net vegetated land (VEG), Croplands (CROP), Forests (FOR), other natural vegetation (GRASS)] and biomes [Tropical (TROP), Temperate (T), Cold (COLD), and Arid (ARID)] during 2000–2019. (d) Change (%) in CGR for (c) during recent decade (2010–2019) from the previous decade (2000–2009).

(Fig. 5d). Among the seasons, greening is enhanced in JJA (4.47%), DJF (0.23%) as these are the periods of small increase in aridity (JJA: CWD, 0.63%; VPD: 2.32%) or increase in SM (DJF: 2.45%). Conversely, slowdown/reversal of greening is observed in SON (−4.53%) and MAM (−0.57%) as these are the seasons (SON: VPD, 8.54%; SM: -1.13%), (MAM: VPD, 5%; CWD: 2%; SM, −4.84%) of increase in aridity and decline in SM (Fig. 5b).

3.6. Sensitivity of photosynthesis to moisture availability/demand

Sensitivity analysis highlights the change in global photosynthesis corresponding to the change in moisture, whether this change (FPAR and moisture availability/demand) is in the same (positive) and opposite direction (negative) across the land cover types and biomes (Fig. S7) and the uncertainties (Table S13). For land evaporative aridity (CWD), photosynthesis (FPAR) has a mixed response of positive and negative sensitivities for various regions. Global vegetated land exhibits a positive sensitivity of FPAR to CWD, which is higher in croplands (0.48), and arid (0.84) and temperate (0.35) biomes (Fig. S7 and Table S13). FPAR has a negative sensitivity to CWD in central and western North America, eastern and western Eurasia, eastern Asia, India, eastern and western Australia, northern and southern Africa, northeastern, and southern South America. Global vegetated land exhibits a positive sensitivity (0.19) of FPAR to VPD and is higher in croplands (0.49), and temperate (1.1) and arid (0.42) biomes. For VPD, FPAR has a positive sensitivity in northern, eastern and southern North America, western Europe, southern India, Indonesia, eastern Australia, northern and central Africa and southwestern South America as there are increases in both VPD and FPAR. However, FPAR has a negative sensitivity to VPD in northern and central North America, northeastern, southern South America, southern Africa, and southern and eastern Eurasia because there is browning due to enhanced VPD. Regions such as eastern China, India and western Australia also exhibit a negative sensitivity of FPAR to VPD due to greening induced by reduced VPD. Global vegetated land demonstrates a negative sensitivity (−0.39) of FPAR to SM, which is consistently negative across all biomes and land cover types. The sensitivity is greater in croplands (−1.35) compared to forests (−0.33) and grasses (−0.31). Temperate (−1.3) and arid (−0.65) biomes demonstrate greater sensitivity compared to tropical (−0.21) and cold (−0.13) biomes (Fig. S7, Table S13). FPAR has a positive sensitivity to SM in central South America, sub-Saharan Africa, northwest India, and eastern China, where moisture-induced greening is evident. Central North America, northeastern South America, southern Africa, western Eurasia, and western Australia show a positive sensitivity as SM drying-induced browning dominates in these regions. Eastern and southern India, eastern Asia, and Indonesia exhibit negative sensitivity owing to greening despite SM-drying.

3.7. Resilience of photosynthesis to moisture stress

Here, we investigate the resilience of global photosynthesis (FPAR) to moisture stress. FPAR is non-resilient to land evaporative aridity (CWD) in northern and northeastern North America, northwestern Amazonia, northern Eurasia, northwest India, west central and southeastern Africa and Indonesia (Fig. 6a). The regions northeast and central South America, western and central Europe, central and southern Africa, Australia, Indonesia, western China, and northeastern Eurasia exhibit non-resilience of photosynthesis (FPAR) to atmospheric aridity (VPD)

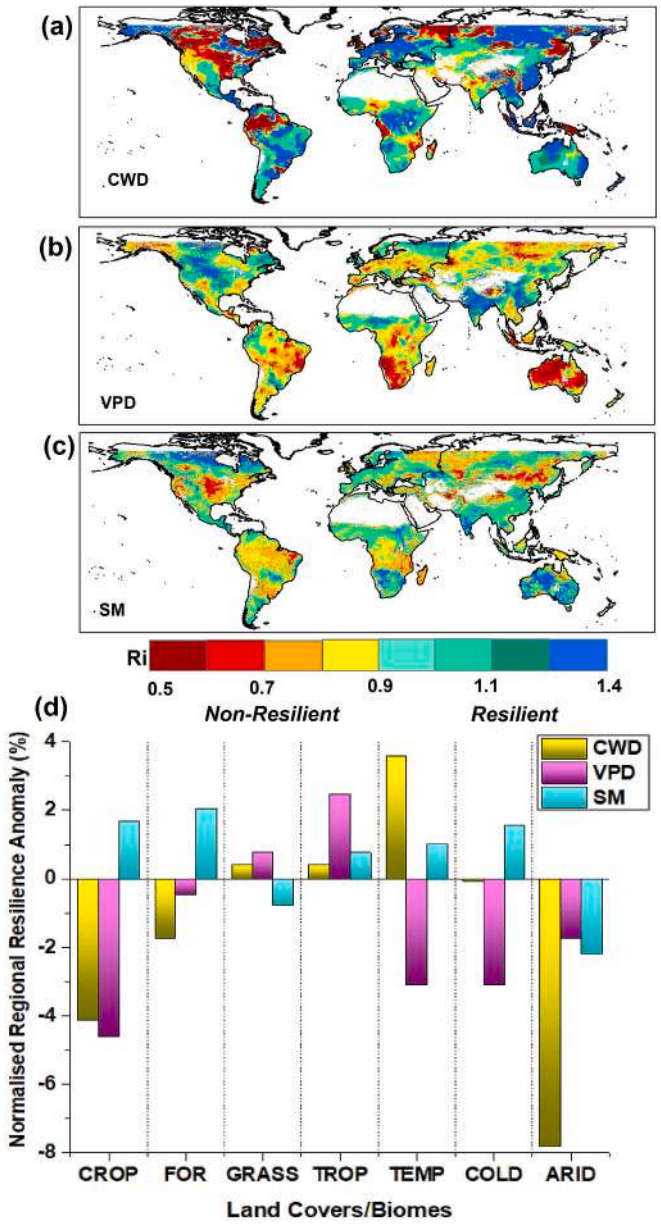

Fig. 6. Resilience index (Ri) of Global Photosynthesis (Fraction of Photosynthetically Active Radiation (FPAR) to (a) Climatic Water Deficit (CWD), (b) Vapour Pressure Deficit (VPD), (c) Soil Moisture (SM) and (d) (a, b, c) for land covers [net vegetated land (VEG), Croplands (CROP), Forests (FOR), other natural vegetation (GRASS)] and biomes [Tropical (TROP), Temperate (T), Cold (COLD), Arid (ARID)] averaged for the period 2000–2019.

(Fig. 6b). The regions of northeastern and western North America, northern and central South America, central Africa, northeastern Asia and northeastern Europe show non-resilience of FPAR to SM drying (Fig. 6c). Furthermore, we also estimated the normalised regional anomaly in resilience score (NRRA) for various land cover types and biomes (Fig. 6d). We find that photosynthesis (FPAR) has weaker resilience to VPD and CWD than SM across the land cover types and biomes, except for grasses. In grasses, FPAR has high resilience to VPD (0.78%) and CWD (0.4%), but weak resilience to SM (−0.78%). FPAR in croplands exhibits weak resilience against VPD (−4.6%) and CWD (−4.1%). In arid biome, FPAR has weak resilience against all, predominantly to CWD (−7.8%). In tropical biome, FPAR exhibits higher resilience to against all, primarily to VPD (2.47%). In temperate biome, FPAR has weak resilience to VPD (−3.1%), but high resilience to CWD (3.57%) (Fig. 6d).

Next, we examine the change in the resilience of global photosynthesis to moisture stress in recent decade (2010–2019) from the previous decade (2000–2009). We find that the FPAR resilience to CWD has declined in northeastern and central North America, northwest South America, central west Africa, Indonesia, Indo-Gangetic Plain, western Eurasia and northeastern Europe in recent decade from the previous. In contrast, FPAR resilience to CWD has increased in most other regions predominantly in Europe, eastern China, eastern Asia and Australia in the same period (Fig. 7a). Overall, the FPAR resilience to CWD has increased by 6.68%. Among the land cover types, croplands (10.9%) and grasses (10%) exhibit enhanced resilience, but forests (−10.45%) show a reduced resilience. All biomes show a gain in resilience, which is highest for temperate (11.5%), followed by cold (7.1%) and arid (4.9%) types, except the tropical (−0.64%) (Fig. 7d). The FPAR resilience to VPD has

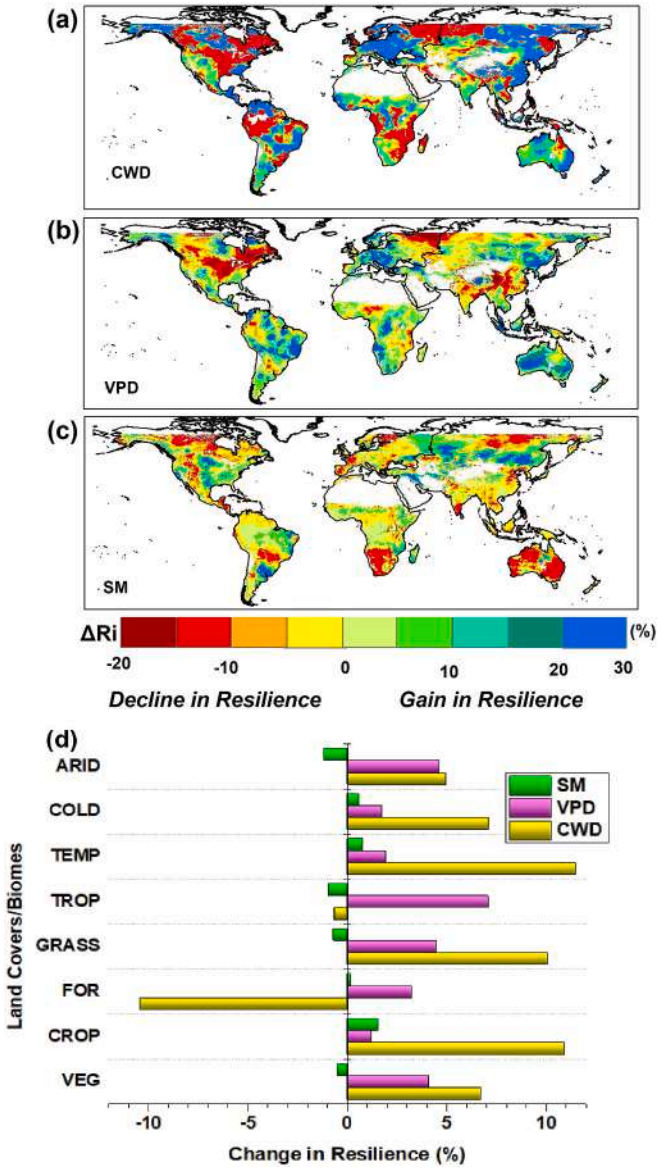

Fig. 7. Change (%) in Resilience index (Ri) of Global Photosynthesis (Fraction of Photosynthetically Active Radiation (FPAR) to (a) Climatic Water Deficit (CWD), (b) Vapour Pressure Deficit (VPD), (c) Soil Moisture (SM) and (d) (a, b, c) for land covers [net vegetated land (VEG), Croplands (CROP), Forests (FOR), other natural vegetation (GRASS)] and biomes [Tropical (TROP), Temperate (T), Cold (COLD), and Arid (ARID)] during recent decade (2010–2019) from previous decade (2000–2009).

declined in northeastern and central Northern America, eastern Europe, western Eurasia, eastern China and northern India. In contrast, most other regions, mainly in western Europe, eastern Eurasia, Indonesia, Australia, central and southwestern Africa and northeastern, central and southern South America show a gain in resilience of FPAR to VPD. Overall, the FPAR resilience to VPD has increased by 4.1% (Fig. 7b). For land cover types, grasses (4.64%) show the largest gain in resilience followed by forests (3.25%). For biomes, tropical (7.1%) and arid (4.6%) types exhibit the largest gain in resilience followed by the temperate (1.9%) and cold (1.7%) (Fig. 7d). The FPAR resilience to SM is weakened in northern, west central and southern North America, western and northern Europe, northern Eurasia, northwestern and southern India, Australia, southern Africa, and northern and central South America. However, northeastern North America, eastern Europe, western Eurasia, Central Africa and South America show a gain in resilience of FPAR to SM drying (Fig. 7c). Overall, the resilience of FPAR to SM has declined by 0.5%. It has increased in croplands (1.53%) and forests (0.15%), but reduced in grasses (−0.68%). For biomes, there is a gain in resilience of FPAR to SM in temperate (0.78%) and cold (0.56%) biomes, but loss of resilience in arid (−1.2%) and tropical (−0.95%) types in recent decade (Fig. 7d).

4. Discussion

Terrestrial carbon uptake has become increasingly constrained by SM drying and it adversely affects global greening (Green et al., 2019; Humphrey et al., 2021; Feng et al., 2021). Concurrently, the global VPD has escalated more rapidly than temperature and carbon dioxide concentration (CO_2), which is detrimental to photosynthesis (Yuan et al., 2019; Song et al., 2024). The global moisture stress is substantial with enhanced VPD and SM drying that limits photosynthesis (Fu et al., 2022; Liu et al., 2024). Moisture-induced greening of sparse canopies like drylands (Patel et al., 2024b; Kashyap et al., 2025b) and croplands due to improved land management and agricultural intensification is reported (Chen et al., 2019; Kuttippurath and Kashyap, 2023). The global browning may have been underestimated or obscured by the extensive greening, particularly in dense canopies (Pan et al., 2018; Qiu et al., 2022; Kashyap and Kuttippurath, 2026). Studies suggest dryness-induced browning in tropical (Feng et al., 2021; Tao et al., 2022) and Arctic (Myers-Smith et al., 2020) regions. Drying-induced browning has intensified after the year 2000 with sustained browning in 35.9% of the global vegetated area with greening levelled off in the last decade (Feng et al., 2021). Therefore, despite current reports on global greening, the increase in browning and rising dryness stress call for a thorough investigation (Liu et al., 2023c; Green, 2024; Kashyap et al., 2025a).

4.1. Growing control of moisture stress on photosynthesis

Therefore, we hereby thoroughly examine the relationship between global photosynthesis and moisture stress across land cover types, biomes and seasons. We find, land evaporative aridity (CWD) and atmospheric aridity (VPD) have negative influence on photosynthesis, which are stronger in croplands, and in arid, temperate (CWD) and tropical (VPD) biomes. Concurrently, readily plant available water (SM) has a strong positive relationship with photosynthesis in tropical and arid biomes. Interestingly, SM has a negative influence on photosynthesis in cold biomes, and both CWD and VPD have a weak negative control there. The water surplus and waterlogging decrease stomatal conductance and photosynthesis (Jiao et al., 2021; Liu et al., 2024). In addition, temperature and solar radiation have stronger control on photosynthesis in cold biome (Nemani et al., 2003; Liu et al., 2020). We find that the FPAR-VPD relationship limiting the role of SM, VPD still has a negative impact on photosynthesis, and is stronger in croplands, forests and cold biome. The FPAR-SM relationship limiting the effect of VPD, is strong in tropical and temperate, but strong negative in cold biomes. SM-VPD link exhibits a strong coupling in mid-latitude regions of southeast Asia, India, sub-Sahara and central South America. Both SM and VPD dryness limit photosynthesis regardless of one another. However, VPD limitation on photosynthesis is largely a result of SM-VPD coupling, dominant in mid-latitudes (Liu et al., 2020; Green, 2024). Broadly, SM (in water-limited) and VPD (in energy-limited) regions controls photosynthesis (Liu et al., 2025b).

The FPAR-VPD relationship has improved in all biomes, which is strongest in cold biome and grasses. Likewise, the FPAR-CWD relationship has enhanced for grasses, forests, and arid and temperate biomes. Concurrently, FPAR-SM coupling has strengthened substantially for croplands and biomes, which is predominant in temperate and arid biomes in recent decade (2010–2019) from the previous decade (2000–2009). Granger Causality reveals causal feedback of photosynthesis with VPD in forests, and tropical, temperate, and cold biomes, but no direct relation with SM (grasses and cold) and CWD (forests, and temperate, and cold biomes). In grasses, SM has a direct causal link with both CWD and VPD that influence FPAR. In cold biome, SM has a causal connection with CWD and feedback with VPD, and CWD has a causal relation with VPD that directly controls photosynthesis. Likewise, in forests and temperate biomes, CWD influences FPAR through VPD. It has been reported that VPD has a strong association with temperature, and has a strong control on photosynthesis in cold biomes (Yuan et al., 2019; Fu et al., 2022). ML based RF model suggests VPD has a greater influence on photosynthesis than CWD and SM for all land cover types and biomes; except temperate biome where SM is the dominant driver. There is a feedback in temperate regions, where greening declines SM as it coincides with warming and increased VPD, and enhanced land-atmosphere coupling that leads to higher ET and depletion of SM there (Liu et al., 2025a).

4.2. Rising moisture stress limits increase in photosynthesis

The influence of VPD on photosynthesis in conjunction with other climatic factors may be greater than previously recognised (Grossiord et al., 2020; Fu et al., 2022). Often a strong SM-VPD coupling is misinterpreted to diminish the control of VPD on global photosynthesis (Liu et al., 2020; Lu et al., 2022). VPD limitations restrict plant growth prior to the onset of SM limitations and contribute to tree mortality, ultimately resulting in vegetation browning, and the reversal from greening to browning (Yuan et al., 2019, 2025; Bauman et al., 2022). We find, the global vegetated land exhibits a substantial rise in land evaporative (CWD, 16.7%), atmospheric (VPD, 4.3%) aridity, and a subsequent decline in plant available soil water (SM, −2.2%) in recent decade. CWD has enhanced in all land cover types and biomes, and is predominant in natural vegetation like forests, grasses, biomes like tropical and cold. Likewise, VPD also exhibits a rise across land cover types and biomes, substantial in grasses, forests, and cold and tropical biomes. Also, SM dying is prevalent in all land cover types and biomes, which is large in tropical biome and grasses. Seasonally, the largest increase in CWD, VPD and decline in SM are found in JJA. During the period, global photosynthesis has enhanced across the land cover types, and is dominant in sparse canopy like temperate, arid biomes and croplands.

The results from growth rate analysis also reveal “Greening Earth” with positive CGR (1.16%) and its rate is higher for croplands (6.4% CGR), and cold (6.5% CGR) and temperate (5.1% CGR) biomes. The rising moisture stress on global vegetated land is attested by high positive CGR in CWD (15.1%), VPD (11.9%) and negative CGR in SM (−0.11%). Both CWD (36.3%) and VPD (19.1%) exhibit large CGR for forests. Furthermore, the global vegetated land exhibits a substantial rise in CGR of CWD (9.85%) and VPD (5%), and there is a reduction in CGR of photosynthesis (FPAR, −2.8%) in recent decades (2010–2019) from the previous (2000–2009). During this period, tropical (−1.8% CGR) and cold (−0.2% CGR) biomes exhibit the largest slowdown/reversal of greening as they also experience large increase in CGR for CWD (tropical: 15.8%, cold: 10.54%) and VPD (tropical: 8.7%, cold: 9.9%). Croplands (1.7% CGR) and forests (0.4% CGR) exhibit enhanced

greening, but a decline for grasses (−4.1% CGR) due to large reduction in SM (−5.1% CGR), and substantial increase in both CWD (8.9% CGR) and VPD (5% CGR). This is consistent with the findings of Winkler et al. (2021) and Feng et al. (2021), who report slowdown/reversal of global greening due to dryness. The grasses face high moisture stress-induced decline in photosynthesis during recent decade, which can adversely impact the vegetation health and functioning, alter the land-atmosphere feedbacks, and threaten the biodiversity in these vulnerable ecosystems.

4.3. Response of photosynthesis to rising dryness

In the future scenario, we find until the end of the century (P3, 2090–2100), from the historical (P1, 2015–2019), SM for the global vegetated land is declined (−0.26%). The future SM drying is stronger in dense canopies of tropical biome (−1.2%), forests (−0.4%) and croplands (−0.35%). Contrarily, sparse canopies of grasses (−0.25%), and cold (−0.2%) and arid (0.4%) biomes show increase or small reduction in SM. SM drying is prominent (< −2.5%) in northern latitudes of North America, Europe and Eurasia, southeast Asia, Indonesia, Australia, northern and central Africa, northern and northeastern South America (Fig. S8). Concurrently, global photosynthesis is enhanced, primarily in sparse canopies of cold (45.9%) and arid (31.6%) biomes. Interestingly, browning is exhibited in dense canopies such as Amazonia, Indonesia and western Africa. Further, we split the periods and examine the changes during the mid-century (P2, 2040–2050) from historical period (P1) and find widespread greening, but browning is projected in northeast Amazonia, India and Australia. Also, for the change in the end-century (P3) from mid-century (P2), greening is predominant, but browning is projected in Amazonia, eastern South America and most of Africa (Fig. S9). It coincides with the regions that show SM drying during the same period. In terms of changes between the mid–end century (F2) and historical–mid-century (F1), SM drying (−0.31%) is stronger in dense canopies like tropical biome (−1.4%) and forests (−0.6%). However, the sparse canopies croplands (−0.1%), grasses (−0.24%), and arid (0.05%) temperate (0.21%) and cold (0.24%) biomes show a small decline or enhanced SM (Fig. S9). It suggests that the moisture availability would play a crucial role in global photosynthesis and sustained carbon sinks in a drier world (Zhao et al., 2020; Wu et al., 2022; Liu et al., 2025a).

We estimate the resilience of vegetation in terms of their photosynthetic ability to moisture stress (Kashyap and Kuttippurath, 2024a, 2025a). This is highly essential to limit current and future global effects of climate change (Smith and Boers, 2023). We find that photosynthesis has a low resilience to VPD stress (croplands, forests, and temperate, cold and arid biomes), CWD stress (croplands, forests and arid biome) and SM stress (grasses and arid biome) in various land cover types and biomes. Generally, higher water availability regions exhibit greater resilience, but lower resilience in grass-dominated ecosystems and regions with high moisture variability (Smith and Boers, 2023). Interestingly, there is a gain in resilience of photosynthesis to CWD stress (6.7%) and VPD stress (4.1%), but loss in resilience to SM stress (−0.5%). This loss in resilience of FPAR to SM stress is predominant in grasses (−0.7%), arid (−1.2%) and tropical (−0.9%) biomes. Forests (−10.5%) and tropical (−0.6%) biomes exhibit loss in resilience of photosynthesis to CWD stress. We find the vegetation in regions such as northern latitudes of North America, eastern Europe, western Eurasia, western Australia, eastern Africa, northeastern South America that are moisture stressed, non-resilient and exhibit decline in resilience results in browning (Fig. 8). The decline in resilience can lead to potential desertification of grasslands and shrublands that may initiate a series of destabilising feedback loops. For instance, diminished vegetation resilience to moisture stress could weaken terrestrial carbon sinks, alter rainfall patterns, change land-atmosphere coupling, decline water storage capacity, and expedite the greenhouse gas emissions due to changes in land covers (Shukla et al., 2019; Smith and Boers, 2023; Kashyap and Kuttippurath, 2025a).

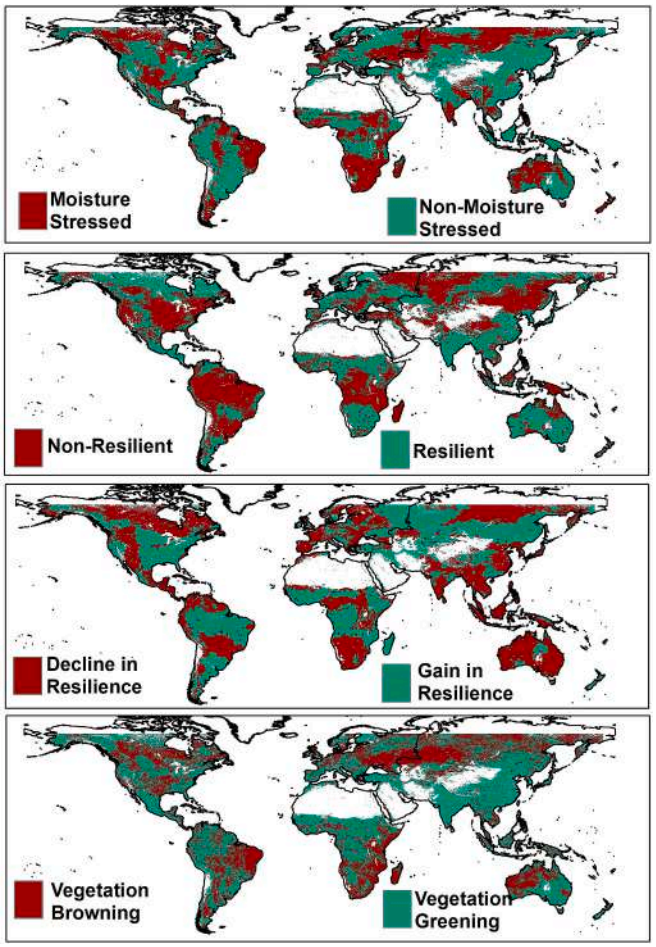

Fig. 8. The concept figure summarising the findings as the vegetation moisture availability (moisture stressed/non-stressed), resilience of vegetation to moisture stress (resilient/non-resilient), change in resilience of vegetation to moisture stress (gain/decline) and the corresponding response of vegetation in terms of change in photosynthesis (increase: greening/decrease: browning) during recent decade (2010–2019) from previous decade (2000–2009).

4.4. Constraints and recommendations

The existing remote sensing measurements are subject to constraints such as background noises, sensor degradation, calibration issues, retrieval problems, sensor saturation and sensitivity loss in very dense vegetation. This calls for improvement of existing remote sensing measurements with ground validation. Also, the tropics and mid-latitude of higher photosynthesis are largely data scare in terms of in-situ measurements. Henceforth, there is a need of expansion of the current ground-based observational networks to capture changing carbon-water cycle across the latitudes. It is of paramount significance to elucidate the future impacts of growing moisture stress control on global photosynthesis for effective climate risk management (Liu et al., 2024). Also, the CMIP6 model projections overestimate the future greening as they fail to efficiently account for SM limitations on photosynthesis (Feng et al., 2021; Wu et al., 2022). Additionally, these climate models underestimate the impacts of VPD stress and compound SM-VPD stress on terrestrial ecosystems, primarily due to the strong SM-VPD coupling, sustained by land-atmosphere feedbacks (Lu et al., 2022; Song et al., 2024; Liu et al., 2025b). Furthermore, these models underestimate the sensitivity of vegetation carbon uptake to extreme climate events caused by El Niño Southern Oscillation (ENSO) and stresses arising from plant hydraulics and low atmospheric humidity in a potentially drier and warmer planet (Wigneron et al., 2020; Feng et al., 2021).

The uncertainties in the data employed in the study will be inherited in the findings. The statistical and machine learning techniques utilised in the study are also constrained by specific limitations. The first-order linear sensitivity analysis is constrained by saturation and threshold behaviour. Granger Causality is effective for extended stationary time series and identifies linear causal relationships. In this context, nonlinear causality inference methods, such as Peter and Clarke's Momentary Conditional Independence (PCMCI) and Convergent Cross Mapping (CCM), may provide additional insights into causal relationships. Nonetheless, these causal frameworks methodologies can yield spurious relations that lack mechanistic plausibility. Machine learning-based methodologies are predominantly data-driven and necessitate substantial data volumes to produce reliable outcomes. Employing process-based terrestrial biosphere models would add to the robustness of the findings. However, their complex attribution methodologies and low-resolution outputs make them highly improbable due to large uncertainties (Ryu et al., 2019; Winkler et al., 2021). Simultaneously, employing geostationary satellites (Xiao et al., 2021) and global navigation satellites systems (GNSS) signals (Yao et al., 2024) enable continuous and frequent monitoring of vegetation stress from space. There is a need for more studies on global scale vegetation-water relationships (Feldman et al., 2024), moisture stress thresholds (Fu et al., 2024) and impact on vegetation (Liu et al., 2025b), and role of vegetation in mediating land-atmosphere feedbacks (Miralles et al., 2025). Additionally, the future studies should focus on microwave remote sensing signals (Wigneron et al., 2024) and in-situ measurements (Xiao et al., 2025). The proliferation of environmental observational networks focused on understanding of plant responses to moisture stress across various spatial scales, coupled with advancements in remote sensing, presents promising avenues. The integration of novel methodologies such as machine learning, enhanced models of stomatal conductance, and innovative vegetation schemes in Earth System Models (ESMs) can reduce uncertainties in the carbon-water cycle estimates for a drier and warmer world.

5. Conclusions

In recent decades, global warming drives higher land evaporative (CWD) and atmospheric aridity (VPD) that dry up the readily plant available soil water (SM). Concurrently, “Greening Earth” continues to be one of the major signatures of changing climate. However, there are reports of browning in dense canopies overshadowed by greening of sparse canopies in recent decades. We comprehensively investigate the response of global photosynthesis to moisture stress across different land cover types, biomes and seasons. We find that the control of SM and VPD on photosynthesis (FPAR) has enhanced for all biomes. CWD has also strengthened relationship with FPAR in arid and temperate biomes. Among land cover types, SM (croplands), VPD (grasses), and CWD (grasses and forests) exhibit enhancement in the influence on photosynthesis. RF model reveals that VPD has a stronger control on photosynthesis than SM and CWD across the land cover types and biomes, except temperate and arid regions where SM has the key control. Granger Causality suggests that VPD has a direct causal connection with FPAR in all biomes and land cover types. CWD and SM influence photosynthesis though VPD where they do not have a direct causal relationship with FPAR. The global vegetated land experiences a substantial increase in land evaporative and atmospheric aridity and SM drying in recent decade from the previous. Concurrently, global greening continues with higher rate in croplands, arid and temperate biomes. However, there is a slowdown/reversal of global greening in recent decade, which is predominant in grasses, tropical and cold biomes due to growing moisture stress. The regions with rising moisture stress that exhibits greening have gained resilience against dryness in recent decade. Contrarily, the regions that show moisture stress-induced browning exhibit a decline in resilience to dryness. The decline in resilience to dryness can lead to potential desertification of grasslands and shrublands, decline water storage capacities, alter rainfall patterns and expedite greenhouse gas emissions. In future, global greening is projected to continue majorly in sparse canopies. However, dense canopies would exhibit a slowdown/reversal in greening due to rising moisture stress. This calls for effective ecosystem planning, climate risk management, employ climate resilient agricultural practices, improve agronomic management to achieve food security. Additionally, there is a need for policies on judicial land management, effective forest conservation and restoration to enhance the resilience of vulnerable ecosystems to rising moisture stress to attain sustainability and food security in a warmer and drier planet in the context of climate change.

CRediT authorship contribution statement

Rahul Kashyap: Writing – review & editing, Writing – original draft, Visualization, Validation, Software, Methodology, Formal analysis, Conceptualization. **Jayanarayanan Kuttippurath:** Writing – review & editing, Visualization, Validation, Supervision, Methodology, Conceptualization.

Consent to participate

Not applicable.

Consent for publication

Not applicable.

Ethics approval

Not applicable.

Funding

This study receives no funding.

Declaration of competing interest

The authors declare that they have no known competing financial interests or personal relationships that could have appeared to influence the work reported in this paper.

Acknowledgements

We thank the Director, Indian Institute of Technology Kharagpur (IIT Kgp), Chairman of CORAL IIT Kgp and the Ministry of Education (MoE) for facilitating the study. RK acknowledges the support from Prime Minister's Research Fellowship (PMRF), MoE. We thank the NASA's LPDAAC team for providing the MODIS landcover, NDVI and EVI products. Giovanni's online data system developed and maintained by the GLDAS for providing soil moisture content, TerraClimate for PET, AET and VPD datasets; CMIP6 for providing future projection of LAI and SM datasets. Special thanks to Jingfeng Xiao for making the GOSIF SIF dataset publicly accessible.

Appendix A. Supplementary data

Supplementary data to this article can be found online at https://doi.org/10.1016/j.scitotenv.2026.181416.

Data availability

All data are publicly available and are listed in Table 1.

References

Abatzoglou, J.T., Dobrowski, S.Z., Parks, S.A., Hegewisch, K.C., 2018. TerraClimate, a high–resolution global dataset of monthly climate and climatic water balance from 1958–2015. Sci. Data 5 (1), 1–12. https://doi.org/10.1038/sdata.2017.191.

Bauman, D., Fortunel, C., Delhaye, G., Malhi, Y., Cernusak, L.A., Bentley, L.P., McMahon, S.M., et al., 2022. Tropical tree mortality has increased with rising atmospheric water stress. Nature 608 (7923), 528–533. https://doi.org/10.1038/s41586-022-04737-7.

Beck, H.E., McVicar, T.R., Vergopolan, N., Berg, A., Lutsko, N.J., Dufour, A., Miralles, D. G., et al., 2023. High-resolution (1 km) Köppen-Geiger maps for 1901–2099 based on constrained CMIP6 projections. Sci. Data 10 (1), 724. https://doi.org/10.1038/s41597-023-02549-6.

Brandt, M., Wigneron, J.P., Chave, J., Tagesson, T., Penuelas, J., Ciais, P., Fensholt, R., et al., 2018. Satellite passive microwaves reveal recent climate-induced carbon losses in African drylands. Nat. Ecol. Evol. 2 (5), 827–835. https://doi.org/10.1038/s41559-018-0530-6.

Cai, W., Zhu, Z., Harrison, S.P., Ryu, Y., Wang, H., Zhou, B., Prentice, I.C., 2025. A unifying principle for global greenness patterns and trends. Commun. Earth Environ. 6 (1), 19. https://doi.org/10.1038/s43247-025-01992-0.

Chen, C., Park, T., Wang, X., Piao, S., Xu, B., Chaturvedi, R.K., Myneni, R.B., et al., 2019. China and India lead in greening of the world through land–use management. Nat. Sustain. 2 (2), 122–129. https://doi.org/10.1038/s41893-019-0220-7.

Chen, X., Chen, T., He, B., Liu, S., Zhou, S., Shi, T., 2024. The global greening continues despite increased drought stress since 2000. Glob. Ecol. Conserv. 49, e02791. https://doi.org/10.1016/j.gecco.2023.e02791.

Cortés, J., Mahecha, M.D., Reichstein, M., Myneni, R.B., Chen, C., Brenning, A., 2021. Where are global vegetation greening and browning trends significant? Geophys. Res. Lett. 48 (6), e2020GL091496. https://doi.org/10.1029/2020GL091496.

Denissen, J.M., Teuling, A.J., Pitman, A.J., Koirala, S., Migliavacca, M., Li, W., Orth, R., 2022. Widespread shift from ecosystem energy to water limitation with climate change. Nat. Clim. Change 12 (7), 677–684. https://doi.org/10.1038/s41558-022-01403-8.

Eyring, V., Bony, S., Meehl, G.A., Senior, C.A., Stevens, B., Stouffer, R.J., Taylor, K.E., 2016. Overview of the Coupled Model Intercomparison Project Phase 6 (CMIP6) experimental design and organization. Geosci. Model Dev. 9 (5), 1937–1958. https://doi.org/10.5194/gmd-9-1937-2016.

Feldman, A.F., Feng, X., Felton, A.J., Konings, A.G., Knapp, A.K., Biederman, J.A., Poulter, B., 2024. Plant responses to changing rainfall frequency and intensity. Nat. Rev. Earth Environ. 5 (4), 276–294. https://doi.org/10.1038/s43017-024-00534-0.

Feng, X., Fu, B., Zhang, Y., Pan, N., Zeng, Z., Tian, H., Penuelas, J., et al., 2021. Recent leveling off of vegetation greenness and primary production reveals the increasing soil water limitations on the greening Earth. Sci. Bull. 66 (14), 1462–1471. https://doi.org/10.1016/j.scib.2021.02.023.

Fu, Z., Ciais, P., Prentice, I.C., Gentine, P., Makowski, D., Bastos, A., Hajima, T., et al., 2022. Atmospheric dryness reduces photosynthesis along a large range of soil water deficits. Nat. Commun. 13 (1), 989. https://doi.org/10.1038/s41467-022-28652-7.

Fu, Z., Ciais, P., Wigneron, J.P., Gentine, P., Feldman, A.F., Makowski, D., Smith, W.K., 2024. Global critical soil moisture thresholds of plant water stress. Nat. Commun. 15 (1), 4826. https://doi.org/10.1038/s41467-024-49244-7.

Granger, C.W., 1969. Investigating causal relations by econometric models and cross–spectral methods. Econometrica 424–438. https://doi.org/10.2307/1912791.

Green, J.K., 2024. The intricacies of vegetation responses to changing moisture conditions. New Phytol. https://doi.org/10.1111/nph.20182.

Green, J.K., Seneviratne, S.I., Berg, A.M., Findell, K.L., Hagemann, S., Lawrence, D.M., Gentine, P., 2019. Large influence of soil moisture on long–term terrestrial carbon uptake. Nature 565 (7740), 476–479. https://doi.org/10.1038/s41586-018-0848-x.

Grossiord, C., Buckley, T.N., Cernusak, L.A., Novick, K.A., Poulter, B., Siegwolf, R.T., McDowell, N.G., et al., 2020. Plant responses to rising vapor pressure deficit. New Phytol. 226 (6), 1550–1566. https://doi.org/10.1111/nph.16485.

Hartmann, H., 2015. Carbon starvation during drought–induced tree mortality–are we chasing a myth? J. Plant Hydraul. 2, e005. https://hal.science/hal-01230747.

Higgins, S.I., Conradi, T., Muhoko, E., 2023. Shifts in vegetation activity of terrestrial ecosystems attributable to climate trends. Nat. Geosci. 16 (2), 147–153. https://doi.org/10.1038/s41561-022-01114-x.

Holling, C.S., 1973. Resilience and Stability of Ecological Systems. https://doi.org/10.1017/9781009177856.038.

Huang, M., Zhai, P., Piao, S., 2021. Divergent responses of ecosystem water use efficiency to drought timing over Northern Eurasia. Environ. Res. Lett. 16 (4), 045016. https://doi.org/10.1088/1748-9326/abf0d1.

Huete, A., Didan, K., Miura, T., Rodriguez, E.P., Gao, X., Ferreira, L.G., 2002. Overview of the radiometric and biophysical performance of the MODIS vegetation indices. Remote Sens. Environ. 83 (1–2), 195–213. https://doi.org/10.1016/S0034-4257(02)00096-2.

Humphrey, V., Berg, A., Ciais, P., Gentine, P., Jung, M., Reichstein, M., Frankenberg, C., et al., 2021. Soil moisture-atmosphere feedback dominates land carbon uptake variability. Nature 592 (7852), 65–69. https://doi.org/10.1038/s41586-021-03325-5.

Jiao, W., Wang, L., Smith, W.K., Chang, Q., Wang, H., D'Odorico, P., 2021. Observed increasing water constraint on vegetation growth over the last three decades. Nat. Commun. 12 (1), 3777. https://doi.org/10.1038/s41467-021-24016-9.

Kashyap, R., Kuttippurath, J., 2024a. Unraveling the sensitivity and response of ecosystems to rising moisture stress in India. Ecosys. Health Sustain. 10, 0180. https://doi.org/10.34133/ehs.0180.

Kashyap, R., Kuttippurath, J., 2024b. Warming-induced soil moisture stress threatens food security in India. Environ. Sci. Pollut. Res. 31 (49), 59202–59218. https://doi.org/10.1007/s11356-024-35107-7.

Kashyap, R., Kuttippurath, J., 2025a. Weakening of forest carbon stocks due to declining ecosystem photosynthetic efficiency under the current and future climate change scenarios in India. India. Resour. Conserv. Recycl. 222, 108478. https://doi.org/10.1016/j.resconrec.2025.108478.

Kashyap, R., Kuttippurath, J., 2025b. Tropical cyclones enhance photosynthesis in moisture-stressed regions of India. npj Clim. Atmos. Sci. 8 (1), 115. https://doi.org/10.1038/s41612-025-00988-z.

Kashyap, R., Kuttippurath, J., 2026. Changing global vegetation-climate interactions constrain photosynthesis in the 21st century. J. Clean. Prod. 538, 147402. https://doi.org/10.1016/j.jclepro.2025.147402.

Kashyap, R., Kuttippurath, J., Kumar, P., 2023a. Browning of vegetation in efficient carbon sink regions of India during the past two decades is driven by climate change and anthropogenic intrusions. J. Environ. Manage. 336, 117655. https://doi.org/10.1016/j.jenvman.2023.117655.

Kashyap, R., Kuttippurath, J., Patel, V.K., 2023b. Improved air quality leads to enhanced vegetation growth during the COVID–19 lockdown in India. Appl. Geogr. 151, 102869. https://doi.org/10.1016/j.apgeog.2022.102869.

Kashyap, R., Kuttippurath, J., Patel, V.K., 2025a. Ecological droughts increased in India with changing Indian summer monsoon and human interventions. Commun. Earth Environ. 6 (1), 853. https://doi.org/10.1038/s43247-025-02694-3.

Kashyap, R., Kuttippurath, J., Patel, V.K., 2025b. Agriculture intensification and moisture-induced Thar desert greening: implications for energy balance, socio-economy, and biodiversity. GISci. Remote Sens. 62 (1), 2483458. https://doi.org/10.1080/15481603.2025.2483458.

Keenan, T.F., Prentice, I.C., Canadell, J.G., Williams, C.A., Wang, H., Raupach, M., Collatz, G.J., 2016. Recent pause in the growth rate of atmospheric CO2 due to enhanced terrestrial carbon uptake. Nat. Commun. 7 (1), 13428. https://doi.org/10.1038/ncomms13428.

Keenan, T.F., Luo, X., Stocker, B.D., De Kauwe, M.G., Medlyn, B.E., Prentice, I.C., Zhou, S., et al., 2023. A constraint on historic growth in global photosynthesis due to rising CO2. Nat. Clim. Chang. 13 (12), 1376–1381. https://doi.org/10.1038/s41558-023-01867-2.

Krich, C., Runge, J., Miralles, D.G., Migliavacca, M., Perez-Priego, O., El-Madany, T., Mahecha, M.D., 2020. Estimating causal networks in biosphere–atmosphere interaction with the PCMCI approach. Biogeosciences 17 (4), 1033–1061. https://doi.org/10.5194/bg-17-1033-2020.

Kuttippurath, J., Kashyap, R., 2023. Greening of India: forests or croplands? Appl. Geogr. 161, 103115. https://doi.org/10.1016/j.apgeog.2023.103115.

Lal, P., Shekhar, A., Gharun, M., Das, N.N., 2023. Spatiotemporal evolution of global long-term patterns of soil moisture. Sci. Tot. Environ. 867, 161470. https://doi.org/10.1016/j.scitotenv.2023.161470.

Li, X., Xiao, J., 2019. Mapping photosynthesis solely from solar–induced chlorophyll fluorescence: a global, fine-resolution dataset of gross primary production derived from OCO–2. Remote Sens. 11 (21), 2563. https://doi.org/10.3390/rs11212563.

Li, X., Xiao, J., He, B., Altaf Arain, M., Beringer, J., Desai, A.R., Varlagin, A., et al., 2018. Solar-induced chlorophyll fluorescence is strongly correlated with terrestrial photosynthesis for a wide variety of biomes: first global analysis based on OCO-2 and flux tower observations. Glob. Chang. Biol. 24 (9), 3990–4008. https://doi.org/10.1111/gcb.14297.

Li, W., Migliavacca, M., Forkel, M., Denissen, J.M., Reichstein, M., Yang, H., Orth, R., et al., 2022. Widespread increasing vegetation sensitivity to soil moisture. Nat. Commun. 13 (1), 3959. https://doi.org/10.1038/s41467-022-31667-9.

Liu, Y., Liu, Y., Wang, W., 2019. Inter-comparison of satellite-retrieved and global land data assimilation system–simulated soil moisture datasets for global drought analysis. Remote Sens. Environ. 220, 1–18. https://doi.org/10.1016/j.rse.2018.10.026.

Liu, L., Gudmundsson, L., Hauser, M., Qin, D., Li, S., Seneviratne, S.I., 2020. Soil moisture dominates dryness stress on ecosystem production globally. Nat. Commun. 11 (1), 4892. https://doi.org/10.1038/s41467-020-18631-1.

Liu, H., Liu, Y., Chen, Y., Fan, M., Chen, Y., Gang, C., Wang, Z., et al., 2023a. Dynamics of global dryland vegetation were more sensitive to soil moisture: evidence from multiple vegetation indices. Agric. For. Meteorol. 331, 109327. https://doi.org/10.1016/j.agrformet.2023.109327.

Liu, Q., Peng, C., Schneider, R., Cyr, D., Liu, Z., Zhou, X., Kneeshaw, D., et al., 2023b. Vegetation browning: global drivers, impacts, and feedbacks. Trends Plant Sci. 28 (9), 1014–1032. https://doi.org/10.1016/j.tplants.2023.03.024.

Liu, X., Sun, G., Fu, Z., Ciais, P., Feng, X., Li, J., Fu, B., 2023c. Compound droughts slow down the greening of the Earth. Glob. Chang. Biol. 29 (11), 3072–3084. https://doi.org/10.1111/gcb.16657.

Liu, Q., Guo, H., Zhang, J., Li, S., Li, J., Yao, F., Peng, J., et al., 2024. Global assessment of terrestrial productivity in response to water stress. Sci. Bull. https://doi.org/10.1016/j.scib.2024.05.033.

Liu, Y., Li, Z., Chen, Y., Jin, L., Li, F., Wang, X., Kayumba, P.M., et al., 2025a. Global greening drives significant soil moisture loss. Commun. Earth Environ. 6 (1), 600. https://doi.org/10.1038/s43247-025-02470-3.

Liu, J., Wang, Q., Zhan, W., Lian, X., Gentine, P., 2025b. When and where soil dryness matters to ecosystem photosynthesis. Nat. Plants 11 (7), 1390–1400. https://doi.org/10.1038/s41477-025-02024-7.

Lu, H., Qin, Z., Lin, S., Chen, X., Chen, B., He, B., Yuan, W., et al., 2022. Large influence of atmospheric vapor pressure deficit on ecosystem production efficiency. Nat. Commun. 13 (1), 1653. https://doi.org/10.1038/s41467-022-29009-w.

McDowell, N.G., Sevanto, S., 2010. The mechanisms of carbon starvation: how, when, or does it even occur at all? New Phytol. 186 (2), 264–266. https://www.jstor.org/stable/27797544.

McDowell, N.G., Sapes, G., Pivovaroff, A., Adams, H.D., Allen, C.D., Anderegg, W.R., Xu, C., et al., 2022. Mechanisms of woody–plant mortality under rising drought, CO2 and vapour pressure deficit. Nat. Rev. Earth & Environ. 3 (5), 294–308. https://doi.org/10.1038/s43017-022-00272-1.

Miralles, D.G., Vilà-Guerau de Arellano, J., McVicar, T.R., Mahecha, M.D., 2025. Vegetation–climate feedbacks across scales. Ann. N. Y. Acad. Sci. 1554 (1), 27–41. https://doi.org/10.1111/nyas.15286.

MODIS Land Team, 2014. Status for: land cover/dynamics (MCD12), validation. http://landval.gsfc.nasa.gov/ProductStatus.php?ProductID=MOD12. (Accessed 18 March 2023).

Myers-Smith, I.H., Kerby, J.T., Phoenix, G.K., Bjerke, J.W., Epstein, H.E., Assmann, J.J., Wipf, S., et al., 2020. Complexity revealed in the greening of the Arctic. Nat. Clim. Chang. 10 (2), 106–117. https://doi.org/10.1038/s41558-019-0688-1.

Nemani, R.R., Keeling, C.D., Hashimoto, H., Jolly, W.M., Piper, S.C., Tucker, C.J., Running, S.W., et al., 2003. Climate–driven increases in global terrestrial net primary production from 1982 to 1999. Science 300 (5625), 1560–1563. https://doi.org/10.1126/science.1082750.

Otkin, J.A., Anderson, M.C., Hain, C., Mladenova, I.E., Basara, J.B., Svoboda, M., 2013. Examining rapid onset drought development using the thermal infrared–based evaporative stress index. J. Hydrometeorol. 14 (4), 1057–1074. https://doi.org/10.1175/JHM-D-12-0144.1.

Pan, N., Feng, X., Fu, B., Wang, S., Ji, F., Pan, S., 2018. Increasing global vegetation browning hidden in overall vegetation greening: insights from time–varying trends. Remote Sens. Environ. 214, 59–72. https://doi.org/10.1016/j.rse.2018.05.018.

Patel, V.K., Kuttippurath, J., Kashyap, R., 2024a. Increased global cropland greening as a response to the unusual reduction in atmospheric $PM_{2.5}$ concentrations during the COVID–19 lockdown period. Chemosphere 358, 142147. https://doi.org/10.1016/j.chemosphere.2024.142147.

Patel, V.K., Kuttippurath, J., Kashyap, R., 2024b. Rise in water vapour driven by moisture transport facilitates water availability for the greening of global deserts. Sci. Total Environ. 946, 174111. https://doi.org/10.1016/j.scitotenv.2024.174111.

Peng, C., Zeng, J., Chen, K.S., Li, Z., Ma, H., Zhang, X., Bi, H., et al., 2023. Global spatiotemporal trend of satellite–based soil moisture and its influencing factors in the early 21st century. Remote Sens. Environ. 291, 113569. https://doi.org/10.1016/j.rse.2023.113569.

Piao, S., Wang, X., Park, T., Chen, C., Lian, X.U., He, Y., Myneni, R.B., et al., 2020. Characteristics, drivers and feedbacks of global greening. Nat. Rev. Earth Environ. 1 (1), 14–27. https://doi.org/10.1038/s43017-019-0001-x.

Qiu, B., Ye, Z., Chen, C., Tang, Z., Chen, Z., Huang, H., Berry, J., et al., 2022. Dense canopies browning overshadowed by global greening dominant in sparse canopies. Sci. Total Environ. 826, 154222. https://doi.org/10.1016/j.scitotenv.2022.154222.

Reichstein, M., Bahn, M., Ciais, P., Frank, D., Mahecha, M.D., Seneviratne, S.I., Wattenbach, M., et al., 2013. Climate extremes and the carbon cycle. Nature 500 (7462), 287–295. https://doi.org/10.1038/nature12350.

Ryu, Y., Berry, J.A., Baldocchi, D.D., 2019. What is global photosynthesis? History, uncertainties and opportunities. Remote Sens. Environ. 223, 95–114. https://doi.org/10.1016/j.rse.2019.01.016.

Sellers, P.J., Tucker, C.J., Collatz, G.J., Los, S.O., Justice, C.O., Dazlich, D.A., Randall, D. A., 1996. A revised land surface parameterization (SiB2) for atmospheric GCMs. Part II: the generation of global fields of terrestrial biophysical parameters from satellite data. J. Climate 9 (4), 706–737. https://doi.org/10.1175/1520-0442(1996)009<0706:ARLSPF>2.0.CO;2.

Sharma, A., Goyal, M.K., 2018. Assessment of ecosystem resilience to hydroclimatic disturbances in India. Glob. Chang. Biol. 24 (2), e432–e441. https://doi.org/10.1111/gcb.13874.

Shekhar, A., Buchmann, N., Gharun, M., 2022. How well do recently reconstructed solar-induced fluorescence datasets model gross primary productivity? Remote Sens. Environ. 283, 113282. https://doi.org/10.1016/j.rse.2022.113282.

Shukla, P.R., Skeg, J., Buendia, E.C., Masson-Delmotte, V., Pörtner, H.O., Roberts, D.C., Malley, J., et al., 2019. Climate Change and Land: An IPCC Special Report on Climate Change, Desertification, Land Degradation, Sustainable Land Management, Food Security, and Greenhouse Gas Fluxes in Terrestrial Ecosystems.

Smith, T., Boers, N., 2023. Global vegetation resilience linked to water availability and variability. Nat. Commun. 14 (1), 498. https://doi.org/10.1038/s41467-023-36207-7.

Song, J., Zhou, S., Yu, B., Li, Y., Liu, Y., Yao, Y., Fu, B., et al., 2024. Serious underestimation of reduced carbon uptake due to vegetation compound droughts. npj Clim. Atmos. Sci. 7 (1), 23. https://doi.org/10.1038/s41612-024-00571-y.

Song, J., Zhou, S., Yu, B., Li, Y., Liu, Y., Yao, Y., Fu, B., 2024. Serious underestimation of reduced carbon uptake due to vegetation compound droughts. NPJ Clim. Atmos. Sci. 7 (1), 23. https://doi.org/10.1038/s41612-024-00571-y.

Su, F., Fu, D., Yan, F., Xiao, H., Pan, T., Xiao, Y., Liu, G., et al., 2021. Rapid greening response of China's 2020 spring vegetation to COVID-19 restrictions: implications for climate change. Sci. Adv. 7 (35), eabe8044. https://doi.org/10.1126/sciadv.abe8044.

Tao, S., Chave, J., Frison, P.L., Le Toan, T., Ciais, P., Fang, J., Saatchi, S., et al., 2022. Increasing and widespread vulnerability of intact tropical rainforests to repeated droughts. Proc. Natl. Acad. Sci. U. S. A. 119 (37), e2116626119. https://doi.org/10.1073/pnas.2116626119.

Wigneron, J.P., Fan, L., Ciais, P., Bastos, A., Brandt, M., Chave, J., Fensholt, R., et al., 2020. Tropical forests did not recover from the strong 2015–2016 El Niño event. Sci. Adv. 6 (6), eaay4603. https://doi.org/10.1126/sciadv.aay4603.

Wigneron, J.P., Ciais, P., Li, X., Brandt, M., Canadell, J.G., Tian, F., Fensholt, R., et al., 2024. Global carbon balance of the forest: satellite-based L-VOD results over the last decade. Front. Remote Sens. 5, 1338618. https://doi.org/10.3389/frsen.2024.1338618.

Winkler, A.J., Myneni, R.B., Hannart, A., Sitch, S., Haverd, V., Lombardozzi, D., Brovkin, V., et al., 2021. Slowdown of the greening trend in natural vegetation with further rise in atmospheric CO 2. Biogeosci 18 (17), 4985–5010. https://doi.org/10.5194/bg-18-4985-2021.

Wu, J., Wang, D., Li, L.Z., Zeng, Z., 2022. Hydrological feedback from projected Earth greening in the 21st century. Sustain. Horiz. 1, 100007. https://doi.org/10.1016/j.horiz.2022.100007.

Xiao, J., Fisher, J.B., Hashimoto, H., Ichii, K., Parazoo, N.C., 2021. Emerging satellite observations for diurnal cycling of ecosystem processes. Nat. Plants 7 (7), 877–887. https://doi.org/10.1038/s41477-021-00952-8.

Xiao, J., Baldocchi, D., Ichii, K., Li, F., Papale, D., 2025. Insights into terrestrial carbon and water cycling from the global eddy covariance network. Nat. Rev. Earth & Environ. 1–20. https://doi.org/10.1038/s43017-025-00743-1.

Yao, Y., Humphrey, V., Konings, A.G., Wang, Y., Yin, Y., Holtzman, N., Frankenberg, C., 2024. Investigating diurnal and seasonal cycles of vegetation optical depth retrieved from GNSS signals in a broadleaf forest. Geophys. Res. Lett. 51 (6), e2023GL107121. https://doi.org/10.1029/2023GL107121.

Yuan, W., Zheng, Y., Piao, S., Ciais, P., Lombardozzi, D., Wang, Y., Yang, S., et al., 2019. Increased atmospheric vapor pressure deficit reduces global vegetation growth. Sci. Adv. 5 (8), eaax1396. https://doi.org/10.1126/sciadv.aax1396.

Yuan, W., Tian, J., Wang, M., Wang, S., Xu, W., Wang, Y., Chen, X., et al., 2025. Impacts of rising atmospheric dryness on terrestrial ecosystem carbon cycle. Nat. Rev. Earth & Environ. 1–16. https://doi.org/10.1038/s43017-025-00726-2.

Zeng, Y., Hao, D., Park, T., Zhu, P., Huete, A., Myneni, R., Chen, M., et al., 2023. Structural complexity biases vegetation greenness measures. Nat. Ecol. & Evol. 7 (11), 1790–1798. https://doi.org/10.1038/s41559-023-02187-6.

Zhang, L., Jiao, W., Zhang, H., Huang, C., Tong, Q., 2017. Studying drought phenomena in the Continental United States in 2011 and 2012 using various drought indices. Remote Sens. of Environ. 190, 96–106. https://doi.org/10.1016/j.rse.2016.12.010.

Zhao, Q., Zhu, Z., Zeng, H., Zhao, W., Myneni, R.B., 2020. Future greening of the Earth may not be as large as previously predicted. Agric. For. Meteorol. 292, 108111. https://doi.org/10.1016/j.agrformet.2020.108111.

Zhu, Z., Piao, S., Myneni, R.B., Huang, M., Zeng, Z., Canadell, J.G., Zeng, N., et al., 2016. Greening of the Earth and its drivers. Nat. Clim. Chang. 6 (8), 791–795. https://doi.org/10.1038/nclimate3004.